

Dissertation zur Erlangung des Doktorgrades
der Fakultät für Chemie und Pharmazie
der Ludwig-Maximilians-Universität München

New Approaches to Optimize Freeze-Drying of Monoclonal Antibodies



Julian Hendryk Gitter

aus

Dessau, Deutschland

2020

Erklärung

Diese Dissertation wurde im Sinne von §7 der Promotionsordnung vom 28. November 2011 von Herrn Prof. Dr. Gerhard Winter betreut.

Eidesstattliche Versicherung

Diese Dissertation wurde eigenständig und ohne unerlaubte Hilfe erarbeitet.

München, den 01. September 2020

(Julian Hendryk Gitter)

Dissertation eingereicht am:	07. September 2020
1. Gutachter:	Prof. Dr. Gerhard Winter
2. Gutachter:	Prof. Dr. Wolfgang Friß
Mündliche Prüfung am:	15. Oktober 2020

To my family

Acknowledgments

Wistful and joyful at the same time, this is the place to honor the ones who supported me on my four years lasting Ph.D. journey.

Most notably, I want to express my sincere gratitude to my supervisor Prof. Dr. Gerhard Winter. Thank you for accepting me in your research group and the continuous support, scientific and personal guidance and, encouragement throughout all phases of this work. I am grateful for the questions you raised during our discussions and the challenges you posed to me. The creative and supportive working atmosphere that you created in your team was fabulous. Thank you for that. I am also thankful for both the opportunities for scientific exchange and for presenting my work at conferences worldwide.

Secondly, I would like to thank Raimund Geidobler and Ingo Presser for their support, guidance, and the fun we regularly had during our telephone conferences and face-to-face meetings. Thank you for the valuable discussions, your honest opinions, your mentoring, and for the co-supervision of my thesis; I very much appreciated our cooperation. I am also grateful for the constant supply with Kinderschokolade.

Other special thanks go to Professor Dr. Wolfgang Frieß for the fruitful scientific discussions, the contribution to my thesis as a committee member and as second assessor as well as for keeping up the great atmosphere at the chair, also by being quick with a joke.

The company PÜSCHNER GMBH + CO KG MicrowavePowerSystems and here, in particular, Peter Püschner, Michael Eggers, and Mirko Diers are kindly acknowledged for all the efforts related to tweaking the prototype microwave-dryer as well as their practical support and the helpful scientific and technical discussions around the physics of microwave drying.

I highly appreciated the collaboration with Dr. Alexander Tambovzev and Matthias Kopp from OPTIMA pharma GmbH. Thanks to you for all the engineering skills provided, technical and scientific input, and the discussions while enjoying one of Mesut's delicious Döner.

Moreover, I want to thank Dr. Frank Harms from Martin Christ Gefriertrocknungsanlagen GmbH for the fruitful discussions on freeze-drying and far beyond.

Furthermore, Steffen Schmidt, Christian Minke, and Wolfgang Wünschheim from LMU are kindly acknowledged for their help with certain measurements. In particular, Dr. Christoph Müller is kindly acknowledged for his help and development work in the establishment of a GC-MS headspace method for tert-Butyl alcohol quantification.

However, the best-equipped laboratory is not enough if you do not have a supportive working atmosphere. Therefore, I want to say thanks a lot to all the nice people from the research groups of Prof. Dr. Winter, Prof. Dr. Frieß, and Prof. Dr. Merkel who helped to make all the setbacks less bad and all the successes even greater. I am most grateful for all the (scientific) discussions and the great time I had with Leticia Rodrigues Neibecker, Katharina Geh, Mariam Mohammadi, Teresa Kraus, Andreas Tosstorff, Christoph Marschall, Andreas Stelzl, Ute Rockinger, Tobias Keil, Oliver Blümel, Weiwei Liu, Sebastian Groël and Dennis Krieg.

In particular, I enjoyed the time with Hristo Svilenov, who was not only the best labmate to wish for but became a friend for a lifetime. I will miss our lab discussions, music sessions, and (regular) workouts.

Special thanks also go to my students who supported the project with their good work during internships, namely Patrizia Zill, Fabian Schmitt, Moritz Schneider, Julia Kaulich, Franziska Freitag, Robin Endter, David Schmidt and Anian Thaller. Particularly, Benedikt Häupler is kindly acknowledged for his engaged work during his master thesis. It was my pleasure working and discussing with you, and coaching you.

Last but not least, I want to deeply thank my family and friends. Your continuous support, encouragement, and patience made this work become a success. Foremost, I want to thank my mother, Evelyn, my brother, Danny, and my future in-laws, Adelheid and Eckhard, as well as my future brother-in-law, Benedikt, for supporting me over all the time and being my family. I am deeply grateful as much for the continuous encouragement and longstanding deep friendship with my closest friends Holger Erlen, Hristo Svilenov, and Stephan Rauschenberg. Finally, I want to thank Annabelle from the bottom of my heart. With your patience, support, unconditional love, and for simply being there for me for more than 10 years until now, you played a key role in this successful work. And with our small love Clara, the time of writing this thesis was never boring.

Funding acknowledgment

This work was funded by the company Boehringer Ingelheim Pharma GmbH & Co. KG, Biberach.

Table of Content

Chapter I	General introduction.....	1
I.1	Introduction	1
I.2	The freeze-drying process	1
I.2.1	Freezing	1
I.2.2	Primary drying	4
I.2.3	Secondary drying	6
I.3	Emerging developments in the field of freeze-drying.....	7
I.3.1	Spray freeze-drying.....	7
I.3.2	Microwave-assisted freeze-drying.....	7
I.3.3	Continuous freeze-drying	8
I.4	Aim and outline of the thesis.....	9
Chapter II	Significant drying time reduction using microwave-assisted freeze-drying for a monoclonal antibody	11
II.1	Abstract	12
II.2	Introduction	13
II.3	Materials and methods.....	14
II.3.1	Materials	14
II.3.2	Preparation of formulations	14
II.3.3	Freeze-drying process	15
II.3.4	Residual moisture content.....	16
II.3.5	Specific surface area	16
II.3.6	X-ray powder diffraction	16
II.3.7	Reconstitution of lyophilizates	17
II.3.8	High-performance size exclusion chromatography (HP-SEC).....	17
II.3.9	Light Obscuration	17
II.3.10	Turbidity	17
II.4	Results and discussion.....	18
II.4.1	Applicability to different formulations.....	18
II.4.2	Accelerated stability study.....	21
II.5	Conclusion and outlook.....	22
II.6	Supplementary material.....	24
II.6.1	Materials and methods	24
II.6.2	Results.....	25
Chapter III	Microwave-assisted freeze-drying of monoclonal antibodies: product quality aspects and storage stability	29
III.1	Abstract	30
III.2	Introduction	31
III.3	Materials and methods.....	33
III.3.1	Materials	33
III.3.2	Study design.....	33
III.3.3	Preparation of formulations	34
III.3.4	Freeze-drying process	35
III.3.5	Karl Fischer titration.....	38
III.3.6	Brunauer-Emmet-Teller krypton gas adsorption	38

III.3.7	X-ray powder diffraction	38
III.3.8	Reconstitution of lyophilizates	38
III.3.9	High-performance size exclusion chromatography (HP-SEC).....	39
III.3.10	High-performance cation exchange chromatography (HP-CEX).....	39
III.3.11	Light obscuration	40
III.3.12	Flow-imaging microscopy	40
III.4	Results	41
III.4.1	Solid state.....	41
III.4.2	Protein-related quality attributes.....	43
III.5	Discussion	50
III.5.1	Stability with regard to solid state properties	50
III.5.2	Stability with regard to the protein	52
III.6	Conclusion.....	56
III.7	Supplementary material.....	57
Chapter IV A comparison of controlled ice nucleation techniques for freeze-drying of a therapeutic antibody		
		61
IV.1	Abstract	62
IV.2	Introduction	63
IV.3	Materials and methods.....	63
IV.3.1	Materials	63
IV.3.2	Preparation of formulations	64
IV.3.3	Freeze drying process	64
IV.3.4	Residual moisture content.....	66
IV.3.5	Specific surface area	67
IV.3.6	X-ray powder diffraction	67
IV.3.7	Reconstitution of lyophilizates	67
IV.3.8	High-performance size exclusion chromatography (HP-SEC).....	67
IV.3.9	Flow-imaging microscopy	68
IV.3.10	Turbidity	68
IV.3.11	Statistical tests.....	68
IV.4	Results and discussion.....	69
IV.4.1	Process performance	69
IV.4.2	Solid state properties.....	70
IV.4.3	XRD	71
IV.4.4	Protein analysis	72
IV.4.5	Turbidity	72
IV.4.6	Soluble aggregates	73
IV.4.7	Subvisible particles	74
IV.5	Conclusion.....	75
IV.6	Supplementary material.....	76
IV.6.1	Materials and methods	76
IV.6.2	Results.....	78
Chapter V Study on key variables that can influence controlled ice nucleation in a pilot-scale freeze-dryer		
		81
V.1	Introduction	81
V.2	Materials and methods.....	84
V.2.1	Materials	84

V.2.2	Formulations	84
V.2.3	Experimental setup	84
V.2.4	Design of experiments	86
V.2.5	Regression model.....	88
V.3	Results and discussion.....	90
V.3.1	Occurrence of floating	90
V.3.2	Effect of the investigated factors on the responses.....	90
V.3.3	Implications for controlled ice nucleation process design.....	91
V.3.4	Recommendations for controlled ice nucleation process design	93
V.3.5	Limitations and blind spots of the study	94
V.4	Conclusion and outlook.....	95
Chapter VI 100 % Control of controlled ice nucleation vials by camera-supported optical inspection in freeze-drying.....		97
VI.1	Abstract	98
VI.2	Introduction	99
VI.3	Materials and methods.....	101
VI.3.1	Materials	101
VI.3.2	Preparation of formulations	101
VI.3.3	Freeze-drying processes.....	102
VI.3.4	Karl Fischer titration.....	104
VI.3.5	Brunauer-Emmet-Teller krypton gas adsorption	105
VI.3.6	Reconstitution of lyophilizates	105
VI.3.7	Camera-supported optical inspection.....	105
VI.3.8	Statistical analysis.....	108
VI.4	Results	109
VI.4.1	Residual moisture content and specific surface area	109
VI.4.2	Average edge brightness	111
VI.4.3	Reconstitution time	114
VI.5	Discussion	115
VI.5.1	The feasibility of optical camera inspection for determination of nucleation success.....	115
VI.5.2	Average edge brightness as a surrogate with reservations for specific surface area.....	117
VI.5.3	Limitations	118
VI.6	Conclusion.....	119
Chapter VII Final summary and conclusion of the thesis		121
References		125
Appendix		133
A.1	List of publications	133
A.2	List of presentations	134
A.3	Curriculum vitae.....	135

Chapter I General introduction

I.1 Introduction

The first large-scale commercial implementation of freeze-drying in a pharmaceutical environment was accomplished with freeze-drying of human blood plasma during World War II.^{1,2} Since then, a lot of research into the biophysics of freezing and freeze-drying was made. However, the emergence of widely used recombinant protein pharmaceuticals put freeze-drying on the spot.^{3,4} This is particularly linked to the complexity in both the production and the limited physicochemical stability of proteins.⁴ Most of the typical protein-related degradation pathways like chemical reactions (e.g., hydrolysis) or physical mechanisms (e.g., aggregation) are generally slowed down in the solid state due to the reduction of molecular mobility and significant reduction of water content.⁵⁻⁸ The reader interested in aspects of protein stability in general⁸⁻¹⁰ and protein stability in the solid state in particular^{4,11-13} is referred to literature.

In the following section, the process of freeze-drying will be described at a glance.

I.2 The freeze-drying process

Freeze-drying, synonymously called lyophilization, is a multistage operation which is the drying method of choice for protein pharmaceuticals until today. The classic conventional freeze-drying is performed in a batch-mode and is described as a time-consuming, highly energy consumptive, costly process raising additional challenges during drug product manufacturing.^{3,13,14} Generally, the lyophilization process comprises three process steps, (i) freezing, (ii) primary drying which is characterized by the removal of crystallized water by sublimation under vacuum with gentle heating and (iii) secondary drying in which unfrozen water is desorbed under vacuum by controlled heating to more elevated temperatures.^{13,15}

I.2.1 Freezing

After filling of the liquid in the container and placing it on the shelves of the freeze-dryer, the temperature of the system is lowered until the solvent separates from the solute by crystallization.^{16,17} Searles et al.¹⁸ divided the freezing of water (which normally is the main component of pharmaceutical solutions to be freeze-dried) into four steps which comprised

(1) the cooling of the solution below its equilibrium freezing temperature, i.e. supercooling, (2) the formation of an ice nucleus, i.e. primary nucleation, (3) the instant subsequent growth of an ice nucleus to ice crystals, i.e. secondary nucleation, and (4) the final solidification by the completion of the liquid-to-solid phase transition by proceeding ice crystal growth. The supercooled solution is metastable and is, therefore, prone to spontaneous crystallization of ice. The higher the degree of supercooling the more the number of ice nuclei increases and thus the probability of ice crystallization.^{18–21} Besides, a higher degree of supercooling corresponds with the formation of smaller ice crystals which in turn directly affects the average pore size within the generated cake structure leading to a rather poor drying performance during the subsequent sublimation phase, but an improved desorption drying.^{4,18,22} However, pharmaceutical solutions normally represent multi-component systems which ultimately either leads to eutectic freezing or vitrification upon lowering the temperature. Eutectic freezing refers to the solute crystallization from a cryoconcentrated solution and is characterized by the eutectic melting temperature (T_{eu}). The formation of a eutectic mixture can often be seen for excipients that are known to crystallize upon freezing, e.g. mannitol or glycine. In contrast, the vitrification occurs in systems with excipients that tend to form an amorphous solute phase, e.g. sugars or certain arginine salts²³ and is characterized by the glass transition temperature of the maximally freeze-concentrated solution (T_g'). This occurs in the case of phase separation of a crystalline ice phase and an amorphous solute phase leading to an increase in solute concentration by further crystallization of water. At the T_g' the viscosity of the freeze-concentrate changes approximately four orders of magnitude over a small temperature range leading to a rigid glass system below T_g' .^{17,22} Another characteristic parameter is the collapse temperature (T_c). T_c is the (total) loss of structure caused by viscous flow and, therefore, represents the maximum allowable product temperature that must not be exceeded during the subsequent drying procedure if the pharmaceutical elegant appearance and porous structure of the lyophilizate should be maintained.^{24,25} Generally, T_g' measured by differential scanning calorimetry (DSC) represents an easy to access surrogate for T_c , which is normally determined by laborious and operator-dependent freeze-drying microscopy (FDM). For placebos or low protein concentration amorphous formulations (≤ 25 g/L), Pansare et al. suggest $T_g' \sim T_c$.²⁶ In general, T_c is described to be 1 K to 5 K higher as T_g' , but in certain systems like high protein concentration formulations, higher deviations are reported.^{25–29} All in all, the freezing step may have a detrimental effect on the incorporated protein. Especially when keeping in mind that freezing is associated with several stresses like cold

denaturation^{11,30-32}, freeze- or cryoconcentration^{7,22,33,34}, pH shifts due to crystallization of buffer components^{30,35} and protein interaction with ice indirectly³⁶ or via adsorption to the ice surface at the ice-liquid interface³⁷.

The interested reader is referred to reviews by Kasper et al.¹⁷ and Assegehegn et al.³⁸ for a sound overview of the freezing step in pharmaceutical lyophilization.

I.2.1.1 Annealing

One modification of the freezing step is the addition of a thermal treatment after solidification of the system called annealing. By raising the shelf temperature to a value above the T_g' of the solute, the complete crystallization of crystalline compounds is promoted²². Also, annealing is reported to decrease inter-vial heterogeneity and to improve primary drying rates.^{22,39,40}

I.2.1.2 Controlled ice nucleation

Another modification is the control of the ice nucleation temperature (T_N). Controlled ice nucleation (CN) as such refers to the control of T_N of all vials and thus control of the degree of supercooling of the filled solution by introducing a stimulus to the supercooled solutions. Normally, the ice nucleation among the batch is a stochastic event, leading to a distribution of nucleation temperatures and, hence, to an inter-vial heterogeneity concerning pore size distribution and subsequent drying performance. Moreover, especially when transferring a process from laboratory scale to a production environment, shelf-ramped frozen samples tend to a higher degree of supercooling due to less airborne heterogeneous nucleation sites in a Class 100 environment.⁴¹ By the employment of controlled ice nucleation, these challenges during process transfer and scale-up could be overcome or at least diminished. Moreover, the lowering of the degree of supercooling by application of CN leads to the formation of larger ice crystals and thus larger pores which typically result in lower resistance to water vapor during the sublimation phase, but leading to a reduced specific surface area.^{42,43}

Several techniques for controlled ice nucleation are reported in the literature, some of them with commercial implementation. The most common techniques are based on (1) the introduction of ice seeds by ice fog^{41,44-49}, (2) the application of rapid pressure changes^{48,50,51}, or (3) the application of vacuum to induce local surface freezing⁵²⁻⁵⁴. Although the benefits and advantages of controlled ice nucleation from a process time^{40,43,50,52,53,55}, whole

batch, and/or product quality perspective^{40,43,54–59} have been shown widely, shelf-ramp freezing is still the gold standard in most commercial processes.

The interested reader is referred to a review by Geidobler et al.²¹ for more background on controlled ice nucleation.

I.2.2 Primary drying

The primary drying is the sublimation drying in which the frozen solvent, i.e. in most of the cases water, is removed from the product under vacuum. The basis for this is that the chamber pressure is kept well below the vapor pressure of ice at the target product temperature.^{39,60} As the phase transition from solid to gaseous consumes energy, the sublimation enthalpy needed is provided by the heated shelves to keep the sublimation ongoing. In conventional primary drying, the majority of ice is sublimed in a quasi-steady state which can be expressed as coupled heat and mass transfer and which needs to be balanced during primary drying.⁷ That means, it should be balanced in a way that the product temperature does not exceed the maximum allowable product temperature (e.g. T_c) but is kept as close as possible to it.⁶¹ This necessity becomes obvious when taking into account that an increase in product temperature by 1 °C is reported to decrease primary drying time by around 13 %.⁶² For a rational design of the primary drying step, the chamber pressure and the shelf temperature have to be defined. In the following, three important relations from Tang and Pikal³⁹ explaining the interaction of the variables concerning the heat and mass transfer will be discussed:

- (1) The dependence of the ice sublimation rate dm/dt of the chamber pressure P_c in vials is expressed by Equation I-1 (P_{ice} equilibrium vapor pressure of ice at the sublimation interface temperature; R_p resistance of the dried-product layer above the frozen product):

$$\frac{dm}{dt} = \frac{P_{ice} - P_c}{R_p + R_s + R_c} \quad (\text{Equation I-1, modified from Tang and Pikal }^{39})$$

The sublimation rate is proportional to the pressure difference. Consequently, the lower the chamber pressure, the higher the ice sublimation rate. However, due to technical challenges associated with very low chamber pressures⁶³ and reports on increased heterogeneity in heat transfer⁶⁰, Tang et al.³⁹ recommend an operating space from 66 μbar to 266 μbar . In general, the dried-product layer R_p represents the main hindering factor to water vapor flow,

wherefore the resistance to of the semistoppered vial R_s and the resistance to transfer from drying chamber to the condenser R_c could be neglected. However, care must be taken as R_p increases with progressing drying.⁶⁴

- (2) The general relation between heat transfer rate (dQ/dt) and mass transfer rate (dm/dt) is given by the expression:

$$\frac{dQ}{dt} = \Delta H_s * \frac{dm}{dt} \quad (\text{Equation I-2, from Pikal et al.}^{60})$$

The heat transfer rate is directly proportional to the mass transfer rate via the heat of ice sublimation (ΔH_s) as a proportional factor.

- (3) In vials, the heat transfer rate (dQ/dt) is defined as (Q energy received by each vial from the shelf; A_v outer area of vial bottom; K_v vial heat transfer coefficient; T_s shelf temperature; T_b product temperature at the bottom center of the vial):

$$\frac{dQ}{dt} = A_v * K_v * (T_s - T_b) \quad (\text{Equation I-3, from Pikal et al.}^{60})$$

K_v is the sum of the heat flow contributions from conduction (K_c), thermal radiation (K_r), and gas convection (K_g). The main heat transfer mechanisms in conventional freeze-drying are the conductive heat transfer K_c by direct conduction from shelf to vial at the points of contact and the convective heat transfer K_g which represents the conduction through the gas between shelf and vial bottom with the latter being proportionally related to the chamber pressure.^{60,65} The contribution of radiative heat transfer K_r is normally minor due to the low temperatures encountered in classical freeze-drying operations.⁶⁶ However, the contribution of K_r has to be considered particularly when (1) emerging modified freeze-drying technologies like microwave-assisted freeze-drying (section I.3.2, Chapter II & Chapter III) are used or (2) in terms of altering edge vial effects during scale-up as investigated by Rambhatla et al⁶⁷.

All in all, the time needed for completion of primary drying can be decreased by an optimized sublimation rate which can be enhanced by an increased product temperature. The latter being directly affected by both the pressure difference between the vapor pressure of

ice at the sublimation interface temperature and chamber pressure (Equation I-1) and the temperature difference between shelf temperature and product temperature (Equation I-3). However, dependencies between the variables, maximum allowable temperatures (e.g. T_c , T_{eu}), and product-specific aspects (e.g. R_p) have to be taken into account.

I.2.3 Secondary drying

At the end of primary drying, the frozen water is removed by sublimation leaving only the unfrozen water in the solute phase. In amorphous products, 20 % to 30 % (w/w) residual water on a dried solids basis is still contained.⁶⁸ The applied desorption drying during secondary drying should reduce the residual moisture content within the product in a way to ensure a sufficiently long shelf life, i.e. storage stability, at the desired storage temperature.⁶⁹ Usually, residual moisture levels < 1 % are aimed at.³⁹ However, the optimal residual moisture content for long-term stability can vary for different proteins and formulations^{70,71} and even “over-drying” has been discussed⁷²⁻⁷⁴.

Due to the relatively high residual moisture content at the beginning of secondary drying and, thus, low glass transition temperature, the risk for collapse during the initial heat ramp is increased. To prevent the cake from (partial) collapsing, a rather slow temperature ramp should be applied. In general, the efficacy of secondary drying is a function of the shelf temperature and to a lesser extent of the duration and chamber pressure.⁷⁵ Franks⁶⁸ suggests that the secondary drying is based on diffusion rather than desorption shown by the non-linear drying kinetics seen for Ficoll glass films at different isothermal drying profiles. Hence, the achievable water content at a given temperature is rate limited leading to the general recommendation to run a high shelf temperature for a short time.

Besides the shelf temperature, the residual moisture content is only dependent on the specific surface area which in turn is indirectly proportional to the pore size and, hence, can be directly proportional to the degree of supercooling.⁶⁸

I.3 Emerging developments in the field of freeze-drying

An exhaustive and comprehensive overview of all emerging developments related to freeze-drying is out of the scope of this introduction. However, some selected innovations in the field of pharmaceutical freeze-drying that reached at least prototype status or represent an evolution in the author's view should be highlighted in the following.

I.3.1 Spray freeze-drying

Spray freeze-drying (SFD) represents the combination of spray-drying and freeze-drying. The process comprises three stages which are (1) the atomization of a liquid to generate droplets, (2) the fast freezing of the generated droplets under cryogenic conditions and, (3) the removal of solvent from the frozen bulk pellets employing freeze-drying.^{13,76} The application of SFD may have several benefits over conventional freeze-drying (CFD) like the generation of a porous (sterile) bulk material, improved reconstitution behavior of the product, significantly reduced process times due to improved heat and mass transfer, potential flexibility in dosing and easy to achieve combination products (e.g. for protein co-formulations with contradicting stability profiles or different antigens within one vaccine) by dosing of different bulk powders in one vial and the potential for a (semi)continuous process.^{13,76-79} However, potential downsides could be the generation of a high specific surface area of the bulk powder. The degradation rate in a solid state of human growth hormone was correlated to the protein quantity on the air-solid interface by Xu et al.⁸⁰ Other potential pitfalls could be related to the implementation in a GMP environment, to the challenging process design^{77,78}, additional space demand in height due to the length of the freezing tower, sufficiently free-flowing of the bulk powder, electrostatic charging and accurate filling of the pellets in the final primary container.

I.3.2 Microwave-assisted freeze-drying

Microwave-assisted freeze-drying (MFD) refers to the use of dielectric heating, i.e. the application of microwaves to the frozen good. Durance et al.¹³ describe the process to comprise of freezing at ambient pressure, primary and secondary drying under vacuum; therefore, identical to the CFD at first glance. However, sublimation and desorption are mainly a result of the heat supplied by microwave power. Important to note is that microwaves as electromagnetic waves itself interact with the material, but do not inherently

possess heat to be transferred to the good. More detailed information on the physics of microwaves is given in Chapter II and Chapter III. The application of MFD may have several benefits over conventional freeze-drying like the significant reduction of drying time⁸¹, lower operating costs due to decreased energy consumption, higher throughputs¹³, volumetric heating of the entire sample⁸², the potential for (semi)continuous processing. However, there are several challenges reported for MFD, e.g. larger heterogeneity due to non-uniformity of the electromagnetic field⁸¹⁻⁸⁵, selective heating of single formulation components⁸⁶, challenging equipment and process design for pharmaceutical applications and occurrence of arcing leading potentially to product loss^{13,82}.

I.3.3 Continuous freeze-drying

Bearing in mind that one major disadvantage of the conventional freeze-drying is the limitation to the batch mode, continuous freeze-drying could potentially be a huge evolution in the pharmaceutical manufacturing of solid dosage forms for parenteral administration. The general advantages of a continuous mode over the classic batch-mode comprise operation flexibility, reduced or no scale-up challenges, real-time quality assurance, reductions in footprint, investment, and operative costs.⁸⁷ Pisano et al.⁸⁸ summarized in particular the advantages a continuous freeze-drying process could have, covering operational aspects (e.g. downtimes, batch-to-batch variability) and scale-up aspects (e.g. equipment change, differences in the process caused by equipment/environment).

Two approaches that work with unit-doses shall be presented briefly:

- (1) The spin freezing and subsequent infrared drying concept was first described by Corver with a patent filing in 2012.⁸⁹ Since then, several reports described the procedure in detail.⁹⁰⁻⁹⁴ The process comprises a continuous spin freezing creating a thin frozen product layer spread homogeneously over the inner vial surface followed by a subsequent continuous radiative drying by the employment of infrared radiation to the vial on a moving belt under vacuum. The main advantage of this approach is the continuous processing of unit doses in a rather short time as freezing and particularly drying are faster compared to CFD. Moreover, a 100% process control through process analytical tools like near-infrared spectroscopy is feasible. However, the development of mechanistic models to calculate maximum allowable energy

transfer to the frozen product layer and to enable prediction of process behavior is still needed.⁹⁵ Moreover, the essentially new process and concomitant new appearance of the final dried drug product needs a change in thinking at drug product manufacturers, regulatory agencies, and health care professionals.

- (2) The suspended-vial configuration concept by Capozzi, Pisano, and Trout was first introduced in 2019⁹⁶. In contrast to the spin freezing approach by Corver et al., the suspended-vial configuration appears like a continuously thought conventional freeze-drying, meaning that continuation of the process should be achieved by the introduction of a track system along different separated (vacuum) chambers that are dedicated to a different operation. Nevertheless, the inclusion of a method to apply controlled ice nucleation (vacuum-induced surface freezing) during freezing as well as the employment of radiative heating rather than conductive/convective heating seems to be a promising approach for the future. However, until now, the concept is only of theoretical nature and based on preliminary data from a batch-mode with no proof of concept for the continuously operating plant.⁹⁶

The reader interested in more detailed information about continuous manufacturing in lyophilization is referred to the review by Pisano et al.⁸⁸.

I.4 Aim and outline of the thesis

Over the last years, serious interest in emerging next-generation freeze-drying technologies raised. One promising technology that stands out due to its proven benefits in food technology is microwave-assisted freeze-drying (MFD). As briefly outlined in section I.3.2, MFD has the potential to overcome drawbacks like long drying-times due to its volumetric heating of the entire sample.

However, little is known of its feasibility for pharmaceutical applications, particularly in the field of sensitive biologicals. For this reason, the first part of this thesis, **Chapter II** and **Chapter III**, is dealing with the investigation of vial-based microwave-assisted freeze-drying concerning the applicability to standard lyophilization formulations and effects on protein stability.

In **Chapter II**, the applicability and feasibility of this technology to different monoclonal antibody formulations and the influence on the resulting product properties are subject to investigation. Moreover, the potential for drying time savings is examined.

The product quality of four different pharmaceutically relevant monoclonal antibody formulations over storage and the influence of the microwave generator on batch homogeneity are studied in **Chapter III**.

The second part of this work, **Chapter IV – Chapter VI**, is dedicated to detailed investigations on open questions in controlled ice nucleation (CN) in the field of freeze-drying of biologicals. Although there have been multiple publications, reports and case studies about CN over the last two decades, experts in the freeze-drying community are still lacking essential information on aspects of comparability of different controlled ice nucleation techniques, general good practice of process design and how to monitor the nucleation success of a whole batch non-destructively.

In **Chapter IV**, a case study of three relevant model formulations is presented which aims to investigate if mechanistically different controlled ice nucleation techniques in freeze-drying are comparable to each other concerning drying process performance and product quality attributes.

A study analyzing factors that affect the success of CN and questions of process design are studied and discussed in **Chapter V**.

In **Chapter VI** a new technological solution for control of the nucleation success using a camera-based approach is presented in a proof of concept study.

Chapter VII summarizes and concludes the results of the present thesis and gives an outlook.

Chapter II Significant drying time reduction using microwave-assisted freeze-drying for a monoclonal antibody

This chapter is published as:

Gitter, J. H.¹, Geidobler, R.², Presser, I.² & Winter, G.¹. Significant Drying Time Reduction Using Microwave-Assisted Freeze-Drying for a Monoclonal Antibody. *J. Pharm. Sci.* 107, 2538–2543 (2018).

¹ Ludwig-Maximilians-Universität München, Department of Pharmacy, Pharmaceutical Technology and Biopharmaceutics, Butenandstr. 5, 81377 Munich, Germany

² Boehringer Ingelheim Pharma GmbH & Co. KG, Birkendorfer Str. 65, 88307 Biberach an der Riß, Germany

Author contributions:

Conceptual guidance, I.P. and G.W.; Data curation, J.H.G.; Formal analysis, J.H.G.; Investigation, J.H.G.; Methodology, J.H.G.; Project administration, J.H.G., R.G., I.P. and G.W.; Resources, R.G., I.P., and G.W.; Supervision, R.G., I.P., and G.W.; Visualization, J.H.G.; Writing—Original draft, J.H.G.; Writing—Review & editing, R.G., I.P., and G.W.

Note from the author:

The version included in this thesis is identical to the published article apart from minor changes. The reference, figure, and table numbers were changed to fit into the coherent numbering of this document.

The published article can be accessed online via:

<https://doi.org/10.1016/j.xphs.2018.05.023>

II.1 Abstract

Microwave-assisted freeze-drying is a rapid drying process well-known in food technology. However, little is known about its application to biologicals. In this study, we investigated the applicability and feasibility of this technology to different monoclonal antibody formulations and the influence on the resulting product properties. Moreover, one of our main objectives was to study if significant reductions in drying times could be achieved. Additionally, the effect of the drying process on the accelerated stability of a sucrose-based antibody formulation at 40 °C and 25 °C over 12 weeks was investigated. Microwave-assisted freeze-drying resulted in drying time reduction > 75 %. For all model formulations, cake appearance and solid state properties were found to be comparable to standard lyophilized products. These formulations covered a wider range of lyophilization excipients comprising sucrose and trehalose, semi-crystalline forming solids like mannitol:sucrose-mixtures and others like arginine phosphate and a mixture of HP- β -CD with sucrose. Moreover, comparable low changes in relative monomer content, the relative amount of soluble aggregates, and cumulative particles $\geq 1\mu\text{m}$ per mL were observed over 12 weeks of storage, regardless of the drying technology. This makes MFD a promising innovative alternative for the rapid production of freeze-dried biologicals while maintaining product quality.

Keywords

Freeze-drying/lyophilization; Lyophilization; Drying; Proteins; Stability; Excipients; Solid state; Monoclonal antibody; Glass

Abbreviations

API	Active pharmaceutical ingredient
BET	Brunauer–Emmet–Teller Krypton gas adsorption
CFD	Conventional freeze-drying
HMW	High molecular weight species
HPW	Highly purified water
HP- β -CD	2-Hydroxypropyl- β -cyclodextrin
LMW	Low molecular weight species
mAb	Monoclonal antibody
MFD	Microwave-assisted freeze-drying
MW	Microwave
MWCO	Molecular weight cut-off
PES	Polyethersulfone
rM	Residual moisture content
SEC	Size exclusion chromatography
SSA	Specific Surface Area
XRD	X-ray diffraction

II.2 Introduction

Long process times are a typical shortcoming of conventional freeze-drying (CFD).^{97,98} One approach to reduce drying time is microwave-assisted freeze-drying (MFD) which is a well-known process in food technology for high-value goods needing significantly shorter process times while maintaining the overall quality of the product, i.e. color, taste, texture, shape.^{99–101} Especially in the field of food processing, microwave radiation has versatile applications like cooking, drying, or preservation of food products.⁸⁴ Due to its ability to allow for a rapid heat transfer and because of the volumetric and selective heating of dielectric material, it has major advantages over other conventional drying techniques. In contrast to heating via convection or conduction, microwaves as electromagnetic waves directly interact with dielectric materials such as permanent dipoles, e.g. water or disaccharides, or ions, e.g. buffer salts.⁸² In particular, drying at the typical industrial frequency of 2.45 GHz is mainly driven by the interaction of permanent dipoles and microwaves.¹⁰² The capability of a material to absorb microwaves and thereby to convert electric field energy into thermal energy by molecular interactions with the electromagnetic field is characterized by the frequency-depending absolute complex permittivity.¹⁰³ More detailed information on the physical principles of microwave heating can be found elsewhere^{82,84,103,104}. As typical lyophilization formulations used for biologicals are based on aqueous systems containing polar stabilizers, e.g. sucrose or trehalose, buffer salts, and the API,⁷ suitability for a microwave-assisted drying process is likely. Therefore, MFD also raised interest in pharmaceutical applications recently. As reported by Robert Evans at the CPPR conference in 2014, microwave-assisted drying could be applied to both monoclonal antibody and vaccine formulations.¹⁰⁵ In preliminary data, they found similar aggregation rates as obtained by HP-SEC for two monoclonal antibodies and no severe loss in antigen potency for different vaccine formulations. Based on that an international patent is pending, claiming the formulation and production of thermostable dried vaccine formulations using microwave vacuum drying.¹⁰⁶ The inventors claim for shortened drying processes by MFD. However, high sugar concentrations of 17.5 % (w/w) up to 60 % (w/w) in combination with vaccines were investigated. Therefore, our aim is to have a closer look at the applicability of MFD to various pharmaceutically relevant formulations of a monoclonal antibody with a different experimental setup. In this article, we show the successful implementation of MFD for excipient concentrations of 10% (w/v) or 1% (w/v). Additionally, the main focus will be on maintenance of product quality while shortening the drying time significantly. Moreover,

we study the accelerated stability of a sucrose-based IgG antibody formulation over three months either produced by CFD or MFD.

II.3 Materials and methods

II.3.1 Materials

A monoclonal IgG type 1 antibody (mAb) was kindly provided by Boehringer Ingelheim Pharma GmbH & Co. KG (Ingelheim am Rhein, Germany).

D(+)-Sucrose and L-Arginine were purchased from Sigma-Aldrich (Steinheim, Germany). D(+)-Trehalose dihydrate and D(-)-Mannitol were obtained from VWR International BVBA (Leuven, Belgium). 2-Hydroxypropyl- β -cyclodextrin (HP- β -CD) (Cavasol® W7 HP, Wacker Chemie AG, Burghausen, Germany) was a kind gift of PARI GmbH (Starnberg, Germany). L-Histidine monohydrochloride monohydrate and L-Histidine were purchased from Alfa Aesar (Karlsruhe, Germany). Di-sodium hydrogen phosphate dihydrate and sodium dihydrogen phosphate dihydrate were obtained from AppliChem (Darmstadt, Germany). Sodium chloride was purchased from Bernd Kraft (Duisburg, Germany). Tween 80®, ortho-Phosphoric acid, and sodium hydroxide were obtained from Merck KGaA (Darmstadt, Germany). For the preparation of buffers and stock solutions, highly purified water (HPW; Purelab Plus, USF Elga, Germany) was used.

All excipients had at least analytical grade and were used without further purification.

II.3.2 Preparation of formulations

The mAb was concentrated prior to dialysis by using Vivaspin 20 with PES membrane (MWCO 30,000 Da; Sartorius AG, Goettingen, Germany) and then subsequently dialyzed for 24h using dialysis membranes Spectra/Por® (MWCO 6000 – 8000 Da; Spectrum Laboratories Inc., Compton, CA, USA). After the dialysis concentration of mAb was measured with a NanoDrop™ 2000 UV photometer (Thermo Scientific, Wilmington, Delaware) at 280 nm using an extinction coefficient of $\epsilon^{0.1\%} = 1.49 \text{ g/100 mL}^{-1} \text{ cm}^{-1}$. For the preparation of the final formulations, excipient stock solutions ranging from 1 % to 25 % (w/v) prepared in 10 mM Histidine buffer (pH 6.0) were mixed with the dialyzed mAb solution in 10 mM Histidine buffer (pH 6.0) in a way that final formulations contained either 3 or 5 g/L mAb, 0.02 % (w/v) tween 80® and either 10 % (w/v) sucrose or trehalose or HP- β -CD:sucrose 1:1 or mannitol:sucrose 4:1. For the low stabilizer containing formulation the same procedure was applied but ending up with a lower final sucrose concentration of 1%

(*w/v*), 3 g/L mAb, and 0.02 % (*w/v*) tween 80®. The arginine phosphate formulation contained 10 % (*w/v*) of arginine phosphate to which 5 g/L of mAb dialyzed in 10 mM arginine phosphate (pH 6.0) and 0.02 % (*w/v*) tween 80® prepared in 10 mM arginine phosphate (pH 6.0) were added. A tabular overview of the used formulations could be found in the supplementary data (Table SII-1). The formulation for the accelerated stability study contained 5 g/L mAb and 10 % (*w/v*) sucrose as mentioned above. All formulations were filtered using 0.2 µm Cellulose Acetate Membrane syringe filters (VWR International, Radnor, PA, USA) prior to filling of the vials. 2.3 mL of each formulation was filled in 10R tubing vials (MGlas AG, Muennerstadt, Germany) and semi-stoppered with lyophilization stoppers (FluroTec® rubber stopper, West Pharmaceuticals, Eschweiler, Germany). The vial population for conventional freeze-drying was arranged on a lyophilization tray and surrounded with one row of 10 % (*w/v*) sucrose shielding vials.

II.3.3 Freeze-drying process

All samples were frozen in the same freezing step using a Christ ε2-6D laboratory-scale freeze-dryer (Martin Christ, Osterode am Harz, Germany) with equilibration at -5 °C for 1 h followed by ramping down the shelf with 1 K/min to -60 °C set point. The frozen samples were subjected to one of the following drying protocols:

II.3.3.1 Conventional freeze-drying (CFD)

Primary Drying was carried out at a pressure of 0.1 mbar and a shelf temperature of -20 °C. T-type thermocouples were used to determine primary drying time. Secondary drying was carried out at 0.05 mbar applying a 0.05 K/min ramp to 0 °C and subsequently, a ramp of 0.2 K/min to 20 °C which was held for 6h. After completion of the drying, samples were stoppered at approximately 600 mbar in a nitrogen atmosphere and kept refrigerated until analysis.

II.3.3.2 Microwave-assisted freeze-drying (MFD)

Drying was conducted on a modified laboratory-scale Püschner µWaveVac 0250fd vacuum dryer (Püschner GmbH + Co KG, Schwanewede, Germany) ^{107,108} equipped with a 2 kW/2450 MHz magnetron, a condenser (-80 °C) and a vacuum system comprising a root pump and a rotary vane pump. The tuner, which was located between the magnetron and water load, was adjusted that way that approximately 1/10 of the generated microwaves went

into the product chamber. Frozen samples, which were frozen as described above and which were transported on dry ice, were loaded on the pre-cooled rotating sample tray. Drying was carried out at a pressure of 0.008 to 0.03 mbar as measured by Pirani gauge and at a radiated microwave power between 20 W to 110 W as measured by a HOMER™ impedance analyzer (S-TEAM Lab, Bratislava, Slovak Republic) until a constant mass was reached. For process monitoring a glass fiber temperature measurement probe (TS2, Weidmann Technologies Deutschland GmbH, Dresden, Germany) and a balance to determine total weight loss were used. Samples were stoppered externally in a glove bag flushed with dry nitrogen and kept refrigerated until analysis.

II.3.4 Residual moisture content

Karl Fischer titration was used to determine residual water content after freeze-drying. Between 10 and 30 mg of sample aliquots were prepared in a glove box filled with pressurized air with a relative humidity of less than 10%, filled into 2R Vials and stoppered. The samples were then placed in an oven with 100 °C to enable the fast extraction of water. The headspace moisture is transported into a coulometric Karl Fischer titrator (Aqua 40.00, Elektrochemie Halle, Halle (Saale), Germany). Results are calculated in relative water content (*w/w*).

II.3.5 Specific surface area

The specific surface area of dried samples was determined using Brunauer–Emmet–Teller (BET) krypton gas adsorption in a liquid nitrogen bath at 77.3 K (Autosorb 1; Quantachrome, Odelzhausen, Germany). Approximately 80 – 140 mg of a sample was gently crushed with a spatula and weighed into glass tubes. Prior to measurement, an outgassing step was performed for at least 6 h at room temperature. A 9-point gas adsorption curve was measured, covering a p/p_0 ratio of approximately 0.05– 0.25. Data evaluation was performed according to the multipoint BET method fit of the Autosorb 1 software.

II.3.6 X-ray powder diffraction

To determine the solid state of the lyophilizates an XRD 3000 TT diffractometer (Seifert, Ahrensburg, Germany) was used. The device is equipped with a copper anode (40 kV, 30 mA) and has a wavelength of 0.154178 nm. The scintillation detector voltage was 1000 V.

The samples were placed on the copper sample holder and analyzed in the range of 5-45 ° 2-theta with steps of 0.05° 2-theta.

II.3.7 Reconstitution of lyophilizates

The lyophilized cakes were reconstituted by the addition of HPW. The HPW volume for each formulation was calculated to match the volume of the water removed during freeze-drying.

II.3.8 High-performance size exclusion chromatography (HP-SEC)

To determine relative monomer content and the relative amount of soluble aggregates HP-SEC was used. The separation was performed on a Waters 2695 Separation module (Waters GmbH, Eschborn, Germany) with a Tosoh TSKgel G3000 SWxl column (Tosoh Bioscience, Griesheim, Germany) using a Waters 2487 Dual λ Absorbance Detector (Waters GmbH, Eschborn, Germany) at 214 and 280 nm. 10 μ L of reconstituted formulation with a final concentration of either 3 or 5 g/L was injected and separated using a 50 mM PBS running buffer containing 300 mM sodium chloride (pH 7.0) with a flow rate of 0.7 mL/min. Samples were measured as triplicates with three individual injections. Data integration of relative areas was performed using Chromeleon 6.80 (Thermo Scientific, Wilmington, USA).

II.3.9 Light Obscuration

Subvisible particles were determined using a PAMAS SVSS-35 particle counter (PAMAS - Partikelmess- und Analysesysteme GmbH, Rutesheim, Germany) equipped with an HCB-LD- 25/25 sensor which has a detection limit of approximately 120,000 particles $\geq 1 \mu$ m per mL. The rinsing volume was 0.5 mL and was followed by three measurements of 0.3 mL. Before and between samples the system was rinsed with HPW until less than 30 particles/mL $\geq 1 \mu$ m and no particles larger than 10 μ m were present. Data collection was done using PAMAS PMA software and particle diameters in the range of $\geq 1 \mu$ m to 200 μ m were determined. All results are given in cumulative particles per milliliter.

II.3.10 Turbidity

The turbidity of samples was measured as scattered laser light ($\lambda = 860$ nm) detected at an angle of 90 ° using a Hach Lange Nephla nephelometer (Hach Lange GmbH, Düsseldorf,

Germany). 2.0 mL sample was gently pipetted in turbidity glass cuvettes free of particles with a flat bottom and placed into the device. The result is given in FNU (Formazine nephelometric units).

II.4 Results and discussion

II.4.1 Applicability to different formulations

II.4.1.1 Cake appearance

With both microwave-assisted and conventional freeze-drying elegant and look-alike cakes could be produced (Figure II-1). Only for the low concentration stabilizer formulation with 1% (*w/v*) sucrose (Figure II-1, b) and the ionic arginine phosphate-formulation (Figure II-1, f) shrinkage of the cake was observable in both processes.



Figure II-1 Representative photographs of differently dried formulations. Small letters represent the excipient used: **a** 10% sucrose, **b** 1% sucrose, **c** 10% trehalose, **d** 10% mannitol:sucrose 4:1, **e** 10% HP- β -CD:sucrose 1:1, **f** arginine phosphate. **Top picture**: CFD-products; **Bottom picture**: MFD-samples. The asterisk indicates that these formulations contained 5 g/L mAb and were dried in a separate but similar run to the one shown in Figure II-2.

II.4.1.2 Process time reduction

Microwave-assisted freeze-drying resulted in a significantly shorter drying process as shown in Figure II-2. The conventional process (Figure II-2, A) was finished after approximately 77h. Since primary drying was kept longer to allow for complete sublimation in all investigated formulations, the actual drying time in CFD could, therefore, be reduced by about 18h. Additionally, the 16h for the freezing step should be kept out of consideration since both CFD and MFD samples underwent the same freezing procedure. Consequently, the adjusted total drying time, i.e. primary and secondary drying time, for the conventional drying is estimated to be approximately 43h (Figure II-2, A curly brackets b+c). In contrast, the drying procedure using MFD (Figure II-2, B) yielded in a total drying time of nearly 10h, which is a reduction of 77 % in overall drying time. Even though a standardized non-optimized conventional freeze-drying cycle was used, still differences in a large order of magnitude were achieved for the process time reduction using microwave-assisted freeze-drying.

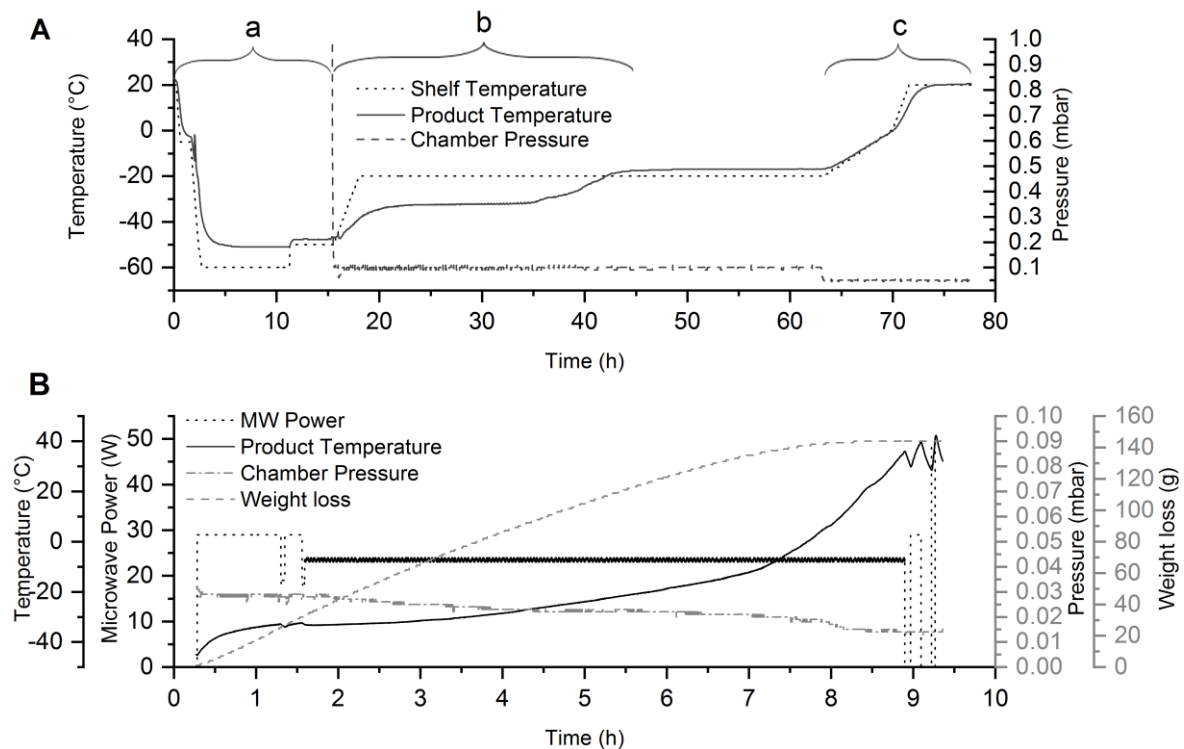


Figure II-2 A Thermocouple and pressure readouts of the conventional freeze-drying cycle. Shelf temperature setpoint is represented by the dotted line, thermocouple readout is depicted with a solid line. The coarse dotted line represents the chamber pressure setpoint. Curly bracket **a** tags the freezing step which is the same for both batches, whereas curly brackets **b** and **c** represent the actual drying time of primary and secondary drying. **B** Glass fiber (solid line), chamber pressure (dash dot-line), microwave power (dotted line), and balance readings (dashed line) of the MFD-cycle. Product temperature measurement was performed in either case in the 10 % sucrose formulation.

II.4.1.3 Residual moisture and specific surface area

For both drying technologies, low residual moisture content was found independent of the excipient system (Figure II-3, A, bars). Only the arginine phosphate formulation showed higher residual moisture of 2.3 % (*w/w*) after MFD. This could be related to the smaller specific surface area which indicates a micro-collapse compared to the conventionally dried product (Figure II-3, A, symbols). Overall, MFD products exhibited low residual moisture contents while the lyophilization-specific porous cake structure represented by the specific surface area was maintained. For some of the MFD samples, a higher variance could be determined, especially in the low concentration sucrose formulation, the 10 % trehalose, and arginine phosphate formulation. This was also observable in a 100 % analysis for solid state properties of a full batch of a sucrose-based formulation produced by MFD (Supplementary Data, Figure SII-1). It is assumed that this is on the one hand caused by the indirect setup of the magnetron to the product chamber via a water load which could favor an inhomogeneous field distribution. On the other hand, the sample handling in the used MFD laboratory setup was not yet optimal. This is due to the fact, that the first samples were frozen externally and kept deep-frozen until processing and second that dried samples were stoppered externally in a dry nitrogen-flushed glove bag.

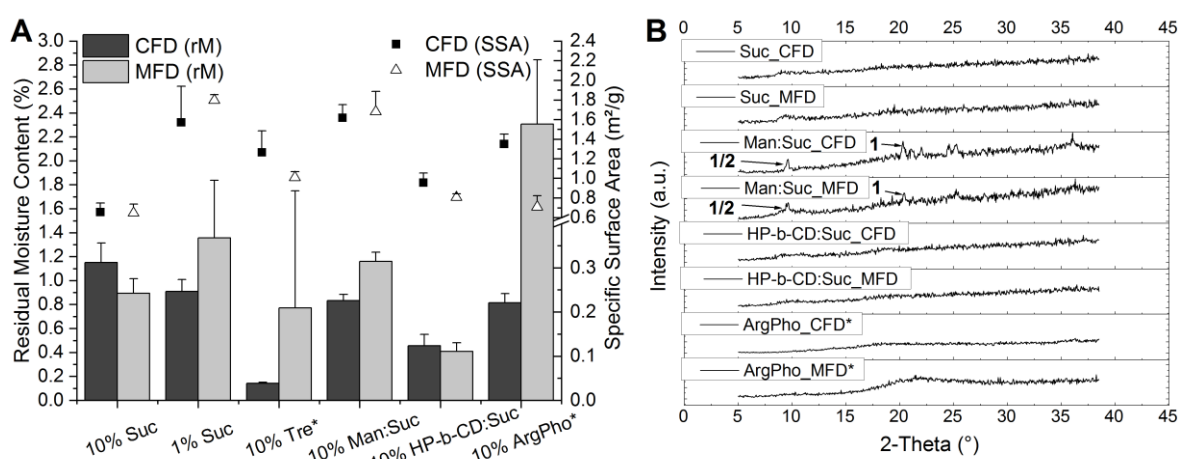


Figure II-3 **A** Residual moisture content (bars) and specific surface area (symbols) for all six formulations and the two respective drying protocols (black: conventional freeze-drying; light grey/white triangles: microwave-assisted freeze-drying). **B** X-ray diffractograms of exemplary formulations. Abbreviations stand for: Suc – 10 % sucrose, Man:Suc – 10 % mannitol:sucrose 4:1-mixture, HP-b-CD:Suc – 10 % HP- β -CD:sucrose 1:1-mixture, ArgPho – 10 % arginine phosphate. **1** represents δ -Mannitol peaks at 9.7° and 20.4°; **2** indicates the overlapping peak of mannitol hemihydrate at 9.6°. Characteristic 2-theta values have been taken from the literature¹⁰⁹. The asterisk indicates that these formulations contained 5 g/L mAb and were dried in a separate but similar run to the one shown in Figure II-2. The shown values represent the mean of measurements from three different vials. Error bars indicate the standard deviation of the mean.

II.4.1.4 XRD

Regardless of the drying approach, the same solid state was found for all formulations as determined by XRD (Figure II-3, B) and confirmed by DSC (Supplementary Data, Figure SII-2). Only mannitol:sucrose 4:1 formulations showed a semi-crystalline structure indicating mainly the formation of δ -Mannitol by characteristic peaks at 9.7°, 20.4°, and 24.6° (Figure II-3, B, arrow 1). A detailed comparison of XRD diffractograms for this formulation is shown in the supplementary data (Figure SII-3). Indications for the formation of mannitol hemihydrate (Figure II-3, B, arrow 2) were found. The crystal modification of mannitol hemihydrate is unfavored due to its destabilizing effect on the dried product.^{109,110} However, it was found to be present in conventionally and microwave-assisted FD samples. The application of a thermal treatment will be taken into consideration to crystallize mannitol in its favored anhydrous crystalline modifications. All other formulations, independent of the drying approach were found to be fully amorphous.

II.4.2 Accelerated stability study

In order to see the influence of the respective drying method on protein stability, a 10% sucrose formulation with 5 g/L mAb produced either by CFD or MFD was stored at 25 °C and 40 °C for 12 weeks. The drying processes which were adjusted to the formulation took 41h 5min and 10h 15min for CFD and MFD, respectively. Although the microwave-assisted drying procedure decreased drying times by 75 %, residual moisture contents after freeze-drying were determined to be similar as 1.1 ± 0.13 % for CFD and 1.0 ± 0.5 % for MFD samples. Over 12 weeks of storage no changes in solid state properties as specific surface area, residual moisture content, glass transition temperature, and solid state were observable (data not shown). Concerning relative monomer content (Figure II-4, A) and the relative amount of soluble species (Figure II-4, B, C) no changes were observed over 12 weeks of storage for both CFD and MFD even at 40 °C. This is confirmed by cumulative subvisible particle counts (Figure II-4, D symbols) and turbidity (Figure II-4, D bars) which show no clear trend and stay at comparably low levels over storage time.

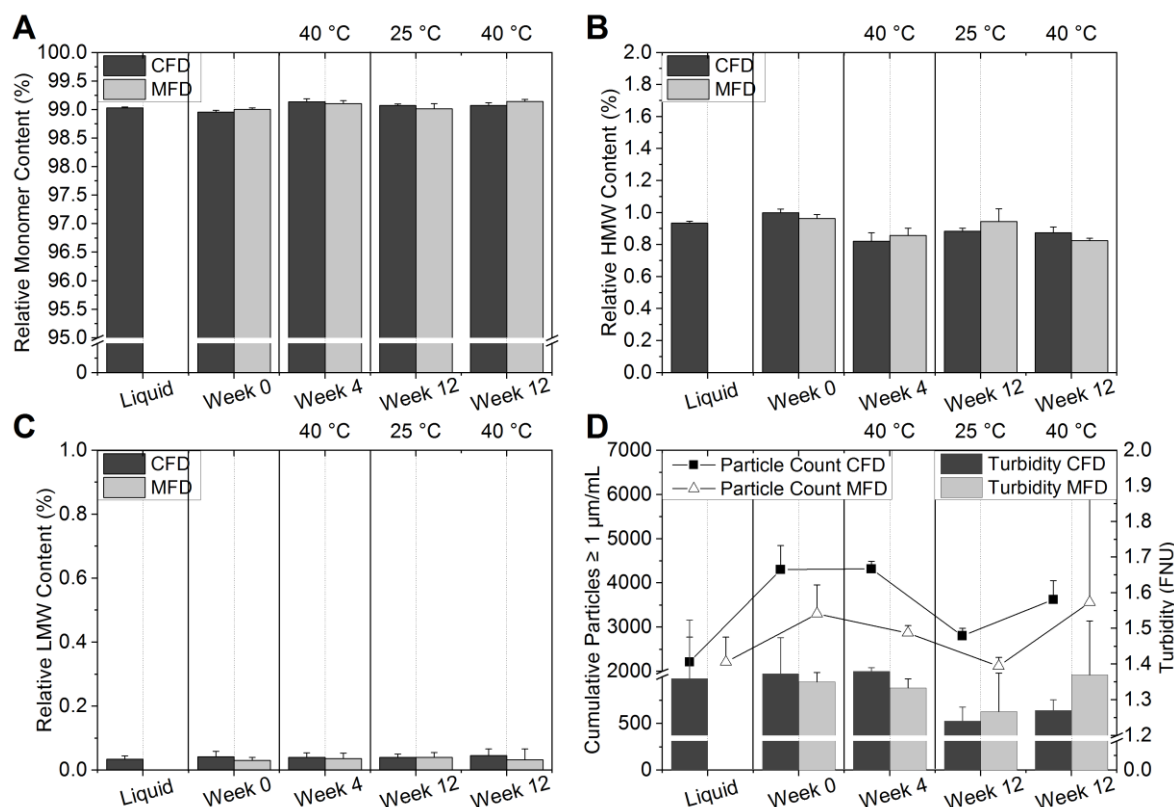


Figure II-4 **A** Relative monomer content of a sucrose-based mAb formulation stored for 12 weeks as determined by HP-SEC; **B** and **C** represent the soluble high molecular weight and low molecular weight species, respectively. **D** Development of cumulative particles $\geq 1 \mu\text{m/mL}$ (symbols) and turbidity (bars) over 12 weeks. The shown values represent the mean of measurements from 3 different vials. Error bars indicate the standard deviation of the mean.

II.5 Conclusion and outlook

With this study, we can confirm that microwave-assisted freeze-drying is able to shorten the freeze-drying process by more than 75 %. Moreover, it is applicable to various relevant antibody formulations while obtaining elegant look-alike cakes and similar solid state properties. The ionic stabilizer system arginine phosphate showed a higher variance in solid state properties and therefore needs to be studied further. Yet, our results show that after 12 weeks of accelerated stability study no differences between conventionally and microwave-assisted freeze-dried products were observable. Neither in solid state properties nor protein-related properties like soluble aggregates and subvisible particles differences occurred for a sucrose-based antibody formulation at two different accelerated storage temperatures. It should be noted, that alternative setups are currently under development since MFD processes are more difficult to control compared to conventional freeze-drying processes. Additionally, typical challenges related to the application of microwaves in freeze-drying

processes should be taken into account like the potential emergence of cold plasma and the potential induction of batch inhomogeneity due to cold and hot spots.

However, microwave-assisted freeze-drying has the potential to become a highly promising alternative to the conventional approach. We were able to confirm its potential to significantly shorten drying times while maintaining product quality, which would be also the main requirement for continuous processing. This, in fact, makes MFD a promising concept for continuous pharmaceutical freeze-drying in the future.

Acknowledgments

The support from the Global Technology Management from Boehringer Ingelheim is kindly acknowledged. In addition, the authors thank Peter Püschner, Michael Eggers, and Mirko Diers from Püschner GmbH + Co KG for the technical support with the microwave vacuum dryer.

II.6 Supplementary material

II.6.1 Materials and methods

II.6.1.1 Modulated dynamic scanning calorimetry (Glass transition temperature)

The glass transition temperature of the lyophilizates was measured using a Mettler Toledo DSC 821e (Gießen, Germany) dynamic scanning calorimeter. Aliquots of 2 to 15 mg of dried lyophilized cake were compacted in an aluminum crucible and crimped in a glove box filled with pressurized air with a relative humidity of less than 10 %. A modulated DSC method heating from either 25 °C to 100 °C for sucrose or from 25 °C to 180 °C for all other formulations with a heating rate of 2 K/min, an amplitude of 1 °C and a period of 2 min was used in order to differentiate between reversed and non-reversed transitions. The glass transition temperature was evaluated from the reversed curve after a 100 point-smoothing operation as the inflection point of the glass transition using the Mettler StarE Software.

II.6.1.2 Preparation of formulations

Table SII-1 Overview of the different investigated formulations.

Formulation	mAb [g/L]	Sucrose [% (w/v)]	Trehalose [% (w/v)]	Mannitol [% (w/v)]	HP-β-CD [% (w/v)]	Arginine phosphate [% (w/v)]	PS 80 [% (w/v)]
10 % Suc	3	10	-	-	-	-	0.02
1 % Suc	3	1	-	-	-	-	0.02
10 % Tre*	5	-	10	-	-	-	0.02
10 % Man:Suc	3	2	-	8	-	-	0.02
10 % HP-β-CD :Suc	3	5	-	-	5	-	0.02
10 % Arg-Pho*	5	-	-	-	-	10	0.02
10 % Suc Stability Study	5	10	-	-	-	-	0.02

All stock solutions used were prepared in 10 mM histidine buffer (pH 6.0) despite the arginine phosphate formulation. For this, all stock formulations were prepared in 10 mM arginine phosphate (pH 6.0). The same is valid for the respective mAb stock solution which was either dialyzed in the respective histidine or arginine phosphate solution at pH 6.0.

II.6.2 Results

II.6.2.1 Full Batch Homogeneity

One hundred percent of a sucrose-based formulation with 3 g/L mAb dried by MFD was analyzed for its solid state properties in order to assess batch homogeneity. For all vials, low residual moisture content could be achieved, although a higher scattering of individual values was found (Figure SII-1, A). One reason may be the wider range of specific surface areas observed (Figure SII-1, B). Another reason could be a potential inhomogeneous microwave field distribution with the setup used which may cause hot and cold spots during the drying procedure.

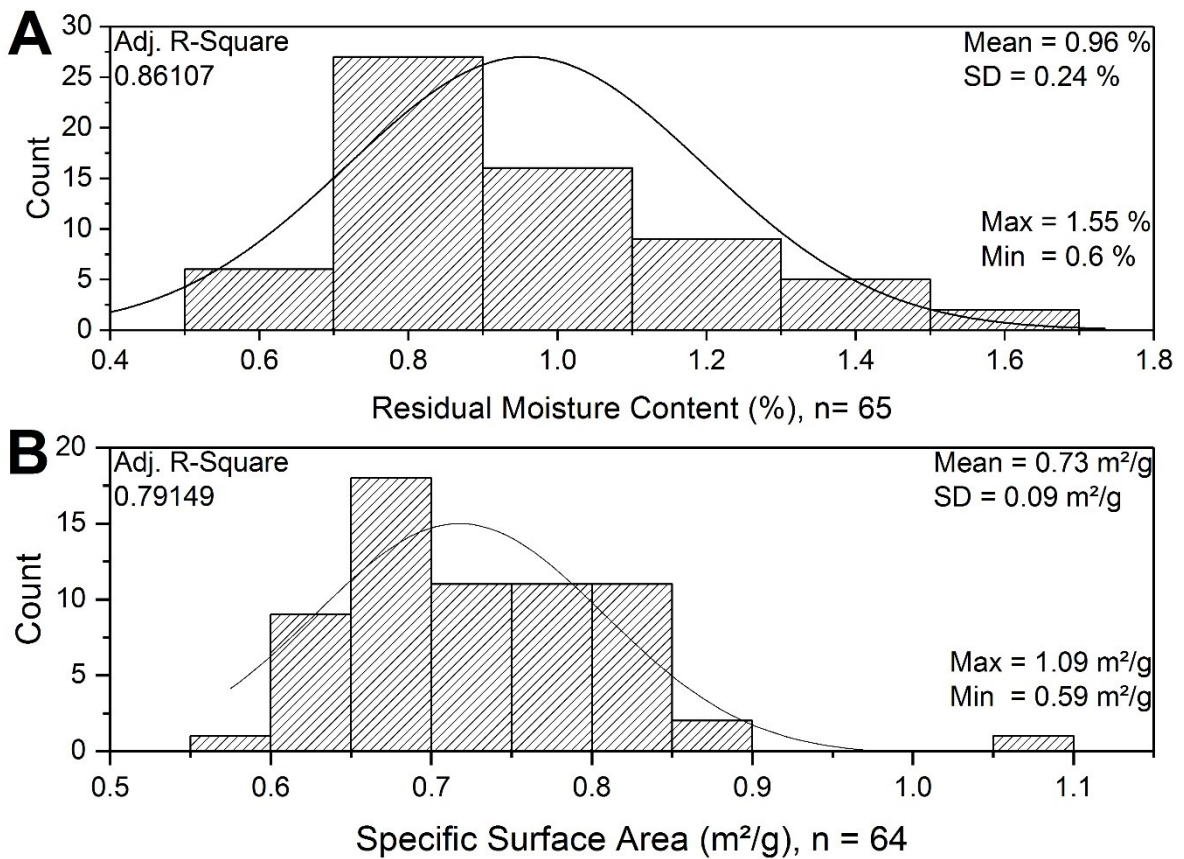


Figure SII-1 A Grouped distribution of residual moisture content of a full batch of a sucrose-based formulation with 3 g/L mAb as described in materials and methods produced by MFD, fitted to Gaussian distribution. **B** Grouped distribution of the specific surface area of the same batch as in A with a Gaussian fit. The drying process was similar to the one shown in Figure II-2.

II.6.2.2 DSC and solid state

DSC analysis confirmed the results obtained by XRD. In Figure SII-2, example thermograms of formulations containing either sucrose or trehalose or arginine phosphate which were produced by MFD are shown. No indication for crystalline proportions was found.

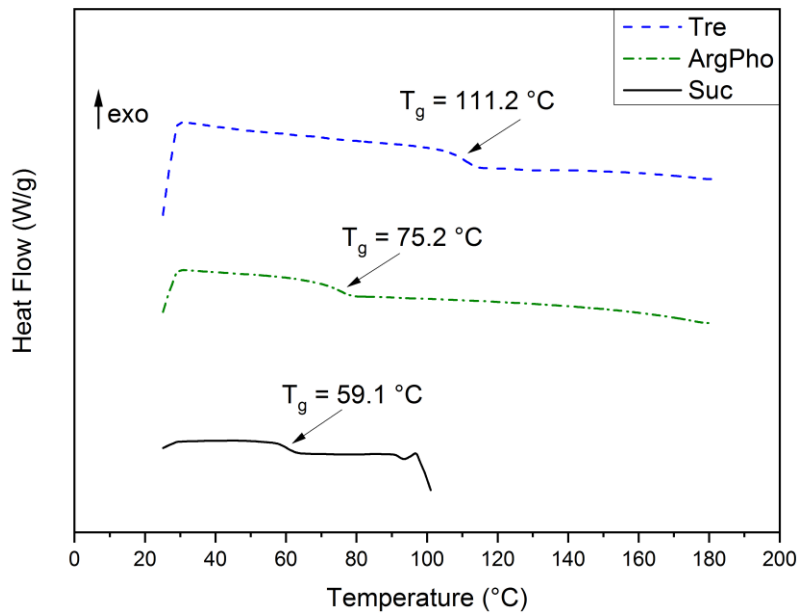


Figure SII-2 Example DSC thermograms that are complementary to Figure II-3B showing the reversed curves of microwave-assisted freeze-dried sucrose (Suc), trehalose* (Tre), and arginine phosphate* (ArgPho) formulations. The asterisk indicates that these formulations contained 5 g/L mAb and were dried in a separate but similar run to the one shown in Figure II-2.

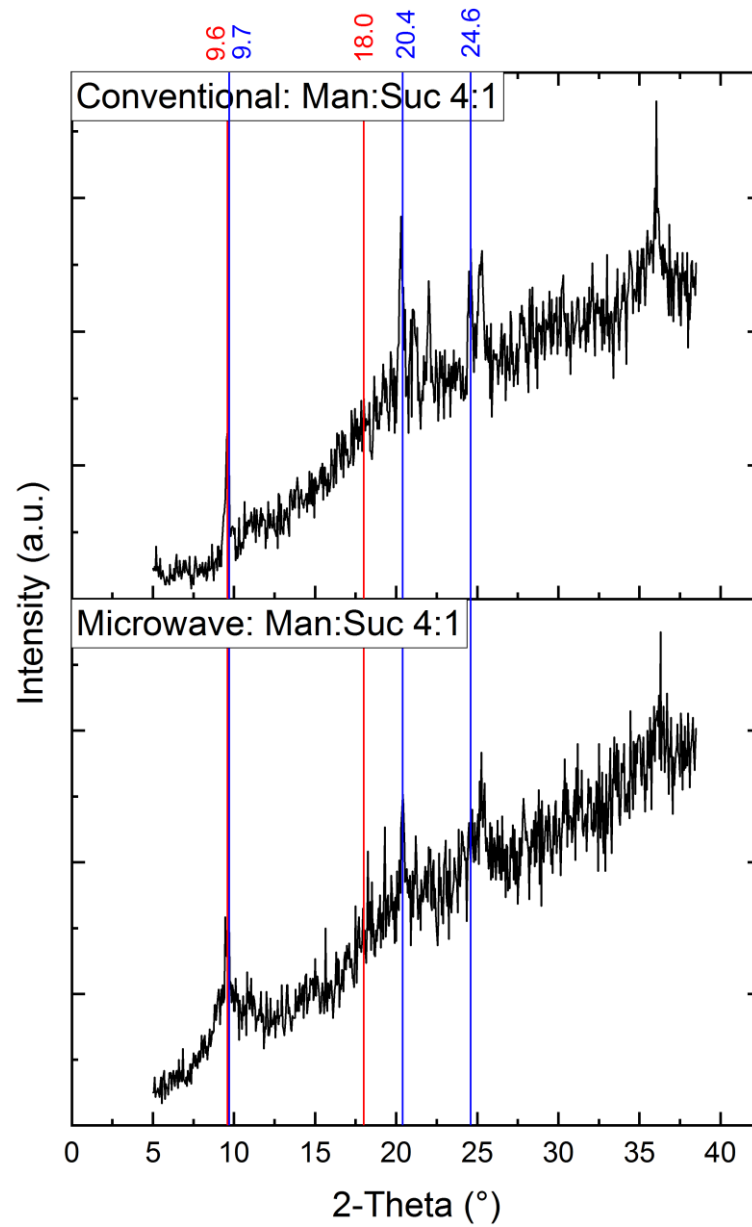


Figure SII-3 X-ray diffractograms of semi-crystalline mannitol:sucrose formulations for the respective drying protocol with characteristic peaks for δ -mannitol (blue) or mannitol hemihydrate (red) at 9.7°, 20.4°, and 24.6° or 9.6° and 18.0° 2-Theta, respectively.

Chapter III Microwave-assisted freeze-drying of monoclonal antibodies: product quality aspects and storage stability

This chapter is published as:

Gitter, J. H.¹, Geidobler, R.², Presser, I.² & Winter, G.¹ Microwave-Assisted Freeze-Drying of Monoclonal Antibodies: Product Quality Aspects and Storage Stability. *Pharmaceutics* 11, 674 (2019).

¹ Ludwig-Maximilians-Universität München, Department of Pharmacy, Pharmaceutical Technology and Biopharmaceutics, Butenandstr. 5, 81377 Munich, Germany

² Boehringer Ingelheim Pharma GmbH & Co. KG, Birkendorfer Str. 65, 88307 Biberach an der Riß, Germany

Author contributions:

Conceptual guidance, I.P. and G.W.; Data curation, J.H.G.; Formal analysis, J.H.G.; Funding acquisition, G.W.; Investigation, J.H.G.; Methodology, J.H.G.; Project administration, J.H.G., R.G., I.P. and G.W.; Resources, R.G., I.P., and G.W.; Supervision, R.G., I.P., and G.W.; Validation, J.H.G.; Visualization, J.H.G.; Writing—Original draft, J.H.G.; Writing—Review & editing, R.G., I.P., and G.W.

Note from the author:

This following version is identical to the published article in the special issue “Pharmaceutical Freeze Drying and Spray Drying” of *Pharmaceutics* apart from minor changes. The reference, figure, and table numbers were changed to fit into the coherent numbering of this document.

The published article can be accessed online via:

<https://doi.org/10.3390/pharmaceutics11120674>

III.1 Abstract

In order to overcome the downside of long conventional freeze-drying (CFD) process times for monoclonal antibody formulations, microwave-assisted freeze-drying (MFD) was introduced. Recently, the general applicability and potential shortening of drying times were shown. However, little is known about the storage stability of MFD products compared to CFD references. Additionally, batch homogeneity issues were seen within MFD in the past. In this study, we examined four different formulations of two different monoclonal antibodies using three different glass-forming excipients: sucrose, trehalose, and arginine phosphate. These formulations were freeze-dried with two different drying protocols (CFD and MFD), stored for 24 weeks, and analyzed for solid-state and protein-related quality attributes. Moreover, a new microwave generator setup was investigated for its potential to improve batch homogeneity. In all investigated formulations, comparable stability profiles were found, although the classical magnetron generator led to inferior batch homogeneity with respect to residual moisture distribution. In contrast, the new MFD setup indicated the potential to approximate batch homogeneity to the level of CFD. However, for future applications, there is an unabated need for new machine designs to comply with pharmaceutical manufacturing requirements.

Keywords

freeze-drying; lyophilization; drying; microwave; protein; monoclonal antibody; stability

Abbreviations

τ^{β}	Relaxation time (global mobility)
BET	Brunauer–Emmet–Teller Krypton gas adsorption
CEX	Weak cation exchange chromatography
CFD	Conventional freeze-drying
ESD	Equivalent spherical diameter
FD	Freeze-drying/Freeze-dryer
FT-IR	Fourier-transform infrared spectroscopy
HMW	High molecular weight species
HP	High performance
LC-MS	Liquid chromatography coupled with mass spectrometry
LO	Light obscuration
mAb	Monoclonal antibody
MFD	Microwave-assisted freeze-drying
MW	Microwave
MW Power	Microwave power input
MWCO	Molecular weight cut-off
p_{Chamber}	Chamber pressure setpoint
PES	Polyethersulfone

PS80	Polysorbate 80
RM	Residual moisture content
SEC	Size exclusion chromatography
SSA	Specific Surface Area
SvP	Subvisible particles
T _c	Product temperature
T _{Shelf}	Shelf temperature setpoint
WFI	Water for injection
XRD	X-ray diffraction

III.2 Introduction

Conventional freeze-drying (CFD), also referred to as lyophilization, is a gentle drying method to improve the long-term stability of pharmaceuticals, specifically of protein drugs.⁶⁹ The method is used for pharmaceutical industrial purposes since World War II for the preparation of human blood plasma⁷ and the demand for freeze-drying remains high. By 2018, one-third of all parenteral protein formulations approved by the European Medicines Agency were freeze-dried products.¹¹¹ During lyophilization, the protein drug is immobilized in the solid state, by that slowing down chemical and physical degradation reactions.^{5-8,112} Additionally, freeze-dried solids may have other benefits with respect to shipping and storage.³⁹

In general, freeze-drying comprises three steps: freezing, primary drying (= sublimation drying), and secondary drying (= desorption drying). Typically, the sublimation step is widely described to be the most time-consuming, and conventional freeze-drying is associated with lengthy process times.^{7,27,48,113,114} One alternative drying method utilizing microwaves is known from the food industry: microwave-assisted freeze-drying.¹¹⁵ Here, it is specifically used for high-value goods like dry fruits.¹¹⁶ Similar to the conventional freeze-drying process, the material to be dried first needs to be frozen. In a second step, the drying itself takes place. In contrast to CFD, the main heat transfer mechanism is radiation rather than convection and conduction. Especially polar substances, e.g. water, sugars, amino acids show good absorption of electromagnetic waves of wavelengths of 12.2 cm and frequencies of 2.45 GHz.^{82,104} In brief, the heating mechanism in pharmaceuticals occurs due to dipolar and ionic mechanisms. When such a polar good is placed in an oscillating field, dipoles or ions try to realign in the direction of the electric field. Due to the ultra-rapid change in the direction of the electric field internal friction of the molecules is caused leading to heating within the material, i.e. volumetric heating. In the case of ions, a charge-driven migration is discussed.^{82,84,117} MFD has clear advantages over conventional drying processes, like significantly shorter process times^{81,118} and in the field of food processing, maintenance of

shape, color, taste, odor, and texture^{99–101,116}. In the transition area between food and pharmaceutical technology, MFD was used for the gentle drying of bacteria suspensions. Ambros et al.¹¹⁸ investigated the survival rate and viability of different bacteria cultures. They found comparable survival rates of the investigated cultures produced by MFD compared to conventional freeze-drying but were able to shorten process times by up to 80%. The first usage in pharmaceutical freeze-drying was presented by Evans et al.¹⁰⁵ at the CPPR conference in 2014 showing the general applicability to monoclonal antibody and vaccine formulations. On this basis, a handful of international patents were filed claiming engineering-¹¹⁹ or formulation/process-focused^{106,120} intellectual property. In a previously published work from our group⁸¹ the general applicability to various pharmaceutical freeze-drying excipient systems containing a monoclonal antibody was underlined. Moreover, the potential for process drying time reductions was discussed. However, two major questions have been raised and have not been answered yet: (1) how do different microwave-assisted freeze-dried antibody formulations perform in accelerated stability studies with respect to solid state and protein stability compared to a conventionally freeze-dried reference? (2) Is the inferior batch homogeneity found for MFD samples a general issue associated with microwave drying or are there ways to improve it?

The current study examines four different formulations of two different monoclonal antibodies in the presence of three different glass-forming excipients: sucrose, trehalose, and arginine phosphate. These formulations were freeze-dried with two different drying protocols, i.e. using conventional freeze-drying and microwave-assisted freeze-drying. Moreover, a new microwave setup equipped with a semiconductor solid-state microwave generator was used for one of the formulations. Samples were stored for 24 weeks at different temperatures (2 - 8°C and 40°C) and analyzed at fixed times for their solid state and protein-related quality attributes. We hypothesize that on the one hand irrespective of the monoclonal antibody formulation comparable stability profiles can be found for CFD and MFD. On the other hand, we anticipate the new microwave machinery set up to have a positive effect on batch homogeneity in microwave-assisted freeze-dried products.

III.3 Materials and methods

III.3.1 Materials

Two different IgG type 1 monoclonal antibodies (mAb) were investigated. mAb1 was kindly provided by Boehringer Ingelheim Pharma GmbH & Co. KG (Ingelheim am Rhein, Germany). mAb2 was an on stock at Ludwig-Maximilians-Universität München (LMU).

For mAb1-formulations, the following excipients were used: ACS certified D(+) Sucrose, which was purchased from Sigma-Aldrich (Steinheim, Germany), D(+) Trehalose dihydrate (min. 99% purity) was obtained from VWR International BVBA (Leuven, Belgium). EMPROVE[®] exp L-Arginine (Ph. Eur. certified), EMSURE[®] ortho-Phosphoric acid 85% and Ph. Eur. certified Tween 80[®] were obtained from Merck KGaA (Darmstadt, Germany). For mAb2-formulation, EMPROVE[®] exp sucrose (Ph.Eur.-certified) purchased from Merck KGaA (Darmstadt, Germany) was used.

L-Histidine monohydrochloride monohydrate (min. 99% purity) and L-Histidine (Cell culture reagent) were purchased from Alfa Aesar (Karlsruhe, Germany). Di-sodium hydrogen phosphate dihydrate and sodium dihydrogen phosphate dihydrate were obtained from AppliChem (Darmstadt, Germany). Trizma[®] base BioXtra (>99.9%) and Trizma[®] hydrochloride BioXtra (>99.0%) were purchased from Sigma-Aldrich (St. Louis, MO, USA). Sodium chloride was obtained from Bernd Kraft (Duisburg, Germany). Sodium hydroxide was purchased from Merck KGaA (Darmstadt, Germany).

For the preparation of buffers and stock solutions, water for injection (WFI; Purelab Plus, USF Elga, Celle, Germany) was used.

III.3.2 Study design

The four different formulations, F1–F4, which were dried either by microwave-assisted freeze-drying (MFD) or by conventional freeze-drying (CFD), were stored for 24 weeks at refrigerator temperature 2–8 °C, at 25 °C (F1), and 40 °C (Table III-1). The low concentration mAb formulations (F1–F3) were produced using a previously described MFD setup with a 2 kW/2450 MHz magnetron⁸¹, whereas the high concentration mAb formulation (F4) was processed using a novel semiconductor solid-state microwave radiation source tunable from 5 W to 450 W/2450 MHz.

III.3.3 Preparation of formulations

mAb1 was dialyzed against 10 mM histidine buffer (F1, F2) or 10 mM arginine phosphate (F3) at pH 6.0 for 24 h using dialysis membranes Spectra/Por® (MWCO 6000–8000 Da; Spectrum Laboratories Inc., Compton, CA, USA) with two buffer exchanges. After dialysis, the concentration of mAb1 was measured with a NanoDrop™ 2000 UV photometer (Thermo Scientific, Wilmington, Delaware) at 280 nm using an extinction coefficient of $\epsilon_{0.1\%} = 1.49 \text{ g/100 mL}^{-1} \text{ cm}^{-1}$.

mAb2 (F4) was dialyzed and concentrated using a cross-flow filtration unit Minimate™ TFF capsule with omega polyethersulfone (PES) membrane (MWCO 30,000 Da; Pall Corporation, New York, NY, USA) by adding a 10-fold excess of 10 mM histidine buffer (pH 5.5). After reaching the desired volume, the concentration of the mAb was measured with a NanoDrop™ 2000 UV photometer at 280 nm using an extinction coefficient of $\epsilon = 225,000 \text{ M}^{-1} \text{ cm}^{-1}$ and a molecular weight of MW = 145.5 kDa.

Formulations were prepared according to the composition shown in Table III-1.

Table III-1 Formulations used in this study.

Ingredient	F1	F2	F3	F4
mAb1 [g/L]	5	5	5	/
mAb2 [g/L]	/	/	/	50
Sucrose [% (w/v)]	10	/	/	5
Trehalose [% (w/v)]	/	10	/	/
Arginine phosphate [% (w/v)]	/	/	10	/
Polysorbate 80 [% (w/v)]	0.02	0.02	0.02	/

Formulations F1 and F2 were formulated in 10 mM histidine buffer (pH 6.0), whereas F3 contained no additional buffer salt but was formulated and adjusted to pH 6.0. F4 was formulated in 10 mM histidine buffer (pH 5.5). mAB = monoclonal antibody.

F1–F3 were filtered using 0.2 μm PES membrane syringe filters (VWR International, Radnor, PA, USA), whereas F4 was filtered using a 0.22 μm PES Sartolab® RF vacuum filter unit (Sartorius AG, Goettingen, Germany). For each formulation, 2.3 mL was filled in 10R tubing vials (MGlas AG, Muennerstadt, Germany) and semi-stoppered with lyophilization stoppers (FluroTec® rubber stopper, West Pharmaceuticals, Eschweiler, Germany). The vial population for conventional freeze-drying was arranged on a lyophilization tray and surrounded with at least one row of 10 % (w/v) sucrose shielding vials.

III.3.4 Freeze-drying process

All samples of a corresponding formulation were frozen in the same freezing step. The formulations F1–F3 were frozen in a Christ ε2-6D laboratory-scale freeze-dryer (Martin Christ, Osterode am Harz, Germany) with equilibration at $-5\text{ }^{\circ}\text{C}$ for 1 h, followed by ramping down the shelf with 1 K/min to a $-60\text{ }^{\circ}\text{C}$ set point.

Formulation F4 was frozen in an FTS Systems LyoStar™ 3 freeze-dryer (SP Scientific, SP Scientific, Stone Ridge, NY, USA) with equilibration at $5\text{ }^{\circ}\text{C}$ for 1 h, followed by ramping down the shelf with 1 K/min to a $-50\text{ }^{\circ}\text{C}$ set point.

The frozen samples were subjected to one of the following drying protocols:

III.3.4.1 Conventional Freeze-Drying (CFD)

The conventional freeze-drying cycles are summarized in Table III-2. The freeze-dryer used for cycle F1 and F2/F3 was not equipped with process analytical technologies for sublimation endpoint determination like comparative pressure measurement. Several different formulations were dried in one run at the same time. The holding time for primary drying, therefore, was chosen to allow for completed sublimation.

Table III-2 Overview of the conventional freeze-drying (CFD) processes for the respective formulations.

FD Process	Setpoint	Freezing			Primary Drying	Secondary Drying	
CFD cycle F1	T _{Shelf} [°C]	20	-5	-60	-20	0	20
	Ramp [K/min]	–	1	1	0.2	0.05	0.2
	Hold time [min]	5	60	2580 ^a	2700 (1120) ^b	–	360
	p _{Chamber} [μbar]	–	–	–	100	50	50
CFD cycle F2/3	T _{Shelf} [°C]	20	-5	-60	-25	0	20
	Ramp [K/min]	–	1	1	0.2	0.05	0.2
	Hold time [min]	5	60	3610 ^a	5760 (1400) ^b	-	360
	p _{Chamber} [mbar]	–	-	–	100	50	50
CFD cycle F4	T _{Shelf} [°C]	20	5	-50	-20	5	35
	Ramp [K/min]	–	1	1	1	0.15	0.3
	Hold time [min]	5	60	1006 ^a	1868 (1058) ^b	–	420
	p _{Chamber} [mbar]	–	–	–	100	100	100

^a Freezing times were held longer than usual due to logistical reasons caused by the need to split up the batch before proceeding with the drying process. ^b Estimated time needed for complete sublimation based on the time the last thermocouple in the respective formulation needed to reach the shelf temperature setpoint.

III.3.4.2 Microwave-assisted freeze-drying (MFD)

Microwave-assisted freeze-drying was conducted on a modified laboratory-scale Püschner μWaveVac 0250fd vacuum dryer prototype (Püschner GmbH + Co KG, Schwanewede, Germany).

For the formulations F1 – F3 the setup described previously⁸¹ was used. Briefly, it contained a 2 kW/2450 MHz magnetron, a condenser (-80°C), and a vacuum system comprising a root pump and a rotary vane pump. The tuner, which was located between the magnetron and water load, was adjusted that way that approximately 1/10 of the generated microwaves went into the product chamber. For a schematic overview of the general setup, the reader is referred to reference¹⁰⁸. In the setup used for F1 – F3, water load and product cavity were interchanged. Drying was carried out at a pressure of 8 μbar to 30 μbar measured by Pirani gauge and at a microwave power between 23 W to 110 W measured by a HOMER™ impedance analyzer (S-TEAM Lab, Bratislava, Slovak Republic) until a constant mass was reached. The drying process used for F1 and F2/F3 is presented in Figure III-1a,b, respectively.

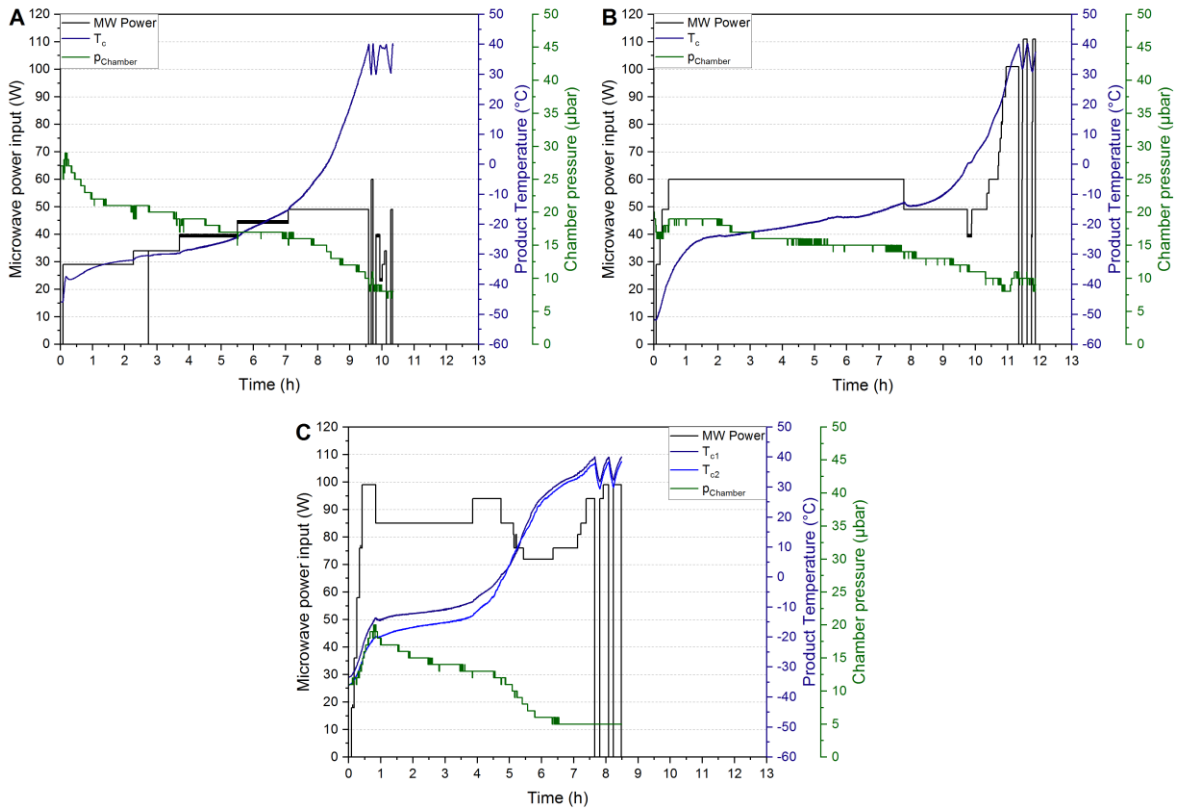


Figure III-1 Graphical overview of the microwave-assisted freeze-drying (MFD) processes for **A** F1, **B** F2/F3, and **C** F4. Microwave power input (MW Power) is the actual measured radiated microwave power, the chamber pressure is the Pirani gauge readout (p_{chamber}), and T_c represents the readout of the glass fiber temperature probe.

In contrast, F4 was processed with a partially modified setup comprising a semiconductor solid-state 500 W/2450 MHz microwave radiation source tunable from 5 W to 450 W which directly emitted its radiation into the product chamber.¹⁰⁸ Moreover, the vacuum system was complemented by the addition of a turbopump to allow for lower chamber pressures. Drying, as it is shown in Figure III-1c, was carried out at a pressure of 5 µbar to 20 µbar measured by Pirani gauge and at a microwave power between 18 W to 99 W measured by a HOMER™ impedance analyzer (S-TEAM Lab, Bratislava, Slovak Republic).

For process monitoring, two glass fiber temperature measurement probes (TS2, Weidmann Technologies Deutschland GmbH, Dresden, Germany) were used. Stoppering of the samples was carried out externally in a glove bag flushed with dry nitrogen. The dried crimped samples were kept refrigerated until analysis.

III.3.5 Karl Fischer titration

Karl Fischer titration, equipped with a headspace module, was used to determine residual water content after freeze-drying. Between samples, aliquots of 9 mg and 28 mg were prepared in a glove box filled with pressurized air with a relative humidity of less than 10 %, placed into 2R vials, and stoppered. The samples were then placed in an oven with 100 °C to enable the fast extraction of water. The headspace moisture is transported into a coulometric Karl Fischer titrator (Aqua 40.00, Elektrochemie Halle, Halle (Saale), Germany). Results were calculated in relative water content (*w/w*). For verification of equipment performance, three aliquots of Apura[®] water standard oven 1 % by Merck KGaA (Darmstadt, Germany) were measured within a sequence.

III.3.6 Brunauer-Emmet-Teller krypton gas adsorption

The specific surface area of dried samples was determined using Brunauer–Emmet–Teller (BET) krypton gas adsorption in a liquid nitrogen bath at 77.3 K (Autosorb 1; Quantachrome, Odelzhausen, Germany). Samples of 90–200 mg were gently crushed with a spatula and weighed into glass tubes. Prior to measurement, an outgassing step was performed for at least 6 h at room temperature. An 11-point gas adsorption curve was measured, covering a p/p_0 ratio of approximately 0.05–0.30. Data evaluation was performed according to the multi-point BET method fit of the Autosorb 1 software.

III.3.7 X-ray powder diffraction

To determine the solid-state of the lyophilizates, an XRD 3000 TT diffractometer (Seifert, Ahrensburg, Germany) was used. The device was equipped with a copper anode (40 kV, 30 mA) and had a wavelength of 0.154178 nm. The scintillation detector voltage was 1000 V. The samples were placed on the copper sample holder and analyzed in the range of 5–45° 2-theta, with steps of 0.05°.

III.3.8 Reconstitution of lyophilizates

The lyophilized cakes were reconstituted by the addition of WFI. The WFI volume for each formulation was calculated to match the volume of the water removed during freeze-drying. Reconstitution time was determined by recording the time between adding the respective formulation-specific volume of water for injection and obtaining a clear solution without

visible matter. This observation was performed by manual visual inspection. Reconstitution was performed applying gentle swirling for 5 s directly after the addition of water.

III.3.9 High-performance size exclusion chromatography (HP-SEC)

A Waters 2695 Separation module (Waters GmbH, Eschborn, Germany) equipped with a Waters 2487 Dual λ Absorbance Detector (Waters GmbH, Eschborn, Germany) at 214 and 280 nm was used. Isocratic elution with a 25 mM sodium phosphate running buffer containing 200 mM sodium chloride (pH 7.0) was performed.

For mAb1-formulations (F1–F3), 10 μ L of a reconstituted solution corresponding to a loading of 50 μ g protein were loaded on a Tosoh TSKgel G3000SWxl, 7.8 \times 300 mm, 5 μ m column (Tosoh Bioscience, Griesheim, Germany) and separated with a flow rate of 0.7 mL/min.

For mAb2 (F4), samples were diluted with 10 mM histidine buffer (pH 5.5) to 1 g/L protein concentration, and 25 μ L was injected, corresponding to a load of 25 μ g protein. A YMC-Pack Diol-300, 300 \times 8.0 mm, 5 μ m column (YMC Europe GmbH, Dinslaken, Germany) with a flow rate of 0.8 mL/min was used for separation. Samples were measured in triplicates with three individual injections. Data integration of relative areas at 280 nm was performed using Chromeleon 6.80 (Thermo Scientific, Wilmington, DE, USA), provided that every peak eluting before the monomer corresponded to high molecular weight (HMW) species. No peaks could be detected after the monomer. For verification of equipment performance, an internal standard of thawed mAb formulation was injected at the beginning and end of a sequence.

III.3.10 High-performance cation exchange chromatography (HP-CEX)

A Waters 2695 Separation module (Waters GmbH, Eschborn, Germany) equipped with a Waters 2487 Dual λ Absorbance Detector (Waters GmbH, Eschborn, Germany) at 214 and 280 nm was used for weak cation exchange chromatography. A linear sodium chloride gradient of 0% to 20% solvent B in solvent A over 30 min was used for elution at a flow rate of 1 mL/min. For all cation exchange (CEX) analysis, a ProPac™ WCX-10G BioLC™ Analytical column 4 \times 250 mm equipped with a ProPac™ WCX-10G BioLC™ guard column 4 \times 50 mm (ThermoFisher Scientific, Waltham, MA, USA) was used.

For mAb1-formulations (F1–F3), the solvents were composed of A: 20 mM TRIS (pH 7.1) and B: 20 mM TRIS (pH 7.1) plus 300 mM sodium chloride. Reconstituted sample aliquots of 10 μ L, corresponding to a loading of 50 μ g protein, were loaded on the column.

For mAb2 (F4), the solvents were composed of A: 20 mM TRIS (pH 7.5) and B: 20 mM TRIS (pH 7.5) plus 300 mM sodium chloride. Before analysis, samples were diluted with solvent A to 1 g/L protein concentration, and 50 μ L was injected, corresponding to a load of 50 μ g protein.

Samples were measured as triplicates with two individual injections. Data integration of relative areas was performed using the Chromeleon 6.80 software (Thermo Scientific, Wilmington, DE, USA), provided that every peak eluting before the main peak corresponded to acidic species and peaks eluting after the main peak corresponded to basic species. For verification of equipment performance, an internal standard of thawed mAb formulation was injected at the beginning and end of a sequence.

III.3.11 Light obscuration

One method used to determine subvisible particles of the formulation F1 was light obscuration. Therefore, a PAMAS SVSS-35 particle counter (PAMAS—Partikelmess- und Analysesysteme GmbH, Rutesheim, Germany) equipped with an HCB-LD 25/25 sensor, which had a detection limit of approximately 120,000 particles \geq 1 μ m per mL, was used. The pre-rinsing volume was 0.4 mL and was followed by three measurements of 0.2 mL. The fill rate, emptying rate, and rinse rate of the syringe were set to 10 mL/min. Before and between samples, the system was rinsed with WFI until less than 30 particles/mL \geq 1 μ m and no particles larger than 10 μ m were present. Data collection was done using PAMAS PMA software, and particle diameters in the range of \geq 1 μ m to 200 μ m were determined. All results are given in cumulative particles per milliliter.

III.3.12 Flow-imaging microscopy

Due to the high transparency of protein particles, an orthogonal method for subvisible particle determination was introduced for formulations F2–F4. Flow-imaging microscopy was performed on a FlowCAM[®] 8100 (Fluid Imaging Technologies, Inc., Scarborough, ME, USA) equipped with a 10 \times magnification cell (81 μ m \times 700 μ m). Prior to a measurement set, the cell was cleaned with a 1% Hellmanex III solution and WFI. For adjustment of the focus, the default autofocus procedure using 20 μ m calibration beads was performed. Sample

solution volumes of 150 μL were measured with a flow rate of 0.10 mL/min, at an image rate of 29 frames per second, and an estimated run time of 1.5 min. After each measurement, the flow cell was flushed with WFI. For particle identification, the following settings were used: 3 μm distance to the nearest neighbor, particle segmentation thresholds for dark pixels and light pixels of 13 and 10, respectively. The particle size was reported as the equivalent spherical diameter (ESD). Frames were collected with VisualSpreadsheet[®] 4.7.6 software and were evaluated for total particle counts of cumulative particles greater or equal to 1 μm , 10 μm and, 25 μm per mL.

III.4 Results

III.4.1 Solid state

III.4.1.1 Residual moisture content and specific surface area

The results for residual moisture (RM) and specific surface area (SSA) determination are presented in Figure III-2. For the low concentrated mAb formulation with sucrose (F1), three different storage temperatures are shown (Figure III-2a). Directly after freeze-drying, the SSA results revealed identical values for CFD, $0.63 \text{ m}^2/\text{g} \pm 0.02 \text{ m}^2/\text{g}$, and MFD, $0.66 \text{ m}^2/\text{g} \pm 0.05 \text{ m}^2/\text{g}$. Irrespective of the storage temperature and time point, neither differences nor relevant changes in specific surface areas were observed. With regard to residual moisture content, analysis showed low values for both CFD and MFD ($1.1 \% \pm 0.1 \%$ and $1.0 \% \pm 0.5 \%$, respectively). These values changed only slightly over 24 weeks at all investigated storage temperatures. However, within the microwave-processed products, some samples exhibited higher variances represented by higher standard deviations, which were not found within the conventionally freeze-dried samples.

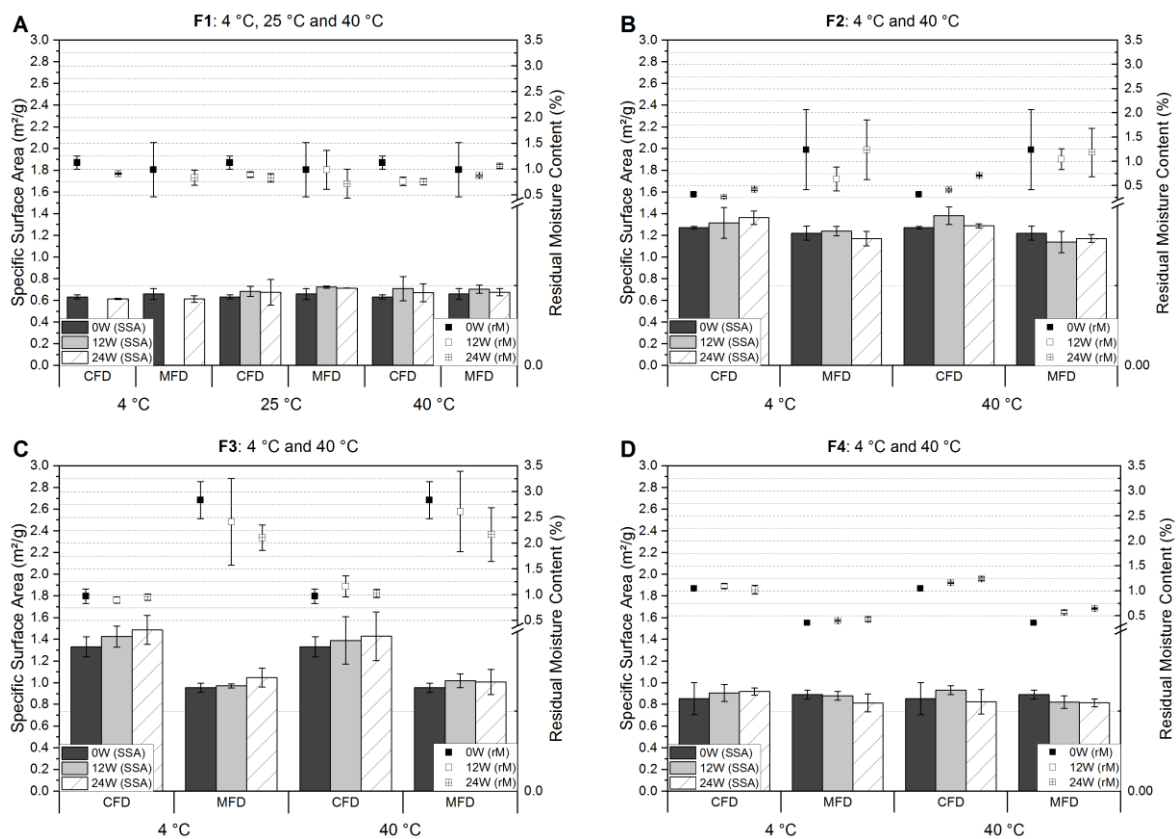


Figure III-2 Specific surface area (bars) and residual moisture content (squares) results over the course of 24 weeks of storage at the respective storage temperature for **A** F1, **B** F2, **C** F3, and **D** F4. Values shown represent the mean value ($n = 3$) \pm standard deviation.

Similar results were found for the low concentrated mAb formulation stabilized with trehalose (Figure III-2b). No relevant differences or changes were observed for the specific surface area over the course of 24 weeks of storage at refrigerator temperature or 40 °C. Mean values almost remained at initial values of $1.27 \text{ m}^2/\text{g} \pm 0.01 \text{ m}^2/\text{g}$ and $1.22 \text{ m}^2/\text{g} \pm 0.06 \text{ m}^2/\text{g}$ for CFD and MFD, respectively. In regards to residual moisture, MFD samples appeared to be moister than CFD samples ($1.2 \% \pm 0.8 \%$ vs. $0.3 \% \pm 0.0 \%$). These differences remained over six months of storage irrespective of the storage temperature. Yet, the moisture content in CFD cakes doubled at 40 °C ($0.7 \% \pm 0.0 \%$), unlike MFD cakes. However, high variances within MFD samples may have masked such effects.

Unlike the sucrose (F1) and trehalose (F2) formulations, low concentration mAb formulations with arginine phosphate (F3) exhibited differences with respect to specific surface area (Figure III-2c). Initial measurements directly after freeze-drying revealed values of $1.33 \text{ m}^2/\text{g} \pm 0.09 \text{ m}^2/\text{g}$ and $0.95 \text{ m}^2/\text{g} \pm 0.04 \text{ m}^2/\text{g}$ for CFD and MFD, respectively. Slight, but non-significant changes over storage were observed. The initially different SSA values

correlated inversely with the observed residual moisture mean values (CFD: 1.0 % ± 0.1 % and MFD: 2.8 % ± 0.4 %). A micro-collapse within MFD samples was assumed.

F4, which was comprised of a 1:1-mixture (weight-wise) of sucrose and mAb2, was dried with a different microwave-setup. By this, high variances in residual moisture, which occasionally occurred before within MFD samples, were not observed anymore (Figure III-2d). For conventional freeze-dried samples, mean values changed from 1.0 % (± 0.0 %) to 1.2 % (± 0.0 %) over 24 weeks of storage at 40 °C. Within MFD samples, a similar increase from 0.4 % (± 0.0 %), initially to 0.6 % (± 0.0%), was observed after six months at 40 °C. In contrast, specific surface areas were found to remain unaffected by accelerated storage conditions at values of 0.85 m²/g ± 0.15 m²/g and 0.89 m²/g ± 0.04 m²/g for CFD and MFD, respectively.

III.4.1.2 X-ray powder diffraction (XRD)

In order to confirm the amorphicity of all formulations, XRD was used. The results for the two sucrose-based formulations, F1 and F4, are presented in Figure SIII-1 and were directly compared to the pure excipient sucrose. No indications of crystallization were found. Amorphous halos and the absence of typical peaks^{121,122} were found for trehalose-based formulations (Figure SIII-2). An overall XRD-amorphicity, represented by an amorphous halo, was also found for the significantly moister arginine phosphate formulations (Figure SIII-3). A reference diffractogram for recrystallized arginine phosphate was derived by intentionally exposing one MFD vial to a moist atmosphere overnight.

III.4.2 Protein-related quality attributes

III.4.2.1 Reconstitution and subvisible particles (SvP)

Before liquid analysis, lyophilized products needed to be reconstituted. Within one formulation, no significant difference between the distinct drying protocols was seen. However, small differences with regard to other formulation were observed (Table III-3).

Table III-3 Reconstitution times of the different formulations.

Formulation	Reconstitution Time (s)
F1	≤ 30
F2	≤ 30
F3	≤ 50
F4	≤ 120

The subvisible particle counts (SvP) obtained by light obscuration for F1 are presented in Figure III-3a,b. All vials analyzed originated from the same filtered bulk formulation, which is why initial particle counts were the same before a certain drying or storage scheme was applied. Light obscuration measurements revealed relatively low particle counts per mL of 2212 ± 565 , 26 ± 2 , and 4 ± 3 for $\geq 1 \mu\text{m}$, $\geq 10 \mu\text{m}$, and $\geq 25 \mu\text{m}$, respectively. An increase of +94 % (4300 ± 546) and +49 % (3303 ± 651) for cumulative particles $\geq 1 \mu\text{m}/\text{mL}$ was observed directly after freeze-drying. In Figure III-3a the results after storage over 24 weeks at 4 °C and 25 °C are shown. After six months at refrigerator temperature, particle counts were stabilized close to values prior to freeze-drying of 2678 ± 307 (CFD) and 2227 ± 225 for particles $\geq 1 \mu\text{m}/\text{mL}$. At 25 °C storage temperature, subvisible particle counts were only slightly elevated for CFD (2953 ± 295), but not for MFD (1937 ± 247). No increase in bigger particles, $\geq 10 \mu\text{m}$, and $\geq 25 \mu\text{m}$, was seen at any of the storage conditions. Figure III-3b shows that storage over 24 weeks at 40 °C caused an increase by factor 2.3 (5106 ± 237) for conventionally FD, and an increase of 36 % (3003 ± 1058) for microwave-assisted FD, in $\geq 1 \mu\text{m}$ particles. However, bigger variances were found for MFD samples.

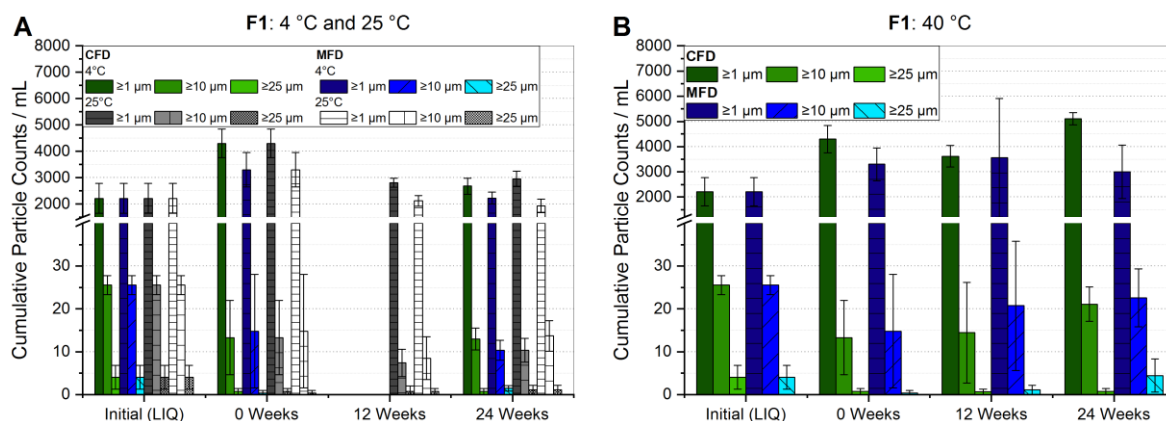


Figure III-3 Subvisible particle (SvP) counts for formulation F1 measured by light obscuration and size-exclusion chromatography results. The bar charts represent the subvisible particle counts for the respective storage temperatures **A** 4 °C, 25 °C, and **B** 40 °C. Bars represent the mean value \pm standard deviation for three individual vials.

Figure III-4 represents the SvP counts analyzed by flow-imaging microscopy for F2. The same filtered bulk formulation was used for all vials analyzed. Initially, relatively low particle counts per mL of 1867 ± 1784 , 90 ± 20 and 20 ± 35 for $\geq 1 \mu\text{m}$, $\geq 10 \mu\text{m}$, and $\geq 25 \mu\text{m}$, respectively, were found. A slight increase by 24% (2320 ± 599) and 37% (2549 ± 677) for cumulative particles $\geq 1 \mu\text{m}/\text{mL}$ was observed directly after freeze-drying. At 4 °C storage temperature, particle numbers $\geq 1 \mu\text{m}/\text{mL}$ settled around initial values after 24 weeks, but the cumulative count of bigger particles increased (Figure III-4a). However, no significant

changes were observed. A dramatic increase for SvP $\geq 1 \mu\text{m/mL}$ was found over the course of six months at 40°C for both CFD (37909 ± 4337) and MFD (18947 ± 6753), as shown in Figure III-4b. The mean SvP count values for $\geq 10 \mu\text{m}$ and $\geq 25 \mu\text{m}$ also increased drastically, even though high standard deviations lowered the significance. However, an upward trend could be assumed for subvisible particles $\geq 10 \mu\text{m/mL}$, in conventionally processed samples.

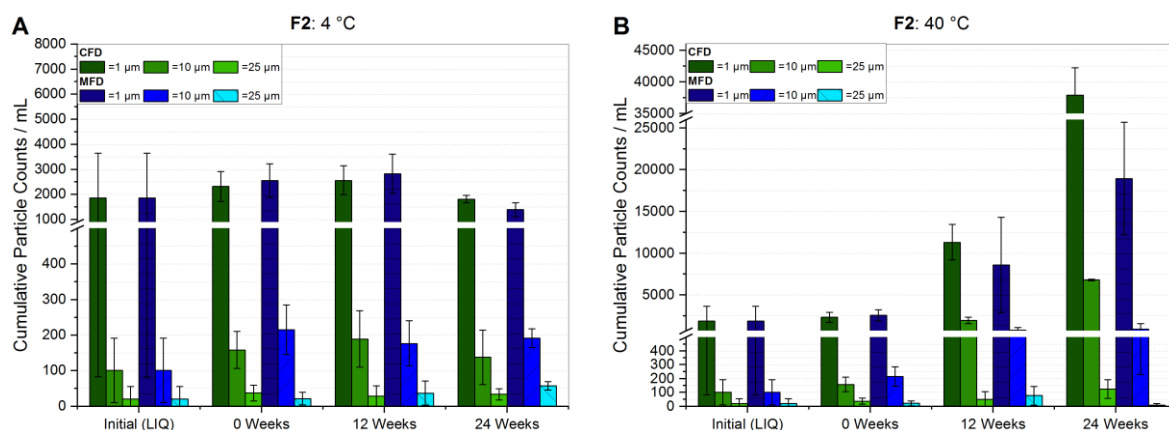


Figure III-4 Subvisible particle (SvP) counts for trehalose-based formulation F2 measured by flow-imaging microscopy. Bar chart **A** represents the SvP counts at refrigerator storage and **B** at 40°C . Bars represent the mean value \pm standard deviation for three individual vials.

The SvP counts for the low concentration mAb formulation stabilized by arginine phosphate, F3, are shown in Figure III-5. Prior to freeze-drying, relatively low particle counts per mL of 1991 ± 1490 , 68 ± 42 and 20 ± 21 for $\geq 1 \mu\text{m}$, $\geq 10 \mu\text{m}$, and $\geq 25 \mu\text{m}$ were found, respectively. At 4°C (Figure III-5a) storage temperature, a small increase in mean values for cumulative particles $\geq 1 \mu\text{m}$ was found over time, although particle counts for this size category settled around the initial values. For particles $\geq 10 \mu\text{m}$ and $\geq 25 \mu\text{m}$, a slightly stronger increase in mean values was observed, although vast standard deviations lowered the significance.

At accelerated storage conditions (Figure III-5b), a moderate increase in all size categories was seen. Especially after six months storage, the conventionally freeze-dried sample showed a significant increase for $\geq 1 \mu\text{m}$, $\geq 10 \mu\text{m}$, and $\geq 25 \mu\text{m}$ with particle counts per mL of 5913 ± 1584 (3 \times higher), 394 ± 97 (6 \times higher), and 78 ± 21 (4 \times higher), respectively. In contrast, the microwave-assisted freeze-dried sample at the same conditions showed no increase for $\geq 1 \mu\text{m}$, and only a modest increase by factor 2.6 and 2.2 for cumulative particle counts $\geq 10 \mu\text{m}$ and $\geq 25 \mu\text{m}$, respectively.

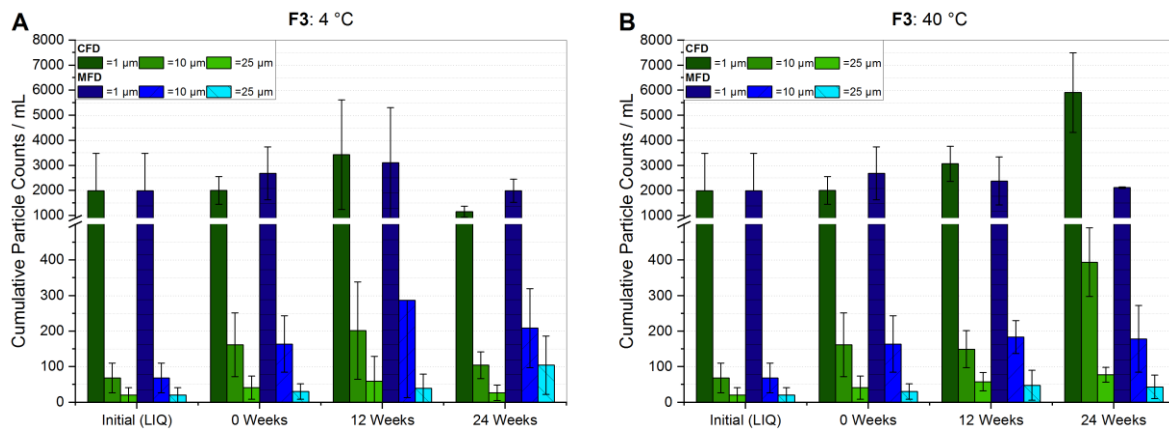


Figure III-5 Subvisible particle (SvP) counts for the arginine phosphate formulation F3 measured by flow-imaging microscopy. Bar chart **A** represents the SvP counts at refrigerator storage and **B** at 40 °C. Bars represent the mean value \pm standard deviation for three individual vials.

For the formulation with 50 g/L of mAb2 and only 5 % (w/v), sucrose-stabilizer neither at refrigerator (Figure III-6a) nor at 40 °C storage temperature Figure III-6b), was a significant change in subvisible particles observed. The initial formulation before FD revealed low particle counts per mL of 2051 ± 1153 , 40 ± 41 and 7 ± 6 for $\geq 1 \mu\text{m}$, $\geq 10 \mu\text{m}$, and $\geq 25 \mu\text{m}$, respectively. The results obtained showed a larger increase by 74 % (3579 ± 2243) for CFD and 25 % (2555 ± 97) for MFD, in regards to cumulative particles $\geq 1 \mu\text{m}$ at four degrees celsius storage over six months, compared to storage at 40 °C.

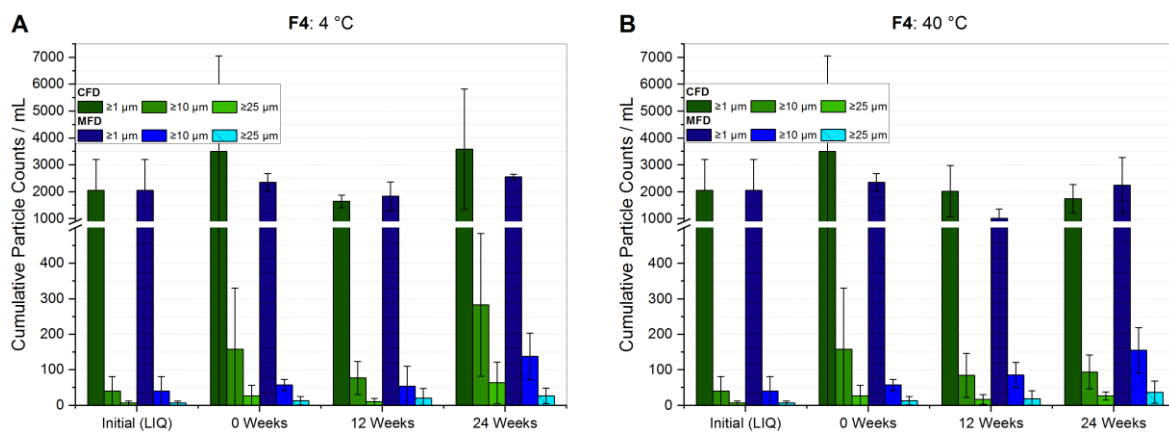


Figure III-6 Subvisible particle (SvP) counts for the high concentration mAb formulation with 50 g/L stabilized by sucrose, measured by flow-imaging microscopy. Bar chart **A** represents the SvP counts at refrigerator storage and **B** at 40 °C. Bars represent the mean value \pm standard deviation for three individual vials.

Yet, at all conditions observed, larger particle categories, i.e., $\geq 10 \mu\text{m}$ and $\geq 25 \mu\text{m}$, revealed an increased number of particle counts. However, due to high standard deviations within a sample, no significant changes were detectable.

III.4.2.2 Weak cation exchange chromatography (CEX)

In order to generically quantify different protein degradation pathways, e.g., deamidation, a salt-gradient weak cation exchange chromatography was used. The CEX data for F1 was not collected. But for the trehalose-based low concentration mAb formulation (F2), data from CEX measurements is shown in Figure III-7a,b for the respective storage temperatures. Directly after freeze-drying, irrespective of the applied drying protocol (CFD or MFD), relative amounts of the different species were found to be alike. For storage at refrigerator temperature, (Figure III-7a) acidic species dropped by roughly one percent for both drying protocols, whereas basic species slightly increased by 1.5 %. Somewhat more pronounced changes were observed for storage at 40 °C (Figure III-7b). While acidic species increased by three percent, basic species rose by 4.7 % and 3.5 % for CFD and MFD, respectively.

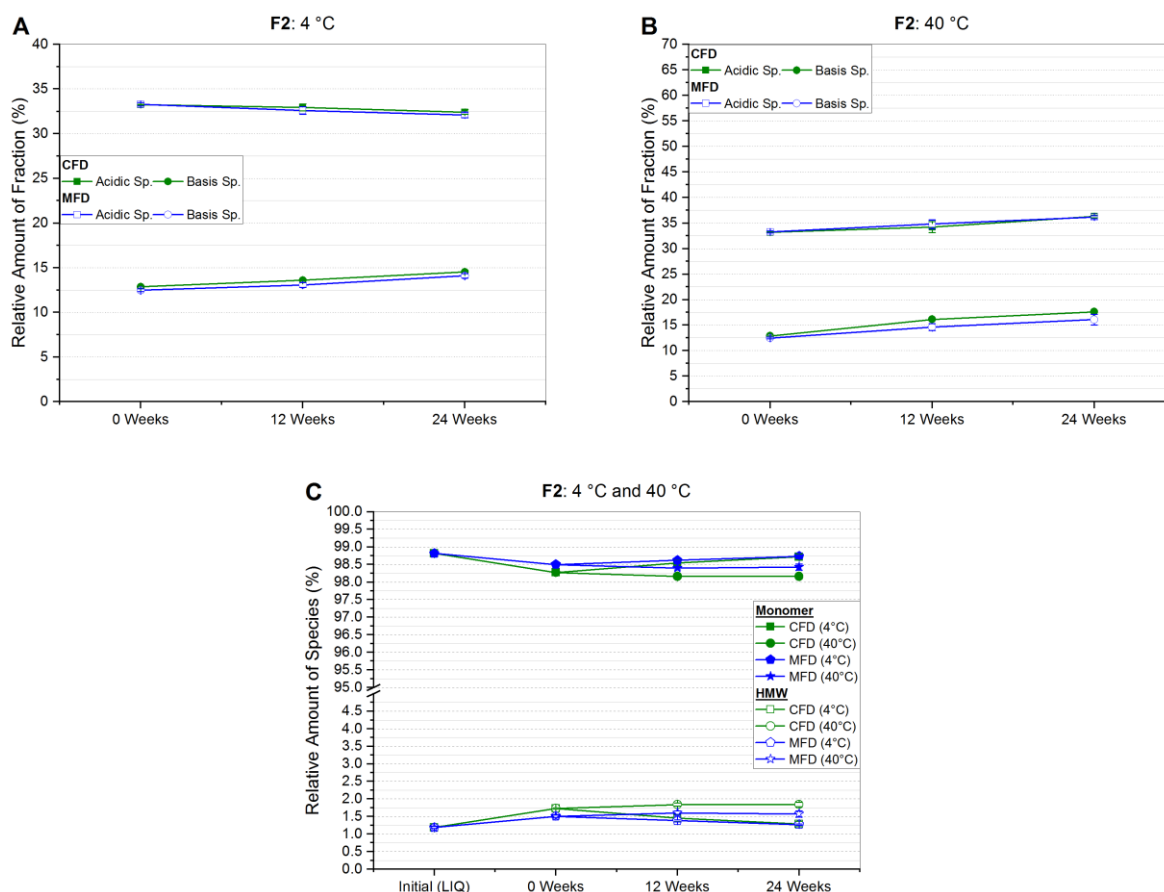


Figure III-7 Relative amount of acidic and basic species obtained by high-performance (HP)-weak cation exchange chromatography for trehalose-based formulation F2 at **A** 4 °C and **B** 40 °C storage temperature. In **C**, the relative percentages of monomer and high molecular weight species (HMW) at the respective storage temperature over storage time gained by HP-size exclusion chromatography (SEC) analysis are presented.

For the arginine phosphate-formulation (F3), CEX data is shown in Figure III-8a,b. A small difference of 1.7 % in the initial relative amount of acidic species was found, which equalized for the two drying protocols over 24 weeks storage time at 4 °C (Figure III-8a). At the same conditions, basic species slightly increased for both CFD (+1.8 %) and MFD (+1.3 %), revealing a small deviation. Acidic species showed a noticeable change by 15.9 % (CFD) and 26.6 % (MFD) at 40 °C storage temperature (Figure III-8b), whereas basic species remained almost the same with changes by 2.5 % (CFD) and –0.5 % (MFD).

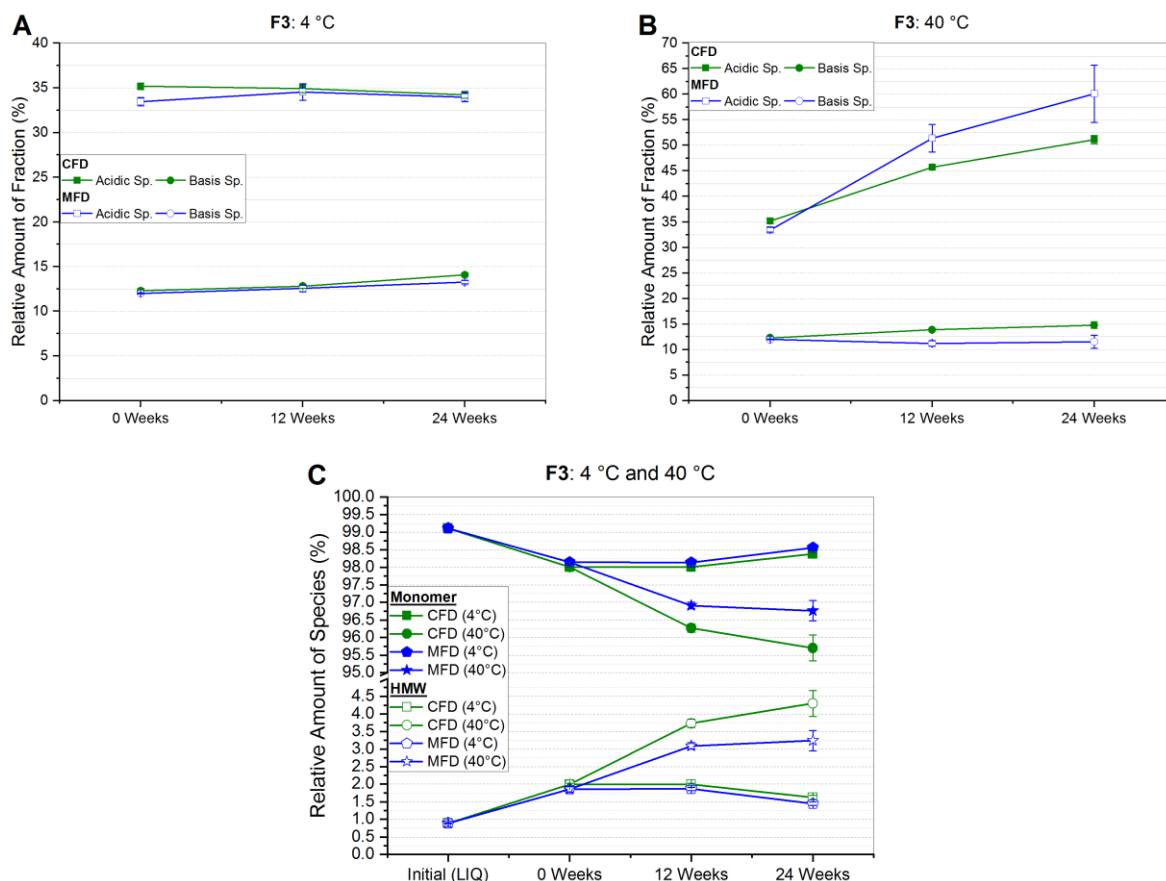


Figure III-8 Relative amount of acidic and basic species obtained by HP-weak cation exchange chromatography for arginine phosphate-based formulation F3 at **A** 4 °C and **B** 40 °C storage temperature. In **C**, the relative percentages of monomer and high molecular weight species (HMW) at the respective storage temperature over storage time gained by HP-SEC analysis are presented.

In the case of the high concentration mAb formulation stabilized with sucrose (F4), almost no differences were found between conventional and microwave-assisted freeze-dried products with regard to CEX results (Figure III-9a,b). At refrigerator temperature (Figure III-9a), changes in both species and both drying protocols ranged within less than 0.5 %. While similar observations were made for the acidic species at 40 °C, basic species slightly

rose by 2.7 % and 3 % for CFD and MFD samples, respectively. However, no difference between the drying procedures was observed.

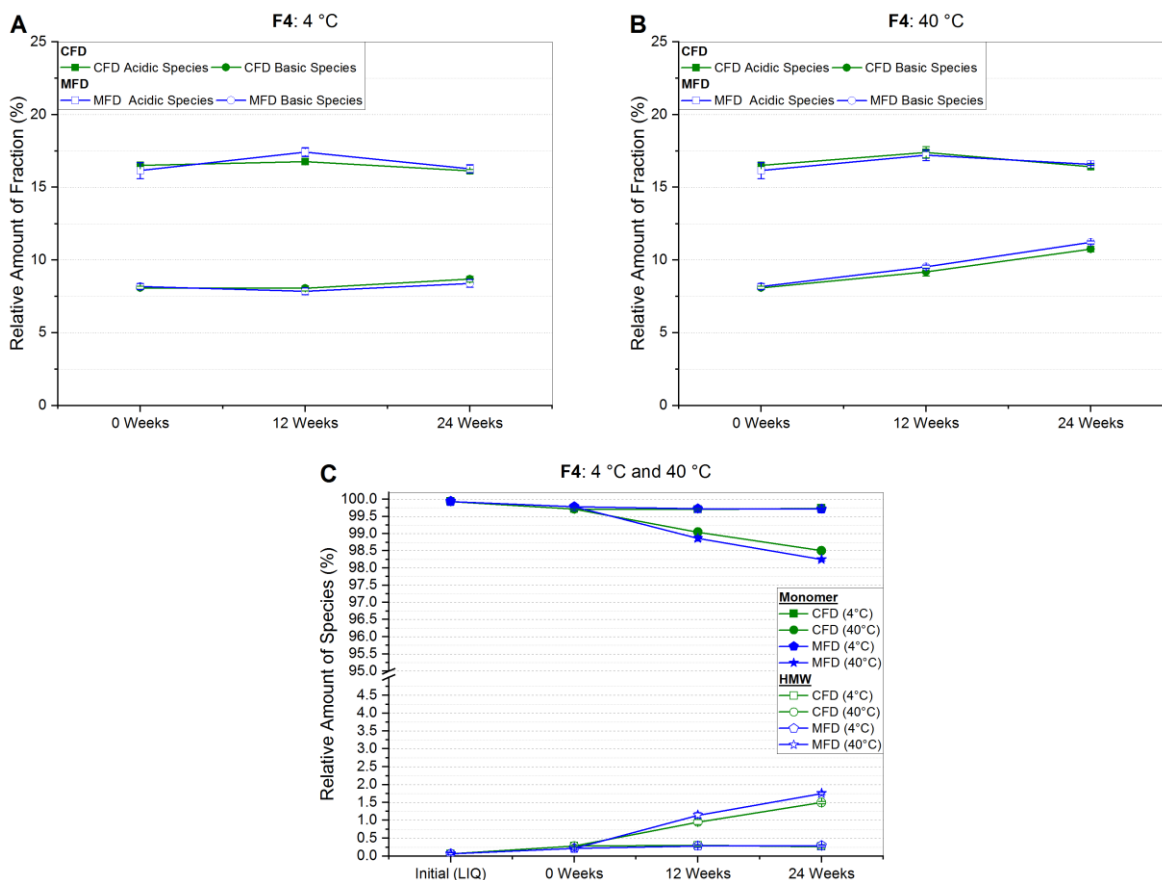


Figure III-9 Relative amount of acidic and basic species obtained by HP-weak cation exchange chromatography for the high concentration mAb formulation with 50 g/L stabilized with sucrose (F4) at **A** 4 °C and **B** 40 °C storage temperature. In **C**, the relative percentages of monomer and high molecular weight species (HMW) at the respective storage temperature over storage time gained by HP-SEC analysis are presented.

III.4.2.3 Size exclusion chromatography (SEC)

The relative amount of monomeric and high molecular weight (HMW) species was assessed by high-performance size-exclusion chromatography. The results of the HP-SEC analysis for the low concentration mAb formulation with 10 % (w/v) sucrose (F1) are displayed in Figure SIII-4. Irrespective of the storage temperature, no changes in monomer content occurred. In other words, the relative amount of monomeric species ranged between 99.0 % to 99.1 % at all analyzed time points, and all investigated storage temperatures.

Only a slightly different picture was seen for the trehalose formulation F2 in Figure III-7c. After six months at 4 °C, the loss of monomer and the complementary rise in HMW was negligibly low, basically within the range of SEC sample standard deviation. A small decrease by -0.6% ($98.2\% \pm 0.1\%$) for CFD and by -0.4% ($98.4\% \pm 0.1\%$) for

microwave-assisted freeze-dried lyophilizates was observed in accelerated storage conditions of 40 °C for 24 weeks.

In arginine phosphate-based monoclonal antibody formulation (F3), more changes were observed (Figure III-8c). At refrigerator temperature, a small decrease by less than one percent in monomer content, and thus, an increase in HMW aggregates to less than 2 % overall HMW species, occurred. However, a significant loss in monomeric content down to 95.7 % \pm 0.4 % and 96.8 % \pm 0.3 % for CFD and MFD, respectively, was seen. This was counterbalanced by an increase in high molecular weight species to 4.3 % \pm 0.4 % and 3.2 % \pm 0.3 % for conventionally and microwave-assisted freeze-dried samples.

The formulation with 50 g/L of mAb2 (F4) showed a higher monomeric SEC-purity of 99.9 % \pm 0.0 %, compared to mAb1 formulations prior to freeze-drying (Figure III-9c). At refrigerator storage temperatures, only a small loss of 0.2 % relative monomer content was observable regardless of the initially used drying procedure. Even for 24 weeks at 40 °C, the monomer content for CFD and MFD samples decreased only slightly to 98.5 % \pm 0.0 % and 98.2 % \pm 0.0 %, respectively. This loss was compensated by an increase in HMW to 1.5 % \pm 0.0 % and 1.8 % \pm 0.0 % for conventionally and microwave-assisted freeze-dried samples, respectively.

III.5 Discussion

III.5.1 Stability with regard to solid state properties

In the case of freeze-dried products, attributes like residual moisture content, solid state, and specific surface area are critical to assess and to monitor over storage and shelf-life.¹²³ With respect to the specific surface area, the low mAb concentration formulations with sucrose and trehalose, F1 and F2 (Table III-1), showed identical values for each formulation for the two distinct drying protocols directly after freeze-drying and no change over the duration of storage. This strongly indicated the absence of a microscopic collapse, which means that the initially determined ice and successive pore structure remained during the two different drying protocols for the respective formulation.¹⁸ Regarding the residual moisture content, similar mean values were found for the sucrose-based formulation F1 with 1.1 % \pm 0.1 % and 1.0 % \pm 0.5 % for CFD and MFD, respectively (Figure III-2a). This moisture level was kept over storage, even at elevated temperatures. However, high variances in some MFD samples were observed. Such high variances among samples of one microwave-batch may have been caused by non-uniform temperature distribution. This non-uniformity in

microwave heating was reported in the literature to be one major challenge associated with that drying technique.^{83,84,104} The resulting appearance of cold and hot spots was described as multifactorial and may be dependent on the chosen mode (multimode, single-mode)^{104,124}, oven design⁸³, composition and geometry of the frozen good^{104,125–127}, the occurrence of standing wave effect¹²⁸ and drying duration¹²⁹.

In contrast, in trehalose samples (F2) residual moisture levels differ already after the freeze-drying step, i.e. $0.3 \% \pm 0.0 \%$ for conventionally dried and $1.2 \% \pm 0.8 \%$ for microwave-assisted dried samples (Figure III-2b). The CFD samples stored at $40\text{ }^{\circ}\text{C}$ showed an increase to $0.7 \% \pm 0.0 \%$. This was most likely due to moisture uptake of the cake from the rubber stopper as it was described by Pikal and Shah¹³⁰. The equilibration of stopper moisture and cake moisture was found to be kinetically dependent on storage temperature in the first place. Because of the high variances in MFD samples, such an effect may have happened but could not be detected.

An arginine phosphate-based formulation (F3) was expected to be different. Firstly, because of the permanently charged character of arginine which causes high dielectric loss, i.e. the ability of a material to absorb electromagnetic energy¹⁰⁴, as reported by Meng et al.¹³¹. Of course, the dielectric properties of a material may vary depending on the exact composition, density, temperature, and frequency.¹⁰⁴ Nevertheless, different behavior of such formulation within the electromagnetic microwave field was expected. Secondly, because of the reported complex molecular structure of arginine phosphate.¹³² Although the reported structure was described for the crystalline state, similar intense interactions in the glassy state were assumed.^{133,134} For formulation F3 specific surface area values were reduced by 39 % to $0.95\text{ m}^2/\text{g} \pm 0.04\text{ m}^2/\text{g}$ for MFD compared to $1.33\text{ m}^2/\text{g} \pm 0.09\text{ m}^2/\text{g}$ for CFD initially after application of the different drying protocols (Figure III-2c). It is assumed that this shift in the SSA is associated with a microscopic collapse within the amorphous matrix which may have been favored by the permanently charged matrix leading to enhanced absorption of microwave energy.¹³¹ As the desorption step of the unfrozen water is highly SSA-dependent⁷⁵, the micro-collapse seems likely to be the cause for higher mean residual moisture in MFD ($2.8 \% \pm 0.4 \%$) compared to CFD ($1.0 \% \pm 0.1 \%$). Over the course of storage, no significant change in glassy state properties was observed.

The 50 g/L mAb2 formulation stabilized with sucrose (F4) appeared to be different with respect to residual moisture content (Figure III-2d). Occasionally emerging high variances within one sample ($n = 3$) produced by MFD was not observed anymore. Two possible reasons are: (1) the formulation which consisted roughly to an extent of 50 % of the

monoclonal antibody by this changing the matrix properties and (2) the newly implemented microwave technical setup as described in the materials and methods section. The authors assume that the increase in batch homogeneity within MFD samples was mainly due to the change in machinery setup. This is believed because: Firstly, similar formulations with the same mAb have been dried with the previously described MFD setup⁸¹ and they revealed the same high deviations that have been observed with the low concentrated mAb formulations F1-F3 in this study (Table SIII-1).

Secondly, with typical sample sizes of $n = 3$ potential batch inhomogeneities were observable. Thirdly, the semiconductor solid-state setup led to a more stable and better tuneable power input during the course of drying. Supportively, Bianchi et al.¹³⁵ simulated the physical behavior of apple slices under microwave-assisted vacuum drying processing comparing magnetron and solid-state technology. They concluded that with the latter an improved heating pattern uniformity can be achieved.

With regard to X-ray diffraction analysis, all formulations revealed an XRD-amorphous solid state exhibiting an amorphous halo (Figure SIII-1 – Figure SIII-3). By that, the authors suppose no adverse effect of microwaves on the crystallization tendency of the investigated matrices. Even moister samples have not revealed any indication of recrystallization.

III.5.2 Stability with regard to the protein

The sucrose-based formulation with 5 g/L of mAb1 (F1) showed no clear trend in subvisible particles (LO) at 4°C and 25°C storage temperature (Figure III-3a) and no difference between CFD and MFD either. Only directly after the freeze-drying procedure an increase of 94 % (4300 ± 546) and 49 % (3303 ± 651) for cumulative particles $\geq 1 \mu\text{m/mL}$ for CFD and MFD, respectively, was observed. Figure III-3b shows that storage over 24 weeks at 40 °C caused an increase by factor 2.3 (5106 ± 237) for conventionally FD and an increase of 36 % (3003 ± 1058) for microwave-assisted FD in $\geq 1 \mu\text{m}$ particles. It was expected that this slight change in SvP at accelerated storage conditions may correlate with an increase in the relative amount of high molecular weight species assessed by HP-SEC. However, no such effect on SEC data was seen (Figure SIII-4). Across all storage temperatures and regardless of the used drying protocol no change in neither soluble aggregates nor loss of monomer was observed.

For the trehalose-based formulation (F2) the more sensitive flow-imaging microscopy technique was used for subvisible particle determination (Figure III-4). Initially, low particle

counts per mL of 1867 ± 1784 , 90 ± 20 and 20 ± 35 for $\geq 1 \mu\text{m}$, $\geq 10 \mu\text{m}$, and $\geq 25 \mu\text{m}$, respectively, were found, but yet bearing unusual high variances. Directly after freeze-drying, most likely due to freeze-drying associated stresses⁴, a slight increase by 24 % (2320 ± 599) and 37 % (2549 ± 677) for cumulative particles $\geq 1 \mu\text{m/mL}$ was observed. No significant changes were observed for SvP at 4 °C storage temperature (Figure III-4a). Taking chromatographic results into account, nor in HP-CEX (Figure III-7a+b) neither HP-SEC (Figure III-7c) changes were observed emphasizing sufficient and comparable stabilization in both drying populations at 4 °C. In contrary, a dramatic increase for subvisible particles $\geq 1 \mu\text{m/mL}$ was found over the course of six months at 40 °C for both CFD (37909 ± 4337) and MFD (18947 ± 6753) as shown in Figure III-4b. A similarly pronounced increase was also for bigger particles observable, although high standard deviations lowered significance. Yet, an upward trend was assumed for subvisible particles $\geq 10 \mu\text{m/mL}$ in conventionally processed samples. With respect to chemical degradation (Figure III-7b), a linear increase with shallow slope was found for both acidic and basic species irrespective of the drying procedure, although basic species increased slightly more in CFD samples. An increase in the different species can be related to several different changes within the protein molecule depending on primary structure, cell line, formulation conditions, and so forth¹³⁶⁻¹³⁸. Reviewed by Du et al.¹³⁶ in 2012, a major contribution to acidic species was assigned to the deamidation reaction of asparagine residues. For basic species, depending on primary structure, they were discussing different causes covering C-terminal basic amino residues, incomplete cyclization of the N-terminal but also the formation of aggregates. It could be suspected that the stronger increase in high molecular weight aggregates (Figure III-7c) at 40 °C in CFD samples is related to the stronger rise of basic species in HP-CEX data. However, no follow-up investigation by (partial) protein digestion or by LC-MS was conducted. Nonetheless, as differences between conventionally dried and microwave-assisted freeze-dried samples were rather marginal, comparable stability in the trehalose formulation is deduced.

Arginine phosphate as discussed in section III.5.1 was expected to be an exceptional formulation, especially challenging when drying with electromagnetic waves. In a recently published review by Stärtzel¹³⁹ several examples of successful stabilization of proteins by arginine salts in the glassy state were shown. Within our study, we found only tiny changes at refrigerator temperature with regard to subvisible particles (Figure III-5a). Primarily the mean values for bigger sized particles ($\geq 10 \mu\text{m}$ and $\geq 25 \mu\text{m}$) increased after 24 weeks of storage, yet not significantly due to higher variances. HP-CEX data (Figure III-8a) and HP-SEC data

(Figure III-8c) supported this. Only slight degradation shown by relative monomer loss of less than 1 % in both CFD and MFD and a small increase in basic species of less than 2 % were found at 4 °C. At accelerated storage conditions (Figure III-5b) a moderate increase in all size categories was seen. Especially the conventionally freeze-dried sample showed a significant increase for cumulative particle counts $\geq 1 \mu\text{m}$, $\geq 10 \mu\text{m}$ and $\geq 25 \mu\text{m}$ with factors of 3x to 6x higher counts after six months of storage. In contrast, the microwave-assisted freeze-dried sample at the same conditions showed only a moderate increase by bigger particles $\geq 10 \mu\text{m}$ and $\geq 25 \mu\text{m}$. Connecting that to the HP-CEX data (Figure III-8b), a contrary picture is drawn. On the one hand, a noticeable change in acidic species by 15.9 % (CFD) and 26.6 % (MFD) at 40 °C storage temperature was found, whereas basic species remained almost the same for both drying procedures. On the other hand, HP-SEC data (Figure III-8c) revealed a loss in monomeric content down to 95.7 % \pm 0.4 % and 96.8 % \pm 0.3 % for CFD and MFD, respectively. Taking all of that into account it appeared that the conventionally dried sample showed a higher degree of degradation exhibiting a higher increase in high molecular weight aggregates accompanied by an increased particle count in flow-imaging microscopy. However, HP-CEX results indicated that a moderate portion of the main charge variant underwent chemical reactions leading to significantly increased acidic species, being more pronounced in MFD samples. Stärtzel et al.¹³⁴ investigated different arginine salts on their stabilizing potential in the glassy state. For that, they also calculated the relaxation time τ^β “which may be regarded as proportional to the inverse of molecular mobility for global motions” (Abdul-Fattah et al., 2007)¹⁴⁰. Subsequently, they related physical aggregation rate constants at 40 °C with the estimated $\ln(\tau^\beta)$. They found that an arginine phosphate formulation (64 g/L L-Arg, 16 g/L sucrose and 50 g/L mAb) revealed longer relaxation times than other arginine formulations. These relaxation times unexpectedly had an inversely proportional correlation to the observed aggregation constants by that, suggesting that increased molecular mobility had a positive effect on protein stability.¹³⁴ This may be one explanation for the stability differences observed between CFD and MFD. Microwave-assisted freeze-dried samples on average revealed higher residual moisture content (Figure III-2c) compared to CFD. Residual water is known as a plasticizer of amorphous matrices which consequently also leads to increased molecular mobility¹⁴¹ and by this potentially to reduced aggregation in an arginine-based system as reported by Stärtzel et al.¹³⁴. However, increased molecular mobility may be associated with increased chemical degradation^{142,143} giving a potential explanation to the more distinct increase in acidic species MFD samples. Another explanation could be based on an advantageous effect

of the partial collapse in MFD samples as it was observed by Schersch et al.¹⁴⁴ for partially collapsed mannitol-sucrose formulation. All in all, microwave-assisted lyophilizates with arginine phosphate, on the one hand, revealed an indication for more pronounced chemical degradation but on the other hand, showed a less severe increase in subvisible particles and aggregates. The authors, therefore, conclude a comparable stability profile for CFD and MFD with reservations.

For the high concentration mAb2 formulation (F4) no clear trend can be derived from subvisible particle analysis. Unexpectedly, particle counts at refrigerator temperature appeared to be higher or at a similar level compared to 40 °C after six months (Figure III-6). With regard to HP-CEX results, no difference between conventionally and microwave-assisted freeze-dried samples was observed (Figure III-9a+b). In size-exclusion chromatography, samples stored at 4 °C exhibited a negligibly small loss of monomer for both drying protocols. At accelerated conditions still a rather low loss in monomeric species of 1.4 % and 1.7 % for CFD and MFD, respectively, was seen after six months of storage. For this reason, the authors conclude that both sample populations derived from the two respective drying protocols were comparable with respect to protein stability.

In the future, an improved prototype dryer with a sophisticated technical setup which provides the operator with standard pharmaceutical freeze-drying features such as freezing and stoppering within the same machine is needed. A combination of current pharmaceutical freeze-drying equipment with modern semiconductor solid-state microwave generators is imaginable in the authors' opinion. For future experiments, a look into relaxation behavior and potential differences between conventionally freeze-dried and microwave-assisted freeze-dried solids could be of interest. Thermal history is expected to be different. Moreover, a deeper look into potential chemical changes that may occur during MFD should be taken. For those analytical techniques focusing on structural changes like FT-IR and circular dichroism, but also methods like (peptide mapping) LC-MS should be considered.

III.6 Conclusion

Microwave-assisted freeze-drying is an emerging technique recently introduced to the field of pharmaceutical freeze-drying of biologicals.^{81,105} Despite potentially huge time savings for vial-based drying achievable by MFD⁸¹, we were able to elucidate comparable stability profiles for different monoclonal antibody formulations over storage times of 24 weeks. Although residual moisture contents were found to be different between CFD and MFD, no adverse effect on protein stability or crystallization tendency in matrices with higher residual moisture was found. Even the occurrence of a microscopic collapse in the microwave-processed arginine phosphate mAb formulation (F3) did not lead to decreased stability with respect to the solid state- and protein-related properties. Moreover, our data indicate that with modern semiconductor solid-state microwave generators batch homogeneities of microwave batches could be approximated to those of conventional freeze-drying. However, the authors see a definite need for new machines complying with the requirements of pharmaceutical manufacturing. The new generator setup presented may open up space for engineering creativity to merge pharmaceutical needs with innovative heating technique.

Acknowledgments

The support from the Global Technology Management of Boehringer Ingelheim Pharma GmbH & Co. KG is kindly acknowledged. In addition, the authors thank Peter Püschner, Michael Eggers, and Mirko Diers from Püschner GmbH & Co KG for technical support with the microwave vacuum dryer experiments.

Conflicts of Interest

The authors declare no conflict of interest. R.G. and I.P. are full-time employees of Boehringer Ingelheim Pharma GmbH & Co. KG. The funders had no role in the design of the study; in the collection, analyses, or interpretation of data; in the writing of the manuscript, or in the decision to publish the results.

III.7 Supplementary material

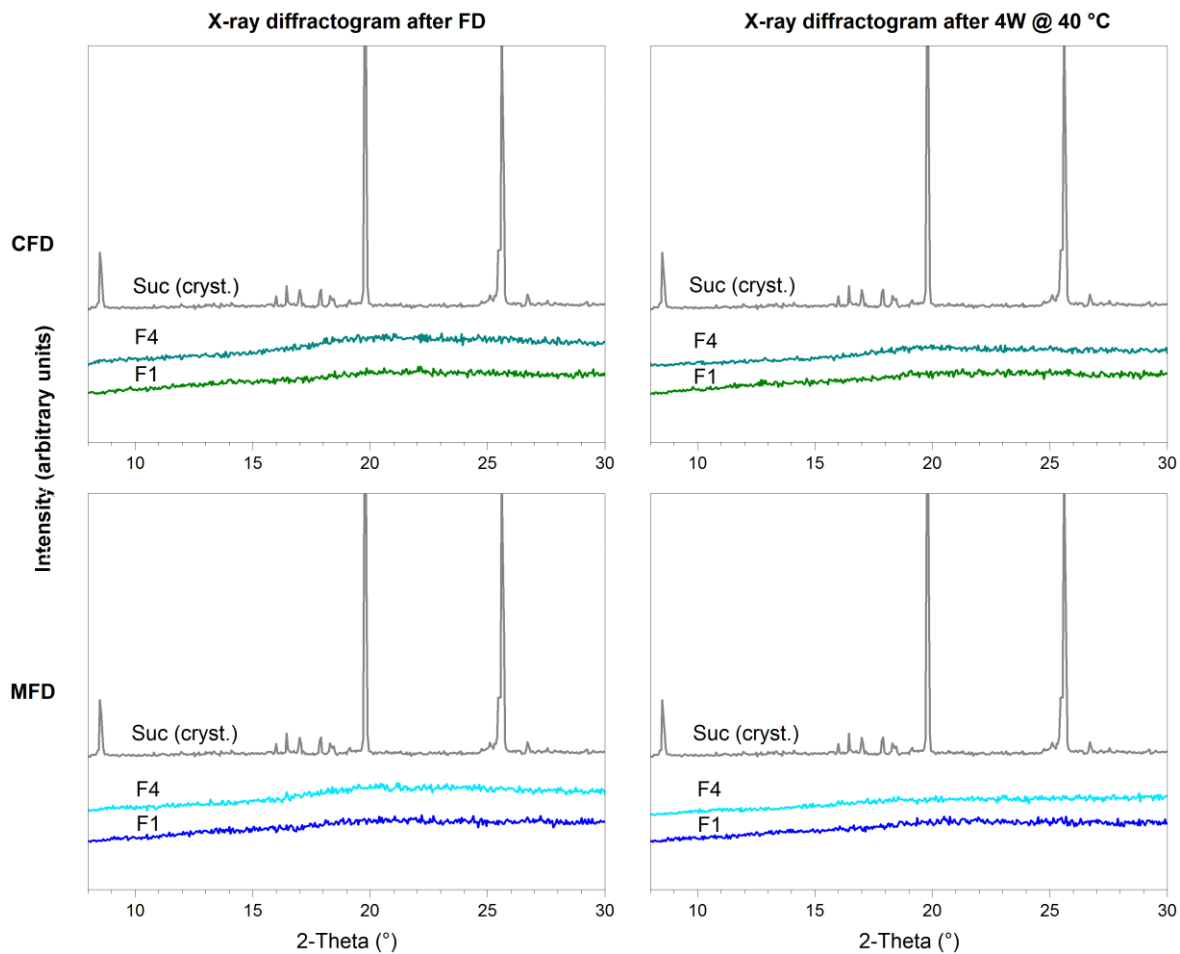


Figure SIII-1 Representative X-ray diffractograms of sucrose-based formulation F1 and F4 compared to unprocessed pure crystalline sucrose (EMPROVE® exp sucrose) from the shelf. Top graphs represent conventionally freeze-dried samples directly after FD (left) and after 24 weeks of storage at 40 °C (right). The same applies to the bottom graphs but with microwave-assisted freeze-dried samples.

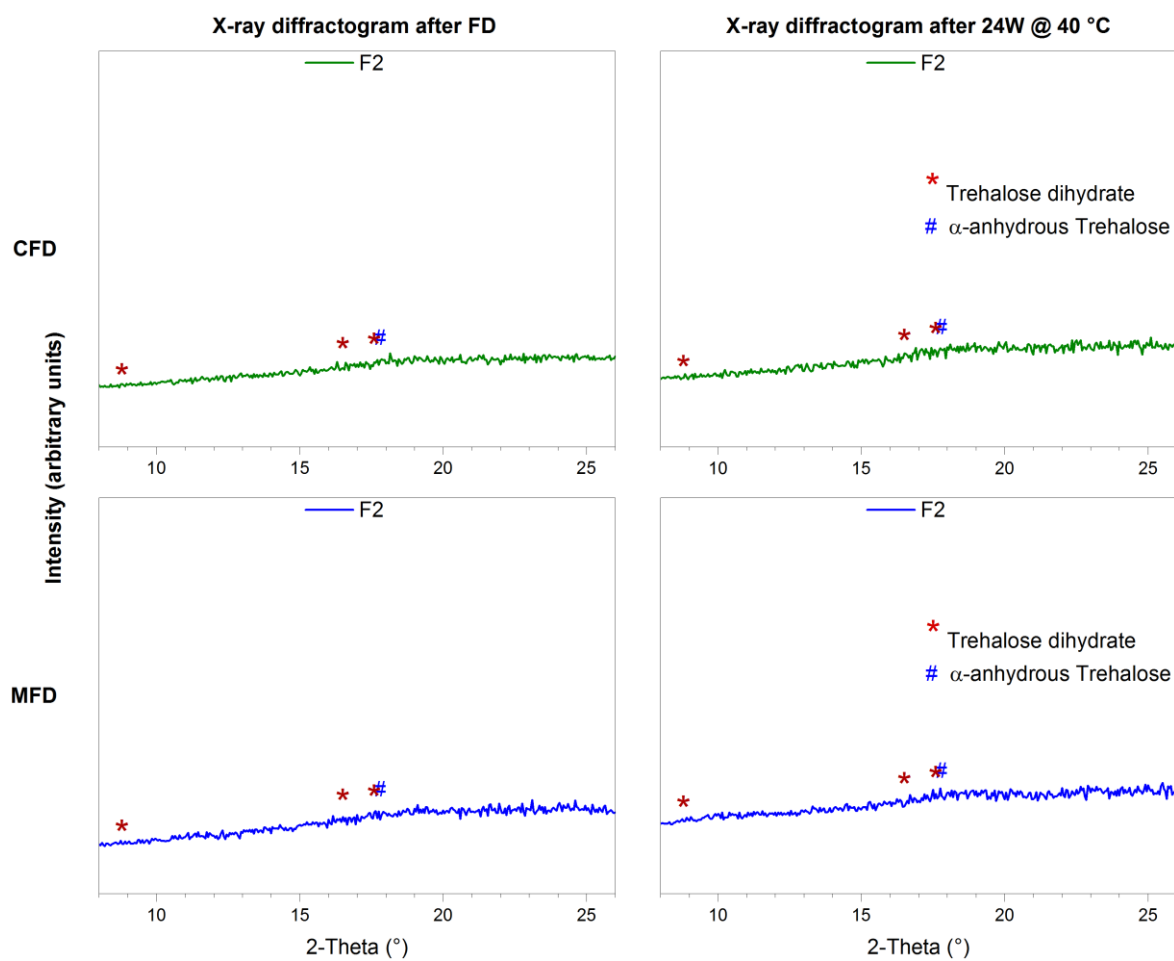


Figure SIII-2 Representative X-ray diffractograms of trehalose-based formulation F2 marked with typical peaks related to trehalose dihydrate (asterisk) and α -anhydrous trehalose (hash) obtained from the literature ¹²¹. Top graphs represent conventionally freeze-dried samples directly after FD (left) and after 24 weeks of storage at 40 °C (right). The same applies to the bottom graphs but with microwave-assisted freeze-dried samples.

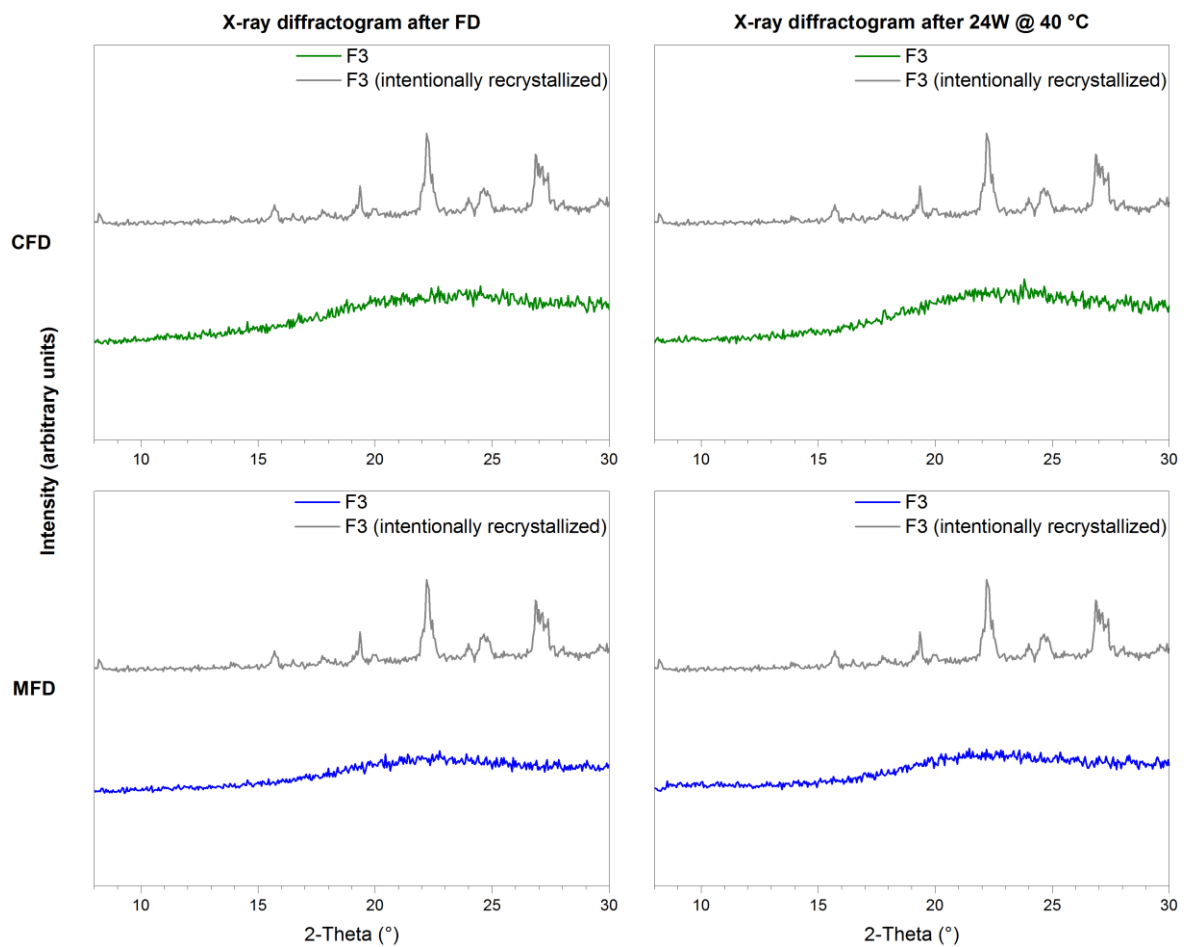


Figure SIII-3 Representative X-ray diffractograms of low concentration mAb formulation with arginine phosphate (F3). The diffractogram of a MFD recrystallized sample of identical composition (gray line) was used for the identification of reference peaks. Top graphs represent conventionally freeze-dried samples directly after FD (left) and after 24 weeks of storage at 40 °C (right). The same applies to the bottom graphs but with microwave-assisted freeze-dried samples.

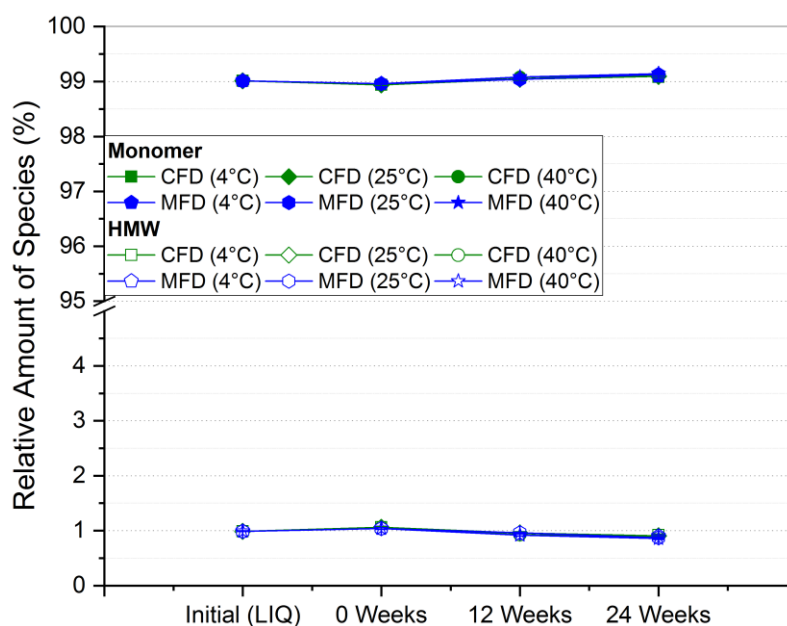


Figure SIII-4 Relative percentages of monomer and high molecular weight species (HMW) at the respective storage temperature over storage time gained by HP-SEC analysis are presented.

Table SIII-1 Residual moisture content from two similar mAb2 formulations produced with the previous microwave setup⁸¹ compared to F4.

Formulation	Residual moisture content \pm standard deviation (n=3) [%]
F4.1: 40 g/L mAb2 + 6% (w/V) sucrose ^a	1.2 \pm 0.7
F4.2: 60 g/L mAb2 + 4% (w/V) sucrose ^a	1.2 \pm 1.1
F4	0.4 \pm 0.0

^a The formulation was buffered with a 10 mM histidine buffer pH 6.0

Relative standard deviations of 58 % and 92 % were found for F4.1 and F4.2, respectively. In strong contrast to that, F4 revealed variances and derived standard deviations which were in the same order of magnitude as those for CFD samples.

Chapter IV A comparison of controlled ice nucleation techniques for freeze-drying of a therapeutic antibody

This chapter is published as:

Gitter, J. H.¹, Geidobler, R.², Presser, I.² & Winter, G.¹ A Comparison of Controlled Ice Nucleation Techniques for Freeze-Drying of a Therapeutic Antibody. *J. Pharm. Sci.* 107, 2748–2754 (2018).

¹ Ludwig-Maximilians-Universität München, Department of Pharmacy, Pharmaceutical Technology and Biopharmaceutics, Butenandstr. 5, 81377 Munich, Germany

² Boehringer Ingelheim Pharma GmbH & Co. KG, Birkendorfer Str. 65, 88307 Biberach an der Riß, Germany

Author contributions:

Conceptual guidance, I.P. and G.W.; Data curation, J.H.G.; Formal analysis, J.H.G.; Funding acquisition, G.W.; Investigation, J.H.G.; Methodology, J.H.G.; Project administration, J.H.G., R.G., I.P. and G.W.; Resources, R.G., I.P., and G.W.; Supervision, R.G., I.P., and G.W.; Validation, J.H.G.; Visualization, J.H.G.; Writing—Original draft, J.H.G.; Writing—Review & editing, R.G., I.P., and G.W.

Note from the author:

The version included in this thesis is identical to the published article apart from minor changes. The reference, figure, and table numbers were changed to fit into the coherent numbering of this document.

The published article can be accessed online via:

<https://doi.org/10.1016/j.xphs.2018.07.019>

IV.1 Abstract

The aim of this study was to investigate if mechanistically different controlled ice nucleation techniques in freeze-drying are comparable to each other with respect to drying process performance and product quality attributes. Therefore, we studied three different model formulations including amorphous (sucrose, trehalose) and semi-crystalline (mannitol:sucrose 4:1) solids containing a monoclonal antibody IgG₁ (5 g/L) processed either by application of ice fog or depressurization technique setting an ice nucleation temperature of -5 °C. Subsequently, the same freeze-drying protocol on identical machinery was applied. The results showed that the techniques are comparable with respect to the thermal history of product temperature sensors and primary drying time, solid state- and protein-related product quality attributes. All analytics comprising Karl Fischer titration, XRD, and BET as well as HP-SEC, turbidity, and subvisible particle counting using flow-imaging microscopy exhibited similarity and comparability among the controlled nucleation protocols.

Keywords

Freeze-Drying; Lyophilization; Protein; monoclonal antibody; Excipients; Drying; Solid-state; Amorphism; X-ray powder diffraction (XRD)

Abbreviations

CN	Controlled ice nucleation
FD	Freeze Drying
FNU	Formazine nephelometric units
HP-SEC	High-performance size-exclusion chromatography
HPW	Highly purified water
MWCO	molecular weight cutoff
p_{chamber}	Chamber pressure
PES	polyethersulfone
SSA	Specific surface area
TN	Ice nucleation temperature
TShelf	Shelf Temperature
XRD	X-ray diffraction

IV.2 Introduction

Freeze-Drying (FD) is a well-established drying process for the stabilization of biologics. However, long drying times^{97,145} and challenges in transferability from the laboratory to pilot or production scale^{41,67,113} are typical shortcomings of FD that increase the production costs. Controlling the ice nucleation temperature (T_N) during freezing is a potential approach to overcome these downsides.^{40,43,55,146} Currently, there are three mechanistically different controlled ice nucleation (CN) techniques on the market which either (1) utilize ice seeds from a generated ice fog as primary nucleation sites^{41,44-47}; or (2) apply an overpressure which is rapidly released, leading presumably to cooling of liquid product surface by the expansion of gas, and inducing hereby ice nucleation^{51,146}; or (3) techniques which utilize vacuum-induced surface freezing by forming an ice layer due to local supercooling¹⁴⁷. Recently, the application of controlled nucleation is getting consistent attention due to its benefits in terms of improving lyophilization process performance^{40,43,55,146} and enhancing product quality attributes of the protein drug product^{40,43,55-58}. Today there are already several commercially available devices for CN, and such processes are on the way to be submitted to the authorities for new biological entities. One major reason may be the lack of knowledge about the comparability of mechanistically different CN techniques in regards to process performance and quality of the resulting product. In fact, this puts transferability into question when different controlled ice nucleation techniques are used in different development stages.

With our study, we aim to reduce this knowledge gap. We apply either ice fog or depressurization at the same T_N during freezing of pharmaceutically relevant formulations that contain a model monoclonal antibody. Subsequently, we investigate process performance and product quality attributes of the resulting lyophilizates. Moreover, we compare the results obtained for the controlled nucleation protocols to a random nucleation reference batch.

IV.3 Materials and methods

IV.3.1 Materials

A monoclonal IgG type 1 antibody (mAb) was kindly provided by Boehringer Ingelheim Pharma GmbH & Co. KG (Ingelheim am Rhein, Germany).

ACS certified D(+)-Sucrose was purchased from Sigma-Aldrich (Steinheim, Germany). D(+)-Trehalose dihydrate (min. 99 % purity) and Ph. Eur. certified D(-)-Mannitol were obtained from VWR International BVBA (Leuven, Belgium). L-Histidine monohydrochloride monohydrate (min. 99 % purity) and L-Histidine (Cell culture reagent) were purchased from Alfa Aesar (Karlsruhe, Germany). Di-sodium hydrogen phosphate dihydrate and sodium dihydrogen phosphate dihydrate were obtained from AppliChem (Darmstadt, Germany). Sodium chloride was purchased from Bernd Kraft (Duisburg, Germany). Ph. Eur. certified Tween 80® and sodium hydroxide was obtained from Merck KGaA (Darmstadt, Germany). For the preparation of buffers and stock solutions, highly purified water (HPW; Purelab Plus, USF Elga, Celle, Germany) was used.

All excipients had analytical or higher grade and were used without further purification.

IV.3.2 Preparation of formulations

The mAb was dialyzed and concentrated using a cross-flow filtration cassette Vivaflow 50 with polyethersulfone (PES) membrane (MWCO 30,000 Da; Sartorius AG, Goettingen, Germany) by adding a 10-time excess of 10 mM histidine buffer (pH 6.0). After reaching the desired volume, the concentration of the mAb was measured with a NanoDrop™ 2000 UV photometer (Thermo Scientific, Wilmington, Delaware) at 280 nm using an extinction coefficient of $\epsilon^{0.1\%} = 1.49 \text{ g}/100 \text{ mL}^{-1} \text{ cm}^{-1}$. To ensure reproducible starting conditions, identical aliquots of dialyzed mAb and excipient stock solutions were frozen at -80 °C and thawed overnight at refrigerator prior to the respective freeze-drying run. Formulations were prepared according to the composition shown in supplementary data (Table SIV-1). All formulations were filtered using 0.2 µm PES membrane syringe filters (VWR International, Radnor, PA, USA) prior to filling of the vials. 2.3 mL of each formulation was filled in 10R tubing vials (MGLas AG, Muennerstadt, Germany) and semi-stoppered with lyophilization stoppers (FluroTec® rubber stopper, West Pharmaceuticals, Eschweiler, Germany). Vials were arranged in the center of a lyophilization tray and surrounded with two rows of 10 % (w/v) sucrose shielding vials. Corresponding T_g' values for the sucrose and trehalose formulation can be found in the supplementary data (Table SIV-2).

IV.3.3 Freeze drying process

All samples were freeze-dried using a Christ ε2-12D pilot-scale freeze dryer (Martin Christ, Osterode am Harz, Germany) which is capable of applying both ice fog and depressurization

ice nucleation technique. For the respective sample population, one of the freeze-drying protocols listed in Table IV-1 was applied. Product temperature was measured by wireless product temperature measurement probes (WTMplus, Martin Christ, Osterode am Harz, Germany). Secondary drying hold time was kept longer for controlled nucleation protocols in order to achieve acceptable low final residual moisture contents comparable to random nucleation processes.

By reaching the end of secondary drying, the product chamber was backfilled with nitrogen to approximately 600 mbar. Vials were fully stoppered by the hydraulic press. Samples were crimped and kept refrigerated until analysis.

Table IV-1 Overview of the applied freezing and drying protocols.

Protocol	Setpoint	Freezing			Primary Drying	Secondary Drying		
Random	T _{Shelf} [°C]	20	-5	-50	-20	5	35	
	Ramp [K/min]	-	1	1	1	0.15	0.3	
	Hold time [min]	10	60	120	2700	-	420	
	p _{Chamber} [mbar]	-	-	-	0.1	0.05	0.05	
Ice Fog^a	T _{Shelf} [°C]	20	-5	-5	-50	-20	5	35
	Ramp [K/min]	-	1	-	1	1	0.15	0.3
	Hold time [min]	10	55	60	120	1380	-	540
	Stabilization time [min]	-	5*	-	-	-	-	-
	p _{Chamber} [mbar]	-	15*	-	-	0.1	0.05	0.05
Depressurization^b	T _{Shelf} [°C]	20	-5	-5	-50	-20	5	35
	Ramp [K/min]	-	1	-	1	1	0.15	0.3
	Hold time [min]	10	55	60	120	1380	-	540
	Stabilization time [min]	-	5*	-	-	-	-	-
	p _{Chamber} [mbar]	-	2200*	-	-	0.1	0.05	0.05

The stabilization time and pressure setpoint marked with an asterisk were applied after the hold time stated in the same section. Settings for the respective ice nucleation technique were as follows: ^a Ice Fog: chamber pressure was set to 15 mbar ± 1.5 mbar with a stabilization time of 5 minutes and a subsequent introduction of ice crystals in the chamber by aeration through the ice condenser utilizing the external volume of the LyoCoN (Martin Christ, Osterode am Harz, Germany). ^b Depressurization: chamber was pressurized to 2.2 bar ± 0.15 bar absolute pressure with pressurized air and nitrogen with a stabilization time of 5 minutes and a subsequent rapid pressure release to introduce controlled nucleation.

IV.3.4 Residual moisture content

Karl Fischer titration was used to determine residual water content after freeze-drying. Between 15 and 50 mg of sample aliquots were prepared in a glove box filled with pressurized air with a relative humidity of less than 10 %, filled into 2R vials and stoppered.

The samples were then placed in an oven at 100 °C to enable the fast extraction of water. The headspace moisture is transported into a coulometric Karl Fischer titrator (Aqua 40.00, Elektrochemie Halle, Halle (Saale), Germany). Results are calculated in relative water content (*w/w*).

IV.3.5 Specific surface area

The specific surface area of dried samples was determined using Brunauer–Emmet–Teller (BET) krypton gas adsorption in a liquid nitrogen bath at 77.3 K (Autosorb 1; Quantachrome, Odelzhausen, Germany). 80 – 140 mg of a sample was gently crushed with a spatula and weighed into glass tubes. Prior to measurement, an outgassing step was performed for at least 6 h at room temperature. An 11-point gas adsorption curve was measured, covering a p/p_0 ratio of approximately 0.05–0.30. Data evaluation was performed according to the multi-point BET method fit of the Autosorb 1 software.

IV.3.6 X-ray powder diffraction

To determine the solid state of the lyophilizates an XRD 3000 TT diffractometer (Seifert, Ahrensburg, Germany) was used. The device is equipped with a copper anode (40 kV, 30 mA) and has a wavelength of 0.154178 nm. The scintillation detector voltage was 1000 V. The samples were placed on the copper sample holder and analyzed in the range of 5-45° 2-theta with steps of 0.05° 2-theta.

IV.3.7 Reconstitution of lyophilizates

The lyophilized cakes were reconstituted by the addition of HPW. The HPW volume for each formulation was calculated to match the volume of the water removed during freeze-drying. Reconstitution time was determined by recording the time between adding the respective formulation-specific volume of HPW and obtaining a clear solution without visible matter. This observation was performed by visual inspection. Reconstitution was performed by applying gentle swirling for 5 s directly after the addition of water.

IV.3.8 High-performance size exclusion chromatography (HP-SEC)

To determine relative monomer content and the relative amount of soluble aggregates HP-SEC was used. The separation was performed on a Waters 2695 Separation module (Waters

GmbH, Eschborn, Germany) with a Tosoh TSKgel G3000 SWxl column (Tosoh Bioscience, Griesheim, Germany) using a Waters 2487 Dual λ Absorbance Detector (Waters GmbH, Eschborn, Germany) at 214 and 280 nm. 10 μ L of reconstituted formulation with a final concentration of 5 g/L was injected and separated using a 50 mM PBS running buffer containing 300 mM sodium chloride (pH 7.0) with a flow rate of 0.7 mL/min. Samples were measured as triplicates with three individual injections. Data integration of relative areas was performed using Chromeleon 6.80 (Thermo Scientific, Wilmington, USA). An example chromatogram is shown in supplementary data (Figure SIV-1).

IV.3.9 Flow-imaging microscopy

Subvisible particles were analyzed using a FlowCAM® 8100 (Fluid Imaging Technologies, Inc., Scarborough, ME, USA) equipped with a 10x magnification cell (81 μ m x 700 μ m). Prior to a measurement set, the cell was cleaned with a 1 % Hellmanex III solution and HPW. For adjustment of the focus, the default autofocus procedure using 20 μ m calibration beads was performed. 150 μ L sample solution was measured with a flow rate of 0.10 mL/min, an image rate of 29 frames per second, and an estimated run time of 1.5 minutes. After each measurement, the flow cell was flushed with HPW. For particle identification, the following settings have been used: 3 μ m distance to the nearest neighbor, segmentation thresholds for dark pixels, and light pixels of 13.0 and 10.0, respectively. Frames were collected with VisualSpreadsheet® 4.7.6 software and were evaluated for total particle counts of cumulative particles greater or equal to 1 μ m, 10 μ m, and 25 μ m per mL.

IV.3.10 Turbidity

The turbidity of samples was measured as scattered laser light ($\lambda = 860$ nm) detected at an angle of 90 ° using a Hach Lange Nephla nephelometer (Hach Lange GmbH, Düsseldorf, Germany). 2.0 mL sample was gently pipetted in turbidity glass cuvettes free of particles with a flat bottom and placed into the device. The result is given in FNU (Formazine nephelometric units).

IV.3.11 Statistical tests

To determine variance homogeneity a Levene's test was performed. Statistical differences between the means of the different applied freezing protocols were analyzed using either a

one-way ANOVA-test or a Student's t-test between two means. In all statistical tests, differences were considered statistically significant for $p \leq 0.05$.

IV.4 Results and discussion

IV.4.1 Process performance

IV.4.1.1 Nucleation and drying process

Based on observations by the LyoCam¹⁴⁸, it could be seen that with both controlled ice nucleation techniques, i.e. ice fog (Video 1)¹ and depressurization (Video 2)¹ nucleation starts at the surface and slowly propagates bottom-down.

The actual freeze-drying cycles for random nucleation and both CN methods are shown in Figure IV-1A and C, respectively. In order to produce pharmaceutically elegant cakes, an established standardized cycle applicable to various formulations in one run was performed. This cycle was adjusted to the sucrose formulation which is most prone to collapse due to its low T_g '. The Random nucleation process resulted in 62 h total drying time, which could be shortened to approximately 42 h by reducing primary drying time by 19 h (Figure IV-1A, bracket a) to overall 26 h time needed for sufficient sublimation as determined by wireless product temperature probes and differential pressure comparison. The processes in which depressurization and ice fog have been applied ended up with total drying times of 43 h, whereof 22 h were primary drying time. As secondary drying was kept longer in controlled nucleation samples and as settings for primary drying were kept the same among all processes, only a reduction of roughly 14 % of primary drying time was found compared to the reference process. However, process time optimization was not the main focus of this work, the reader interested in drying performance improvement by controlled ice nucleation is referred to the literature^{40,43,55,57,146}. Nonetheless, independent of the applied controlled ice nucleation technique, the thermal history of the product, and the temperature profile of the respective formulations as well as the time to reach a pressure difference of 0 μ bar (Pirani vs. capacitance gauge) were found to be similar. The same was true for the nucleation behavior which is shown in Figure IV-1B and D for random nucleation and the controlled ice nucleation techniques, respectively.

¹ The videos can be accessed via <https://www.sciencedirect.com/science/article/pii/S0022354918304544#ec2>

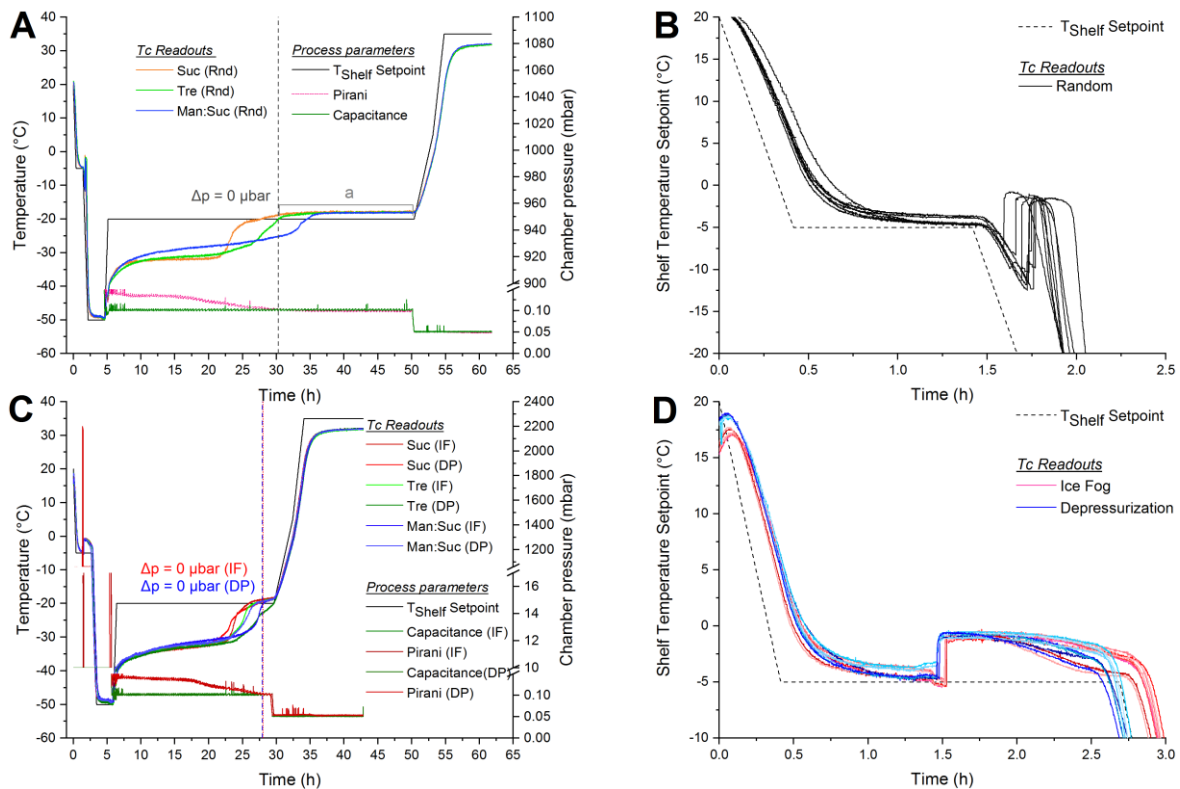


Figure IV-1 Freeze-drying process graphs of **A** random shelf-ramp freezing and **C** ice fog and depressurization. The thermocouples were placed in the formulations (Suc: sucrose, Tre: trehalose, Man:Suc: manitol:sucrose) for the respective freezing protocol (Rnd: random nucleation; IF: ice fog; DP: depressurization). Bracket **a** is described in the main text. Product temperature profiles representing the nucleation behavior during freezing for **B** random shelf-ramp freezing and **D** the controlled ice nucleation protocols are shown. A small time shift between ice fog (red lines) and depressurization (blue lines) protocol is observable which is caused by the slightly different times needed for reaching the desired chamber pressure for the respective nucleation approach.

A small time lag between the two controlled nucleation approaches was observable which was due to technical conditions related to the time needed to evacuate or pressurize the chamber to the desired value. However, regardless of the CN approach, all vials were found to nucleate at the same time within one batch, whereas random nucleated vials show different degrees of super-cooling during freezing.

IV.4.2 Solid state properties

IV.4.2.1 Residual moisture content and specific surface area

We found identical values for SSA in the two amorphous model formulations with either sucrose or trehalose (Figure IV-2A). The same is true for residual moisture which was identical for sucrose and only marginally different for trehalose (1.1 % vs. 1.0 % for ice fog vs. depressurization, respectively). Due to the higher specific surface area which facilitates desorption during secondary drying⁷⁵, random nucleated samples ended up with lower

residual moisture (0.69 % and 0.33 % for sucrose and trehalose, respectively). In contrast, mannitol-containing formulations only differ slightly in residual moisture content (0.43 % vs. 0.52 % or 0.50 % for random vs. ice fog or depressurization, respectively), but show different specific surface areas. Contrary to the expectations the application of controlled ice nucleation to mannitol:sucrose formulations resulted in the formation of larger SSA (38 % and 45 % increase for ice fog and depressurization in comparison to random, respectively), which was seen for this formulation in previous FD experiments applying controlled ice nucleation (Supplementary data, Figure SIV-2). This indicates a certain formulation-dependence for the semi-crystalline model system of the effect of CN on residual moisture and SSA.

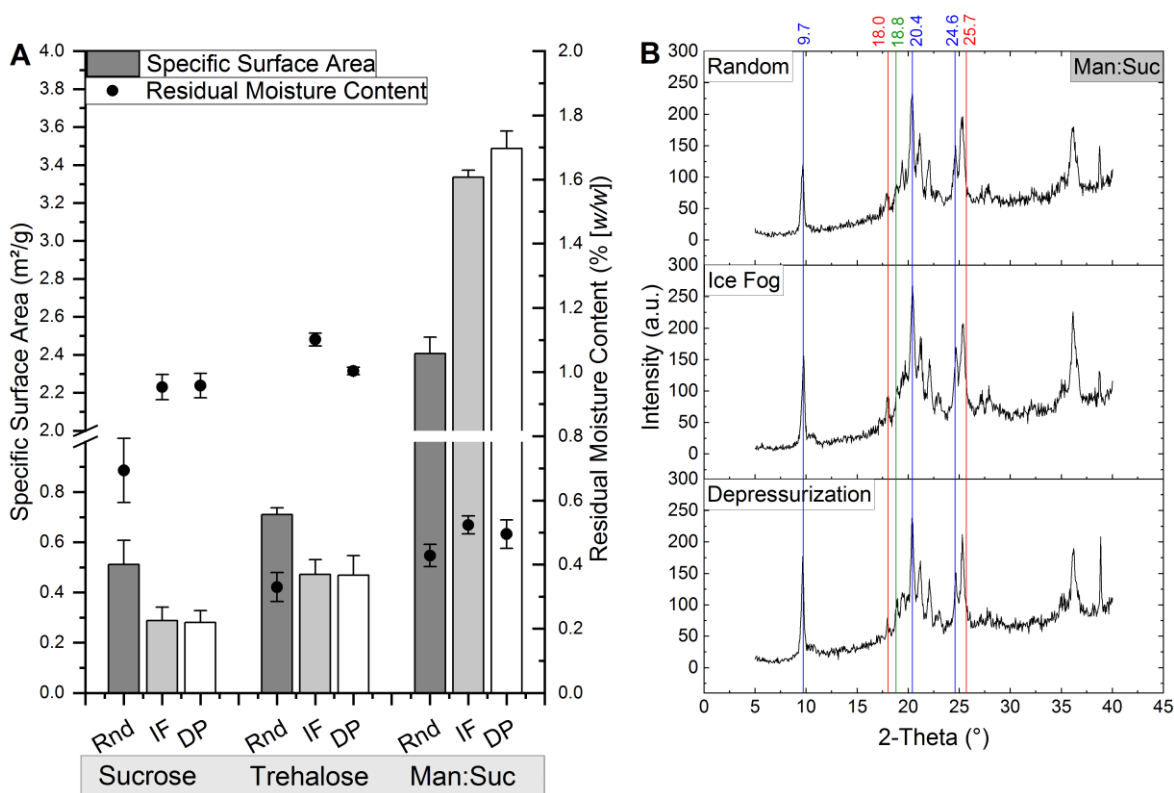


Figure IV-2 **A** Specific surface area (bars) and residual moisture content (circles) for the three different formulations and the applied freezing protocols (Rnd: random nucleation; IF: ice fog; DP: depressurization). **B** X-ray diffractograms of semi-crystalline mannitol:sucrose formulations for the respective freezing protocol with characteristic markers taken from the literature¹⁴⁹ for δ -mannitol, β -mannitol or mannitol hemihydrate at 9.7°, 20.4° and 24.6° (blue) or 18.8° (green) or 18.0° and 25.7° (red) 2-Theta, respectively. The shown values represent the mean of measurements from three different vials. Error bars indicate the standard deviation of the mean.

IV.4.3 XRD

Over the range of all applied freeze-drying protocols sucrose and trehalose formulations resulted in fully amorphous solids represented by an amorphous halo (Supplementary data,

Figure SIV-3). Model systems with mannitol contained a major fraction of δ -mannitol (Figure IV-2B, blue lines), a minor fraction of β -mannitol (Figure IV-2B, green line), and a minor fraction of mannitol hemihydrate (Figure IV-2B, red lines) independent of the freezing protocol. It is of particular interest, that exactly the same diffraction pattern and consequently the same crystalline modifications among the different freezing protocols were found. Due to a missing thermal treatment, metastable crystalline modifications like mannitol hemihydrate formed. Although this is not desired, annealing was not considered as an option for our approach. It potentially changes crystalline modifications. Moreover, annealing would have masked the generation and preservation of particularly thermodynamically unstable mannitol modifications.¹⁵⁰ As annealing also allows at the same time for further Ostwald ice ripening, it consequently would have distorted our results. In fact, potential differences which would be obtained by the application of ice fog and depressurization would have been leveled out by annealing.

IV.4.4 Protein analysis

IV.4.4.1 Reconstitution time

One reason to apply controlled ice nucleation is the potential reduction of reconstitution times.^{55,57} For the investigated formulations a time reduction was found in trehalose and mannitol:sucrose formulations, but not for sucrose-based lyophilizates (Supplementary data, Figure SIV-4). For trehalose, the effect was rather small with a reduction from 34 s for random nucleated samples to 18 s and 21 s after ice fog and depressurization, respectively. Semi-crystalline systems containing an excess of mannitol (4:1 mannitol:sucrose) showed a more pronounced reduction from 72 s for random nucleated samples to 45 s and 52 s compared to ice fog and depressurization, respectively. In contrast, no beneficial effect on reconstitution time was seen in sucrose samples. It was noteworthy that even at the low mAb concentrations in relation to stabilizer used for the present work, this time reducing effect was observable.

IV.4.5 Turbidity

Overall, low turbid samples were found (Figure IV-3, A-C, squares). A slight increase in turbidity due to stresses during freeze-drying was found, but no clear difference between different nucleation approaches was observable.

IV.4.6 Soluble aggregates

In general, a small propensity for the formation of soluble aggregates was found over the range of all formulations directly after freeze-drying (Table IV-2).

Table IV-2 Relative amount of monomer content and high molecular weight (HMW) species obtained by HP-SEC.

Formulation	Freezing Protocol	Monomer (%)	HMW species (%)
Sucrose	Initial (prior to FD)	99.2 ± 0.02	0.8 ± 0.02
	Random	99.2 ± 0.08	0.8 ± 0.08
	Ice Fog	99.2 ± 0.06	0.8 ± 0.06
	Depressurization	99.2 ± 0.07	0.8 ± 0.07
Trehalose	Initial (prior to FD)	99.1 ± 0.02	0.9 ± 0.02
	Random	99.0 ± 0.02	1.0 ± 0.02
	Ice Fog	99.2 ± 0.07	0.8 ± 0.07
	Depressurization	99.2 ± 0.07	0.8 ± 0.07
Mannitol:Sucrose	Initial (prior to FD)	99.1 ± 0.02	0.9 ± 0.02
	Random	99.1 ± 0.09	0.9 ± 0.09
	Ice Fog	99.1 ± 0.03	0.9 ± 0.03
	Depressurization	99.0 ± 0.02	1.0 ± 0.02

Values are expressed as the mean of triple injections out of three individual vials (n=3) ± standard deviation.

Only a tiny amount of HMW formation was seen irrespective of formulation and freezing protocol. For this reason and due to the low mAb:stabilizer-ratio, no significant changes were observable directly after freeze-drying. This finding is supported by a recent systematic investigation by Vollrath et al.¹⁵¹ which showed no adverse effect of controlled nucleation (ice fog) on protein stability in comparison to randomly nucleated samples even after accelerated stability studies. Similar findings related to protein stability in short-term stability were reported for depressurization technique by Awotwe-Otoo and co-workers⁵⁶. A more pronounced decrease in protein stability by either of the investigated CN techniques, therefore, seems unlikely.

IV.4.7 Subvisible particles

For the mannitol-containing formulation no significant difference between the investigated nucleation approaches was observable (Figure IV-3C, bars). In trehalose samples (Figure IV-3B, bars), a small shift towards higher cumulative particle counts $\geq 1 \mu\text{m}$ was found for controlled nucleation protocols (6192 vs. 7068 and 9151 for random vs. ice fog and depressurization, respectively). However, differences were not found to be statistically significant. Moreover, higher counts for $10 \mu\text{m}$ and $25 \mu\text{m}$ were found in random nucleated trehalose samples compared to CN samples whereby this difference was statistically significant for $10 \mu\text{m}$ comparing random nucleation with ice fog. In sucrose samples, a clear and statistically significant difference in cumulative particles greater or equal to $1 \mu\text{m}$ was observable for random nucleation compared to ice fog and depressurization (Figure IV-3A, bars).

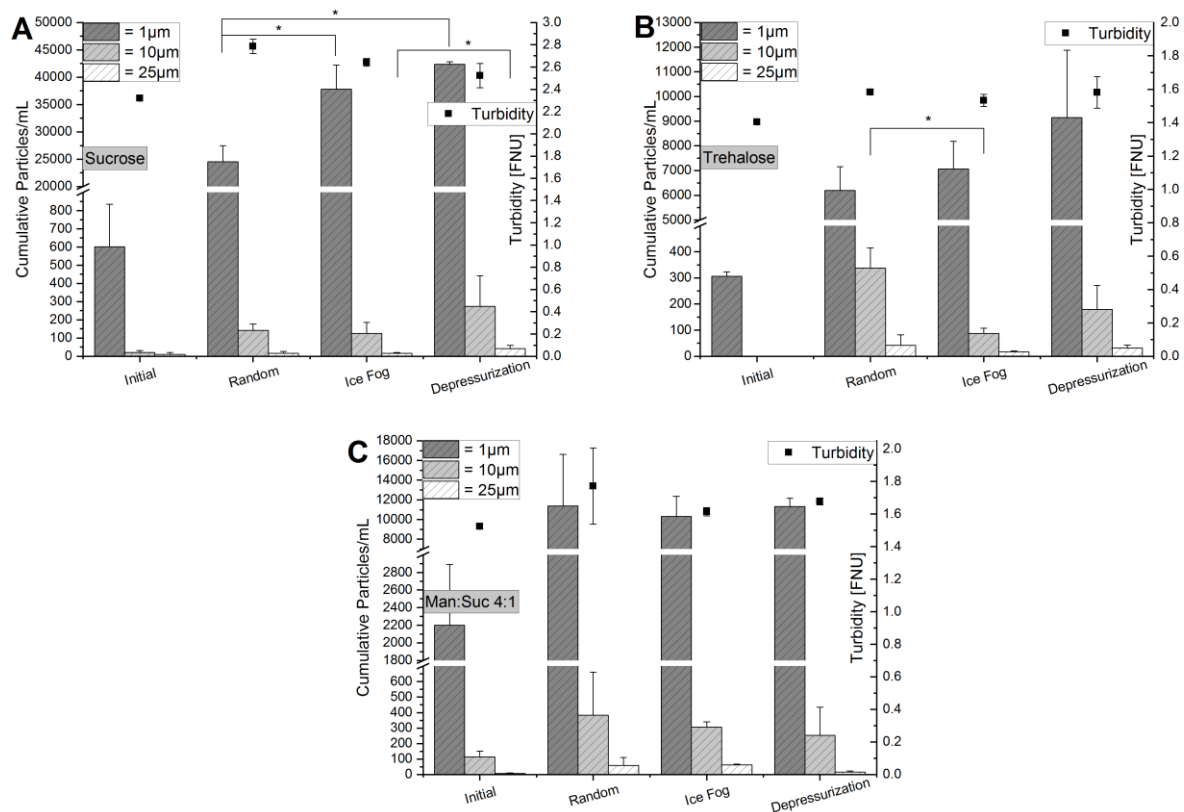


Figure IV-3 A-C Bars represent the cumulative subvisible particle counts per mL for sizes greater or equal $1 \mu\text{m}$, $10 \mu\text{m}$, and $25 \mu\text{m}$ as a function of the nucleation approach used compared to the finally filtered initial formulation before freeze-drying. Turbidity is represented by squares. Values for sucrose- (A), trehalose- (B), and mannitol:sucrose 4:1-formulation (C) are shown in the respective graph. The shown values represent the mean of measurements from three different vials. Error bars indicate the standard deviation of the mean.

The controlled ice nucleation techniques among each other showed no significant difference here. With the exception that for cumulative particles $\geq 25 \mu\text{m}$ interestingly a significant difference between ice fog (16 ± 5) and depressurization (42 ± 18) was found. From our results, we assume formulation dependence for subvisible particle generation if CN is applied. This potential effect needs to be studied further in future experiments.

IV.5 Conclusion

In the present work, we compared ice fog and depressurization which are two mechanistically different and market-dominating controlled ice nucleation methods. With our study, we can confirm that regarding nucleation behavior and process length both techniques are well comparable. We conclude that the control of ice nucleation as such, compared to random nucleation, is more relevant than the applied mechanism for CN. In both, ice fog and depressurization, nucleation starts at the surface and slowly propagates bottom-down based on observations by the LyoCam¹⁴⁸. Therefore, vials nucleated by either of these CN techniques behave practically the same. In contrast, in shelf-ramp freezing, the nucleation typically starts at the bottom due to higher supercooling.

In conclusion, we could show that the resulting product is with respect to solid state properties practically identical over the range of investigated pharmaceutically relevant formulations. From our results, this is also true for soluble aggregates and turbidity measured directly after freeze-drying. We, therefore, assume that a process transfer from one to another controlled ice nucleation technique will be applicable without major challenges caused by the nucleation mechanism which may be different in nature. Based on our results, both ice fog and depressurization lead to similar process performance and similar critical product quality attributes. A change of the applied CN technique during process transfer and scale-up is therefore assumed to be of generally low risk, irrespective of usual scale-up challenges.

Acknowledgments

The support from the Global Technology Management from Boehringer Ingelheim is kindly acknowledged. In addition, the authors thank Manuel Breitfeld, Tobias Diebold, and Frank Botzen from Boehringer Ingelheim Pharma GmbH & Co. KG Biberach for the technical support with the pilot-scale freeze-dryer.

Conflict of interest disclosure

The authors have no conflict of interest to disclose.

IV.6 Supplementary material

IV.6.1 Materials and methods

Table SIV-1 Overview of the different investigated formulations.

Formulation	mAb [g/L]	Sucrose [% (w/v)]	Trehalose [% (w/v)]	Mannitol [% (w/v)]	Polysorbate 80 [% (w/v)]
Sucrose	5	10	-	-	0.02
Trehalose	5	-	10	-	0.02
Mannitol:Sucrose	5	2	-	8	0.02

All stock solutions used were prepared in 10 mM histidine buffer (pH 6.0) The mAb stock solution was dialyzed in 10 mM histidine buffer (pH 6.0), too.

IV.6.1.1 Dynamic scanning calorimetry (T_g')

The glass transition temperature of the liquids prior to freeze-drying was measured using a Mettler Toledo DSC 821e (Gießen, Germany) dynamic scanning calorimeter. 25 μ L of the formulation was pipetted in an aluminum crucible and crimped. A DSC method cooling from 20 °C to -50 °C with a cooling rate of 10 K/min, followed by an isothermal step for 5 minutes and a subsequent ramping to 20 °C with 10 K/min was used. The glass transition temperature of the maximally freeze-concentrated solution was evaluated from the heating step as the inflection point of the glass transition using the Mettler StarE Software.

Table SIV-2 Glass transition temperatures of the maximally freeze-concentrated solutions of the amorphous formulations used.

Formulation	T_g' onset (°C)	T_g' inflection point (°C)
Sucrose	-34.6 \pm 0.2	-33.1 \pm 0.3
Trehalose	-31.7 \pm 0.1	-30.4 \pm 0.2

Values are expressed as the mean of three individual measurements (n=3) \pm standard deviation.

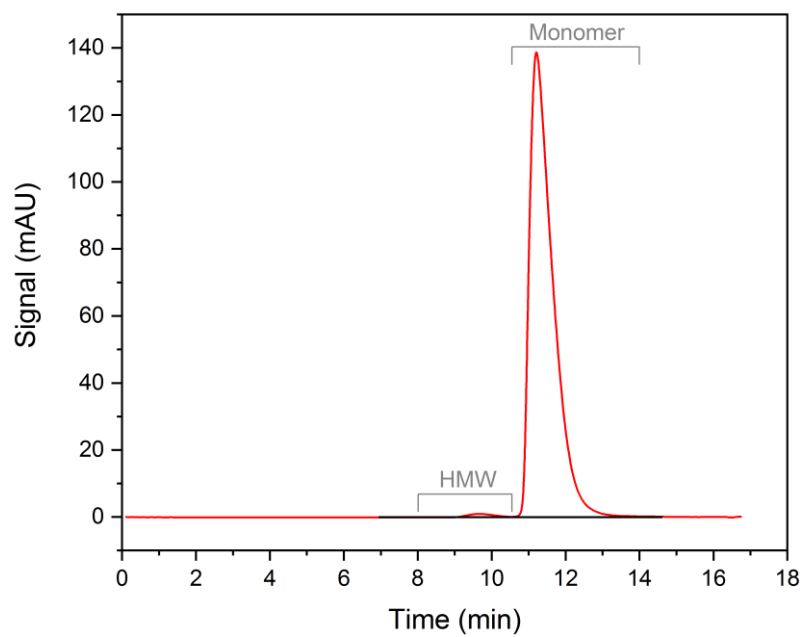


Figure SIV-1 Example HP-SEC chromatogram showing the method of peak separation and integration. HMW represents the relative fraction of high molecular weight species whereas monomer depicts the relative area of the monomer peak. There was no peak eluting later than the monomer in any analyzed sample.

IV.6.2 Results

IV.6.2.1 Specific surface area (previous experiment)

As shown in Figure SIV-2 the same unexpected enlarged SSA was observed for the two controlled ice nucleation techniques in a previous experiment (Figure SIV-2, Experiment 1). Despite holding times during the FD process, all other settings (T_N , exact formulation, freezing/drying protocol) were the same.

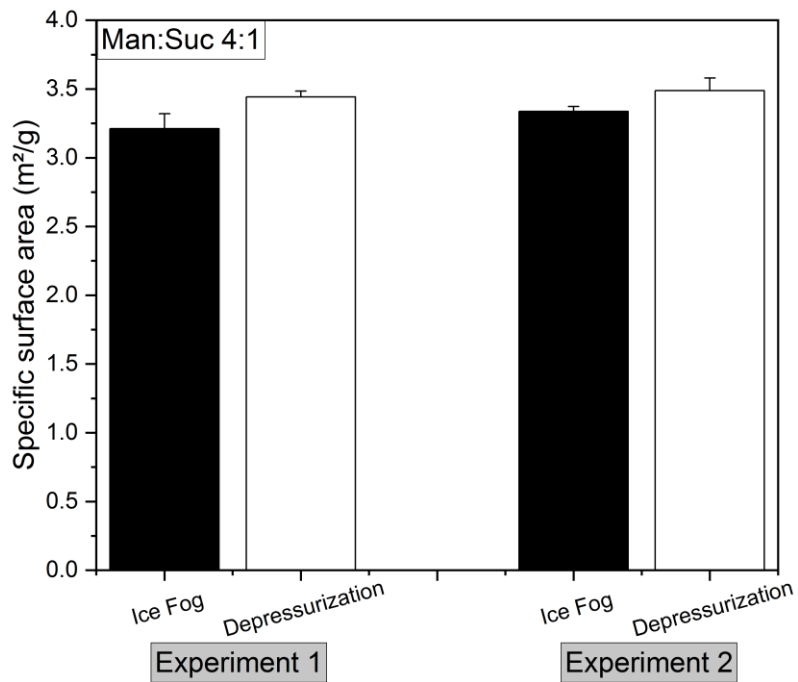


Figure SIV-2 The specific surface area data for mannitol:sucrose 4:1-formulation from a previous experiment (left) and the one described in the main body (right). The shown values represent the mean of measurements from three different vials. Error bars indicate the standard deviation of the mean.

IV.6.2.2 X-ray diffraction of sucrose and trehalose formulations

Independent of the applied freezing protocol sucrose and trehalose formulations ended up as fully amorphous solids represented by an amorphous halo in x-ray diffractogram (Figure SIV-3).

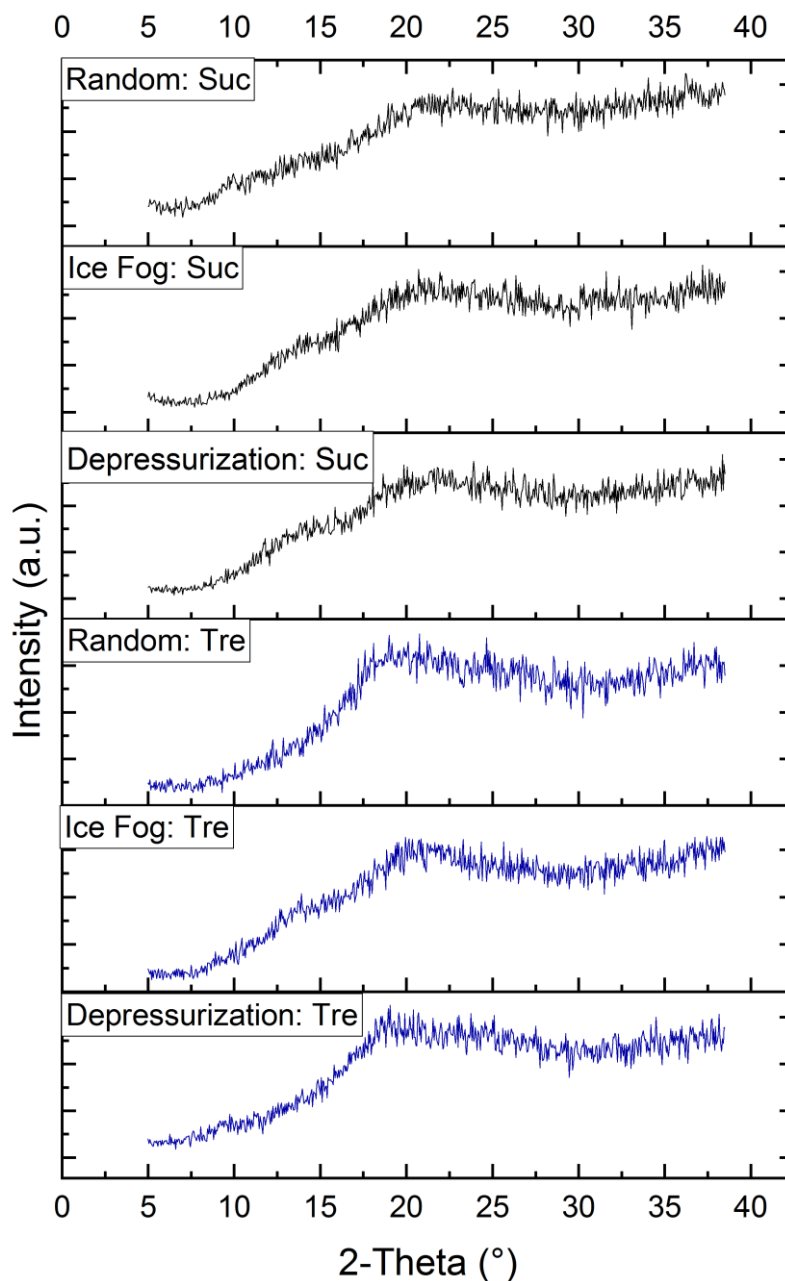


Figure SIV-3 Representative x-ray diffractograms for the respective formulations and freezing protocols.

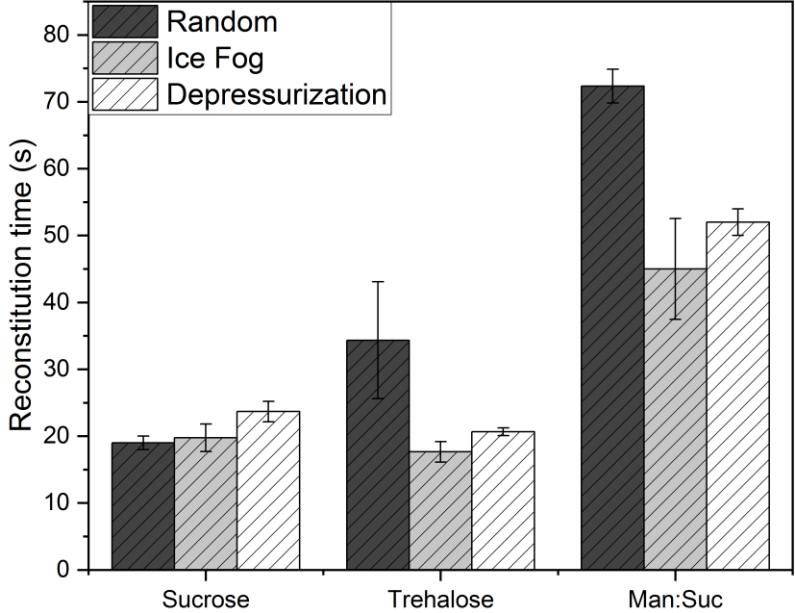


Figure SIV-4 Reconstitution times obtained for the respective formulation and the corresponding freezing protocol. The shown values represent the mean of measurements from three different vials. Error bars indicate the standard deviation of the mean.

Chapter V Study on key variables that can influence controlled ice nucleation in a pilot-scale freeze-dryer

Abbreviations

API	Active pharmaceutical ingredient
CN	Controlled ice nucleation
HES	Hydroxyethyl starch
PES	Polyethersulfone
SV-ratio	Liquid surface area to fill volume-ratio
T _N	Nucleation temperature
T _S	Shelf temperature setpoint
WFI	Water for injection

V.1 Introduction

Freeze-drying is an established unit operation used in the production of parenteral products, e.g. biologics. The current commercial freeze-drying processes rely on random ice nucleation events during the freezing step. Such stochastic nucleation is reported to bear a potential for batch heterogeneity with respect to product characteristics and moisture content within the same batch.^{43,54} Controlled ice nucleation holds a great promise to reduce those inter-vial variations that arise from the freezing step. That is why the control of the nucleation temperature (T_N) during the freezing step of pharmaceutical freeze-drying constantly gained interest over the last two decades. Controlled ice nucleation (CN) as such refers to the control of T_N of all vials and thus control of the degree of supercooling of the filled solution by introducing a stimulus to the supercooled solutions. Several techniques are reported in the literature, some of them with commercial implementation. The most common techniques are based on (1) the introduction of ice seeds by ice fog^{41,44-49}, (2) the application of rapid pressure changes^{48,50,51}, or (3) the application of vacuum to induce local surface freezing⁵²⁻⁵⁴. Although the benefits and advantages of controlled ice nucleation from a process time^{40,43,50,52,53,55}, batch, and/or product quality perspective^{40,43,54-59} have been shown widely, shelf-ramp freezing is still the gold standard in most (commercial) processes. A better understanding of the factors important for a successful CN process and their effects on the product quality will be vital for the implementation of controlled ice nucleation technique in commercial manufacturing.

The risk of failure of the CN step is likely if the critical variables are not well controlled and within a certain range as it was reported by a process scientist (personal communication). During process characterization studies, they observed a floating phenomenon occurring after the induction of controlled ice nucleation. Observed was the literal floating of a frozen layer on top of a liquid-like layer and in some cases even a complete melting of the initially frozen solution was seen. Similar observations with regard to floating were also reported by Oddone et al.⁵⁴. At this point, it is important to look into the physics of freezing and supercooling. Searles et al.¹⁸ divided the freezing of water (which in general is the main component of pharmaceutical solutions to be freeze-dried) into four steps which comprise (1) the cooling of the solution below its equilibrium freezing temperature, i.e. supercooling, (2) the formation of an ice nucleus, i.e. primary nucleation, (3) the instant subsequent growth of an ice nucleus to ice crystals, i.e. secondary nucleation, and (4) the final solidification by the completion of the liquid-to-solid phase transition by proceeding ice crystal growth. The supercooled solution is metastable and is therefore prone to spontaneous crystallization of ice. The higher the degree of supercooling the more the number of ice nuclei increases and thus the probability of ice crystallization¹⁸⁻²¹. In the case of CN, the (secondary) nucleation/crystallization is induced by the introduction of a stimulus. When the nucleation event occurs, the temperature of the liquid-solid mixture increases close to the equilibrium freezing point and the crystallization stops due to the lack of sufficient removal of heat of crystallization. Because of this, only a portion of the crystallizable water instantly freezes during secondary nucleation. Searles et al.¹⁸ calculated that only around 7 % of the freezable water could have crystallized at a nucleation temperature of -5 °C in an aqueous solution of 10 % (w/v) HES. The biggest amount of water crystallization follows with continuous heat removal.^{21,152} Consequently, the degree of supercooling and the subsequent continuous heat removal, e.g. during an isothermal post-CN hold step is critical to a controlled ice nucleation process. Whereas the nucleation temperature mainly determines the ice morphology and thereby the process performance during the subsequent drying steps¹⁸, the post-CN hold step may have implications on both ice crystal properties (ice crystal size, complexity of the ice network) and API integrity. The impact on ice crystal properties is mainly due to Ostwald ripening which leads to a decreased interfacial free energy due to a melting of smaller ice crystals in favor of larger ice crystals.^{21,22,153} In the case of the incorporated API, the isothermal post-CN hold step may play a role with regard to damages resulting from freeze-concentration and/or cold denaturation of protein APIs.^{11,20,31,154}

Two recent studies elucidated the interplay of nucleation temperature and the post-CN hold step on product morphology and process-related parameters. Oddone et al.⁵⁴ on the one hand investigated the influence of different T_N and post-CN shelf temperatures on a 5% mannitol placebo with different filling volumes using vacuum-induced surface freezing. They described a floating of an ice layer on a liquid-like phase when applying $T_N = -5\text{ }^\circ\text{C}$ and observed signs for a meltback if the post-CN shelf temperature was kept at this temperature. In contrast, they found the formation of ice filaments (dendritic structures) when a vial with a high filling volume (corresponding to a filling height of 1.7 cm) was nucleated at $-5\text{ }^\circ\text{C}$ with a subsequent lowering of the T_s to $-10\text{ }^\circ\text{C}$, by this leading to an inhomogeneous middle section of the lyophilized cake. Wenzel et al.¹⁵⁵ on the other hand investigated a buffered system containing 100 g/L of S-Adenosyl-L-methionine disulfate tosylate with approximately 1.5 cm filling height in 10R vials. They applied different controlled nucleation protocols using depressurization with a special focus on post-CN hold time. At this, they found a general trend towards lower product resistance values for higher T_s , but also indications for local micro-collapse with an unfavorable morphology for the highest T_s of $-3\text{ }^\circ\text{C}$ followed by an isothermal hold step at the same shelf temperature setpoint.

Considering the issues with controlled ice nucleation that were reported in literature, it appears important to study the variables affecting the CN process, on the one hand, to better understand the process and interplay of factors, on the other hand to pave the way for the implementation of this technique for the production of drug products. That is why our study aims to provide further insight in the factors for the process characterization of controlled ice nucleation. Significant factors influencing the successful performance of CN should be identified. Moreover, the occurrence of unfavorable events like floating and therewith (some) error limits should be reproduced and studied.

We hypothesize that the appearance of failures during the controlled ice nucleation process is related to an unfavorable combination of different factors. These are versatile and may include, but are not limited to:

- the vial (vial type, size, stopper type),
- the formulation (filling volume and filling height, composition, total solute concentration, solution viscosity, solution density, class of API)
- the nucleation process (cooling ramp and isothermal hold time before CN, features associated with the used technology, nucleation temperature, post-CN hold time and temperature, cooling ramp down to final freezing temperature)

In our study, we investigated placebo sucrose solutions for some of the aforementioned factors which we considered to be the most critical for the occurrence of failure during controlled ice nucleation.

V.2 Materials and methods

V.2.1 Materials

For the representative placebo formulations, the following excipients were used: EMPROVE® exp_D(+)-sucrose (Ph.Eur.-certified) and sodium hydroxide purchased from Merck KGaA (Darmstadt, Germany), L-Histidine monohydrochloride monohydrate (min. 99% purity) and L-Histidine (Cell culture reagent) supplied by Alfa Aesar (Karlsruhe, Germany). Methyl blue microbiology stain BHD prolabo (C.I. 42780) was purchased from VWR International BVBA (Leuven, Belgium). For the preparation of buffers and stock solutions, water for injection (WFI; Purelab Plus, USF Elga, Celle, Germany) was used.

V.2.2 Formulations

The stock solutions of L-histidine buffer, methyl blue and sucrose were mixed in a way to obtain the final placebo formulations covering a range of 5.2 % (w/v) to 15.2 % (w/v) total solute concentration as summarized in Table V-1 Formulations used in the study. The respective filling volume was filled in 10R tubing vials (MGlas AG, Muennerstadt, Germany) and semi-stoppered with lyophilization stoppers (FluroTec® rubber stopper, West Pharmaceuticals, Eschweiler, Germany).

Table V-1 Formulations used in the study.

Formulation	L-Histidine buffer [mM]	Sucrose [% (w/v)]	Methyl blue [ppm]
5 % Sucrose	10	5	5
10 % Sucrose	10	10	5
15 % Sucrose	10	15	5

The L-histidine buffer was adjusted to pH 5.5.

V.2.3 Experimental setup

All experiments were conducted on an FTS Lyostar III pilot-scale freeze-dryer (SP Scientific, Stone Ridge, NY, USA) using the upper and the middle shelf. The product temperature was monitored in one vial of each factor combination placed on the outer edges of all loaded vials using wired thermocouples (Type T, Newport Electronics, Deckenpfronn,

Germany). For the induction of controlled ice nucleation, the ice fog method described by Geidobler et al.⁴⁹ was used. Briefly, the shelves loaded at room temperature were ramped down to the respective shelf temperature setpoint with 1 K/min and held for 1h to allow for equilibration and supercooling. Subsequently, the freeze-dryer was evacuated to roughly 4 mbar and held depressurized for another 5 min to allow for product temperature equilibration and to ensure 100 % nucleation success among the investigated vials. Hereafter, the system was rapidly raised to atmospheric pressure by opening the release valve which ventilated via the cold condenser resulting in almost instant nucleation of the supercooled vials. Nucleation success was determined visually.

For each shelf temperature setpoint and for each response, a separate run was performed, i.e. six runs in total.

V.2.3.1 Residual accessible liquid volume

The vials were placed in the first third of the upper and middle shelves in a central position from the acryl glass door. In order to reduce the radiation effects of the chamber wall, a dummy vial row was placed around the investigated vials. At a desired sampling time point after induction of ice nucleation, one vial per shelf was taken out and immediately analyzed. For that, the liquid portion of the vial content was gently poured either into a 2 mL Eppendorf tube with 0.1 mL marks (Eppendorf AG, Hamburg, Germany) or into a 10 mL measuring cylinder with 0.2 mL marks assuring that no ice or slush was poured into the cylinder.

V.2.3.2 The thickness of the frozen layer

Ten vials, of which the outer were equipped with thermocouples, were placed in the front center of each shelf close to the acryl glass door. A white background was placed behind the vials. Two rulers were attached to the shelves on the left and right sides of the vials. In front of the acryl glass door of the product chamber, a Nikon digital camera D5300 (Nikon GmbH, Düsseldorf, Germany) equipped with a Nikkon DX AF-S Nikkor 18-105 objective was mounted on a tripod. The camera settings were set to ISO 640, aperture 7.1, exposure time 1/80, and manual focus. To assure for uniform illumination of the photograph, two led spotlights were attached to the acryl glass door. With the induction of ice nucleation, an interval photo series was started with a picture taken every minute. Each picture was processed using ImageJ (Version 1.8.0_112, NIH, USA). The raw file was split into the RGB channels, of which the green channel was used for scaling (pixel/cm). For improved

differentiation between transparent liquid and blurry frozen layer, the contrast was increased. Eventually, the height of the frozen layer was determined on an individual vial basis. The two values per process condition of one shelf were averaged and taken as one replicate.

V.2.4 Design of experiments

To systematically investigate the impact of different factors and second-order interactions, an experiment plan using a general multi-stage full factorial design was created. The software Minitab 19 Statistical Software (Minitab, LLC., State College, PA, USA) was used.

V.2.4.1 Factors

From the factors identified in the introduction, those assumed to be most critical are summed up in Table V-2 and were considered in the study design.

Table V-2 Factors included in the general multi-stage full factorial design

Factor	Unit	Type	Levels
Shelf temperature setpoint	°C	quantitative	-3, -7 ^a , -10
Liquid surface area to fill volume-ratio¹	l/cm	quantitative	0.5, 0.8 ^a , 1.0
Total solute concentration	% (w/v)	quantitative	5.2, 10.2 ^a , 15.2
Post-CN hold time	min	multilevel	10, 20, 30, 60, 75, 90, 120

¹ In the following text referred to as Surface-Vol liquid ratio or SV-ratio. ^a "Center point" which was added manually to the study design.

The shelf temperature setpoint was used as a freeze-dryer build-independent and reproducible surrogate for the product temperature and therewith as a surrogate for the nucleation temperature T_N .

The term liquid surface area to fill volume-ratio (SV-ratio) was introduced as a generic vial size-independent term covering aspects of vial format and filling height which in turn is dependent on the filling volume of the vial. For the determination of the respective value, the area of the circle of the inner cylinder of a 10R vial was calculated using:

$$A = \pi * r^2 \quad (\text{Equation V-1})$$

with A representing the surface area and r reflecting the inner radius of the cylindric part of the glass tube, i.e. $r = 2.2$ cm in the case of 10R as stated by the glass vial manufacturer SCHOTT¹⁵⁶. Furthermore, the complementary filling volumes of filling heights 1.0 cm, 1.4 cm (center point), and 2.0 cm were empirically determined to be 3.8 mL, 5.32 mL, and 7.6 mL, respectively. Herewith, the SV-ratio could be calculated using:

$$SV - ratio = \frac{\pi * r^2}{V(filling)} \quad (\text{Equation V-2})$$

resulting in SV-ratios of 0.5, 0.71, and 1.0 for filling heights of 2 cm, 1.4 cm, and 1 cm, respectively.

The total solute concentration represented the overall amount of solutes included in the formulation, which comprised buffer components, sucrose and methyl blue.

The post-CN hold time reflected the time duration starting from the nucleation stimulus. For the stated duration, the shelf temperature setpoint was kept at the same setting used for the initiation of ice nucleation in order to separate effects which may have been caused by a temperature ramp after initialization of the nucleation.

V.2.4.2 Responses

The occurrence of the floating phenomenon and the investigation of the error limits of the controlled ice nucleation process was rarely reported in the literature and was mainly concerning nucleation success in general²¹. Therefore, the best fit responses are not known yet. To be able to prioritize impacting factors, quantitative and easy to assess responses were needed. In this experiment, we investigated two responses in placebo solutions which will be described in the following:

- Relative residual accessible liquid volume
- Relative thickness of the frozen layer

The occurrence of floating of a solid ice layer on top of a liquid layer implies a portion of the filling volume to be in a liquid-like physical state. For the data set underlying the response relative residual accessible liquid volume, the measured volume of a vial was set in relation to the filling volume of the respective vial leading to a value between 0.0 and 1.0. Two replicates of each condition were included in the investigation.

The relative thickness of the frozen layer was determined by the evaluation of photographs taken in a standardized setup (see V.2.3.2). The number of pixels was transformed into a height allowing to measure the thickness of the frozen layer. This value was set in relation to the known filling height of the respective vial. Two replicates of each condition were included in the investigation.

V.2.5 Regression model

All obtained data was fit to a regression model using Minitab statistical software.

V.2.5.1 Relative residual accessible liquid volume

In order to obtain normally distributed data, a constant of $c = 0.01$ needed to be added to allow for a box-cox power transformation with a $\lambda = 0.5$. By that, the square root of the original values was calculated leading to a normally distributed data set. All factors and factor combinations up to second-order interactions were included. A two-sided 95 % confidence interval was used. The model generation was performed by stepwise regression, i.e. that the software automatically added and removed terms to the model to identify a useful subset of the terms. The specified alpha error values to enter or to remove a term from the model based on a comparison to its p-value were set to 0.15 each. This model was analyzed for unusual observations, which are single value combinations that do not follow well the proposed regression equation and which are characterized by absolute standardized residuals greater than 2. The model was adjusted by excluding seven observations based on the standardized residuals. Eventually, the model terms were checked for statistical significance based on $\alpha = 0.05$ which led to no change in the model terms. The second-order regression model for the response relative residual accessible liquid volume was represented by the following equation:

$$\begin{aligned} (\text{Relative residual accessible liquid volume} + c)^{0.5} = & 1.178 - 0.530 \text{ Surface-Vol} \\ & \text{liquid-ratio} + 0.0721 \text{ Shelf Temperature Setpoint} - 0.01054 \text{ Post-CN hold time} + 0.03068 \\ & \text{Total solute concentration} + 0.000042 \text{ Post-CN hold time} * \text{Post-CN hold time} - 0.0383 \\ & \text{Surface-Vol liquid-ratio} * \text{Shelf Temperature Setpoint} - 0.000314 \text{ Shelf Temperature} \\ & \text{Setpoint} * \text{Post-CN hold time} + 0.002847 \text{ Shelf Temperature Setpoint} * \text{Total solute} \\ & \text{concentration} \end{aligned}$$

(Equation V-3)

The final model showed a corrected R² of 77.1 % and a prognostic R² of 75.1 %.

V.2.5.2 The relative thickness of the frozen layer

The obtained data were evaluated for the response as described above. It turned out that the factor combination of the highest shelf temperature setpoint ($T_s = -3$ °C), the biggest filling volume represented by the SV-ratio 0.5, and highest total solute concentration (15.2 %) showed a decrease in the response over time regarding the thickness of the frozen layer. That resulted in a clear liquid solution after approximately 50 minutes of observation. As this was an artificial effect caused by the 5 minutes holding step at vacuum conditions before induction of the nucleation, the dataset based on that factor combination was excluded from the model generation.

All factors and factor combinations up to second-order interactions were included. A two-sided 95 % confidence interval was used. The model generation was performed by a stepwise regression with alpha values of 0.15. This generated model was adjusted by excluding seven observations based on the standardized residuals. Eventually, the model terms were checked for statistical significance based on $\alpha = 0.05$ which led to no change in the model terms. The regression model for the response relative thickness of the frozen layer was represented by the following equation:

$$\begin{aligned} \text{Relative thickness of the frozen layer} = & 0.6426 + 0.2564 \text{ Surface-Vol liquid-ratio} - \\ & 0.01955 \text{ Shelf Temperature Setpoint} + 0.000732 \text{ Post-CN hold time} + 0.02138 \text{ Total solute} \\ & \text{concentration} - 0.002451 \text{ Total solute concentration} * \text{Total solute concentration} + 0.02564 \\ & \text{Surface-Vol liquid-ratio} * \text{Shelf Temperature Setpoint} + 0.000128 \text{ Shelf Temperature} \\ & \text{Setpoint} * \text{Post-CN hold time} - 0.002598 \text{ Shelf Temperature Setpoint} * \text{Total solute} \\ & \text{concentration} + 0.000046 \text{ Post-CN hold time} * \text{Total solute concentration} \end{aligned}$$

(Equation V-4)

The final model showed a corrected R² of 75.4 % and a prognostic R² of 71.1 %.

V.3 Results and discussion

V.3.1 Occurrence of floating

During all experiment runs, no clear floating phenomenon as described in the introduction could be reproduced. However, an iceberg formation was seen at one condition setting which is speculated to be caused by floating (see section V.3.3).

V.3.2 Effect of the investigated factors on the responses

To increase the quality of the fit of the model, second-order interactions were taken into account within the model. However, in the following only the statistically significant single factors are taken into consideration. The extent and direction of the factors on the respective response are shown in Figure V-1 and Figure V-2.

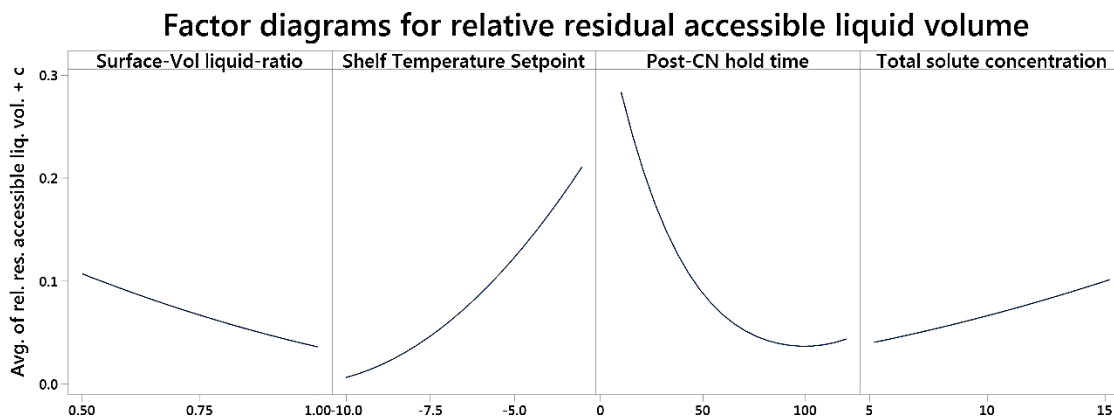


Figure V-1 Factor diagrams for the response relative residual accessible liquid volume.

For mitigation of a failure during controlled ice nucleation, the relative residual accessible liquid volume is ought to be minimized with a certain setting, i.e. a value close to 0 was desirable for this response. It is important to note that the curvature of the post-CN hold time-line is likely to be caused by the not normally distributed data or by artefacts in the data set. Therefore, only the sign of the slope is taken into consideration. Derived from Figure V-1 lowering the shelf temperature setpoint and keeping the post-nucleation hold time between 50 minutes and 100 minutes seemed to have the strongest effect on a reduction of the response. Reducing the filling height (represented by the SV-ratio) and decreasing the total solute concentration also appeared to lead to a reduced relative residual accessible liquid volume, although the impact seemed to be lesser than for shelf temperature setpoint and post-CN hold time.

Concerning the optically measured response, partially concordant results were found (Figure V-2).

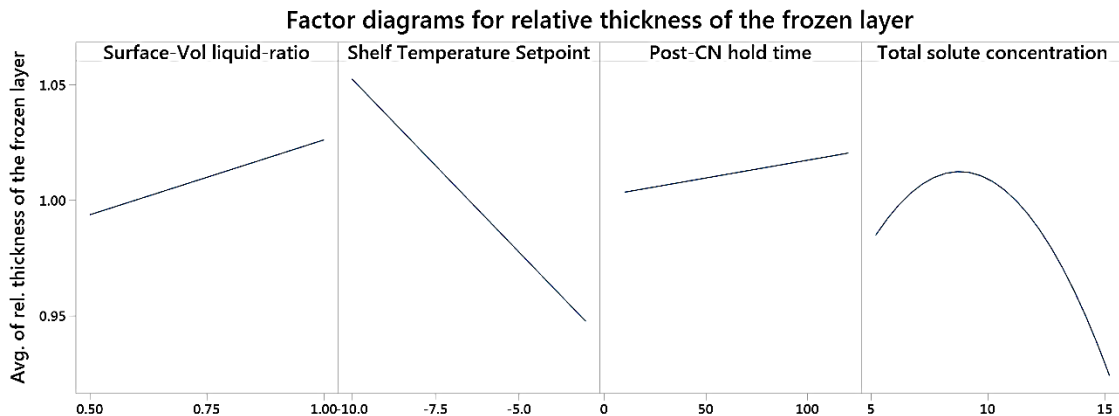


Figure V-2 Factor diagrams for the response relative thickness of the frozen layer.

In that case, a value of the response close to 1.0 was desirable. Like with the residual liquid volume, the impact of a lowered shelf temperature setpoint appeared to have a strong impact. However, the influence of the post-CN hold time was not found to be as strong as for residual volume. Yet, a longer hold time appeared to lead to increased frozen layer thickness. The SV-ratio showed the same trend as for the residual volume, i.e. that a lower filling height increased the thickness of the frozen layer. An artificial finding caused by the results for the manually added “center point” was seen with respect to the total solute concentration. Here, it appeared that a solute concentration close to 10 % would maximize the thickness of the frozen layer (Figure V-2, right graph). This supposed correlation should be taken with caution due to a possible artefact in the model caused by the manually added center point.

V.3.3 Implications for controlled ice nucleation process design

Based on the unclear suitability and reproducibility of the investigated responses and other potential blind spots of the experimental setup (see section V.3.5), all results should be interpreted carefully. However, for the factor combination with the lowest solute concentration of 5.2 %, a time-dependent growth of an iceberg-like spike on top of the frozen good was seen (Figure V-3).

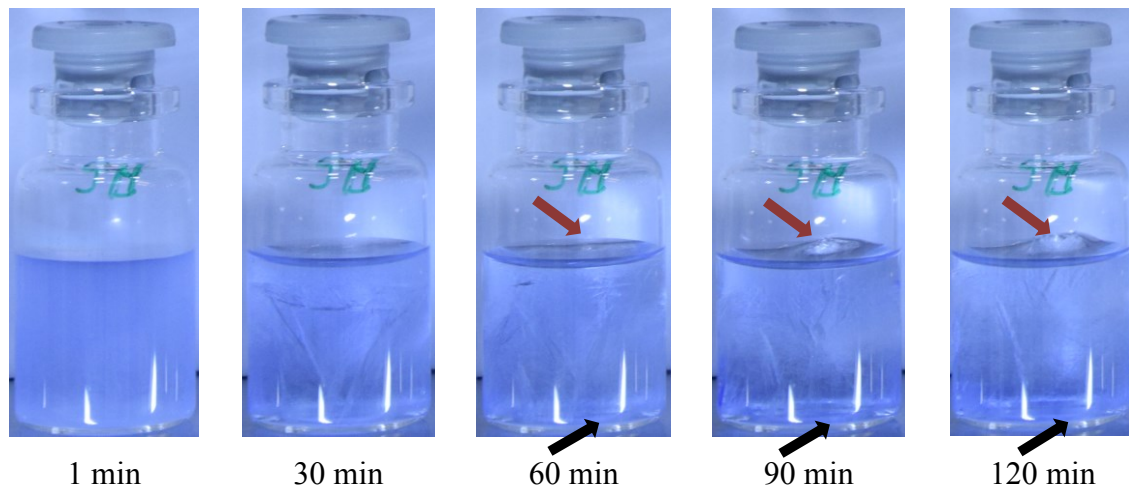


Figure V-3 Photographs showing the time-dependent formation of an iceberg (red arrows) on top of the frozen good for the factor combination: $SV = 0.5$, $T_s = -3$ °C, total solute concentration = 5.2 %. The black arrows point to the area which becomes clearer over holding time.

This could only be observed for that factor combination assumed to be unfavorable regarding filling height (SV-ratio) and insufficient removal of heat of crystallization represented by the high shelf temperature. It is speculated that this iceberg-like formation (Figure V-3, red arrows) may have been caused by floating of a large frozen portion on a small liquid residue (Figure V-3, black arrows). The spike formation already started between 30 min and 60 min. Looking at the raw images, a change in the surface appearance of the top layer of the frozen good was first seen after approximately 45 min. The occurrence of such an optical defect is undesirable and should, therefore be avoided during controlled ice nucleation either by reduction of the filling height or by decreasing the shelf temperature setpoint.

Based on that, an acceptable range for the responses for the generation of overlaid contour plots was defined. The overlaid contour plots help to visually identify an area where the predicted means of the two response variables are likely to be in an acceptable range (Figure V-4). Bearing in mind, that the model-based assumptions should be considered rather qualitative than quantitative, some implications for the controlled ice nucleation process design could be assumed. The graphs A to C (Figure V-4) all represent the case of 2 cm fill height (SV-ratio 0.5) and an increasing solute concentration from 5.2 % to 15.2 %, respectively. For that high filling height, rather low shelf temperature setpoints should be chosen, decreasing with an increasing total solute concentration. Concerning the hold time after the CN stimulus, a longer time would appear to be beneficial. However, the iceberg observations made above should be considered, too. Consequently, a longer holding time (i.e. approximately > 30min) in combination with the highest technically possible shelf temperature setpoint regarding the successful induction of ice nucleation, should be avoided.

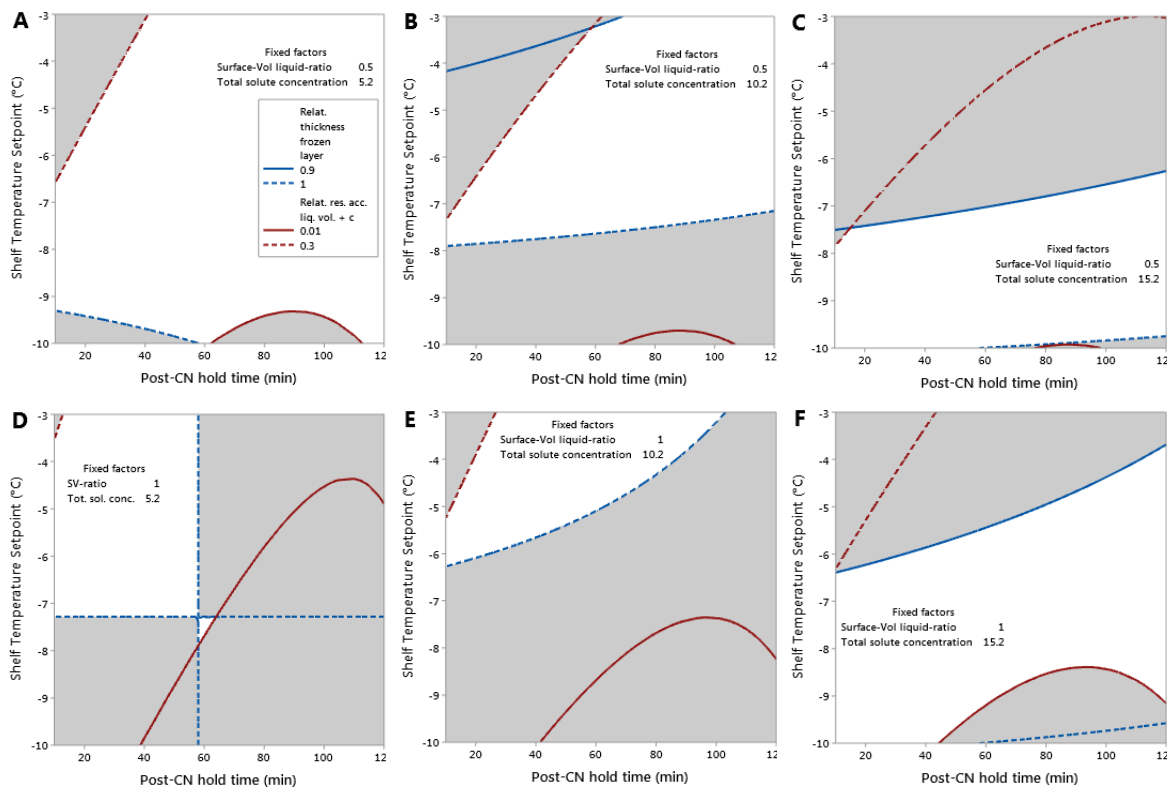


Figure V-4 Overlaid contour plots for both responses. the y-axis represents the shelf temperature setpoint and the x-axis represents the post-CN hold time. All other factors are fixed at different levels from A to F. The red line refers to the response relative residual accessible liquid volume with its set lower limit (solid line) and upper limit (dashed line). The blue line corresponds to the response relative thickness of the frozen layer with its set lower limit (solid line) and upper limit (dashed line). The area marked in white in a graph represents the operational area where the predicted means of the two response variables are within that acceptable range.

The more likely use case of 1 cm filling height (SV-ratio 1), is represented in the graphs D to F (Figure V-4) for an increasing solute concentration from 5.2 % to 15.2 %, respectively. It could be assumed that with lower filling heights, higher shelf temperature setpoints are feasible. Interestingly, the model suggests that with increasing solute concentration the shelf temperature setpoint should be lowered, too, to ensure a successful nucleation process.

V.3.4 Recommendations for controlled ice nucleation process design

Mainly based on relevant recent literature reports by Oddone et al.⁵⁴ and by Wenzel et al.¹⁵⁵ and partly supported by the our data discussed in section V.3.3, the following recommendations can be made:

- filling heights of significantly more than 1 cm (i.e. 1.5 cm and more) should be avoided to decrease intra-vial heterogeneity and micro-collapse independent of the vial size^{54,155,157}

- high shelf temperature setpoints close to the equilibrium freezing point (e.g. -3 °C) during post-CN hold time should be avoided to prevent the system from significant viscous flow and meltbacks (Oddone et al., 2016⁵⁴ and the presented results)
- (too) low shelf temperature setpoints during post-CN hold time (e.g. -20 °C) should be avoided as they could be linked to the unfavorable occurrence of micro collapse and inter-vial heterogeneity due to faster removal of heat of crystallization during secondary nucleation^{54,155}

And, although not investigated in this study, but of importance particularly in relation to process transfer and scale-up and thus worth mentioning as a general recommendation:

- controlled ice nucleation process transfer from depressurization to an ice fog method seems to be feasible⁴⁸, whereas depressurization and vacuum-induced surface freezing does not seem to be interchangeable without major challenges¹⁵⁵

V.3.5 Limitations and blind spots of the study

With the presented approach, we studied one path in the direction of a systematic investigation of the error limits of CN. The phenomenon of floating only occurred in one factor combination. This may be due to some limitations and blind spots the presented work implies. Ambient factors like radiation from the chamber walls and acryl glass door that could not be controlled should have been mitigated, e.g. by standardization or sufficient knowledge from preliminary experiments, as far as possible. The general multi-stage full factorial design could have been replaced by a first screening design to identify significant factors with suitable limits and levels. These factors could have included different vial formats and filling volumes to overcome the generic SV-ratio which may be oversimplified. Additionally, formulation aspects not only limited to the total solute concentration but also to include polymer content (representing a monoclonal antibody) and viscosity could have been of interest. Concerning the responses, there is a high need for a suitable, directly quantitatively measurable and accurately determinable variable as the used responses may not be per se suitable to identify correlations and to investigate all suitable operational spaces. Especially the provisional character of the introduced response variables lacking a high level of objectification and standardization may adversely impact the quality of the regression model. The regression model itself was chosen as simple as possible only incorporating terms to second-order.

V.4 Conclusion and outlook

In this preliminary work, we studied different factors that potentially affect the success of the controlled ice nucleation step in order to broaden the knowledge about the CN process. We introduced two new and highly experimental response variables to determine the effects of several factors on the freezing behavior of selected sucrose-based placebo formulations. The generated regression model suggested a strong influence of the shelf temperature setpoint which in turn correlates with the nucleation temperature, on the success of a controlled ice nucleation process. Moreover, it was found that all other investigated factors, namely the filling height represented by the vial format-independent SV-ratio, the total solute concentration, and also the hold time after the nucleation event are key factors for a successful CN process. Based on these results and recent literature findings, general recommendations for controlled ice nucleation process design were made. However, this investigation could only be a piece in the jigsaw puzzle of characterizing the factors and variables for a stable controlled ice nucleation process.

In the future, the need for a broad systematic investigation on the factors influencing the controlled ice nucleation process the most is consistently high. Especially formulation aspects, as well as the inclusion of critical quality attributes of a drug product, seem important. Moreover, it should be taken into account that vacuum-induced surface freezing was reported to behave both process-wise and product-wise differently than depressurization and most likely also ice fog CN methods. If such a future study is meticulously planned and performed, eventually the generation of a predictive mathematical model to gain an operational design space seems feasible.

Chapter VI 100 % Control of controlled ice nucleation vials by camera-supported optical inspection in freeze-drying

This chapter is prepared for submission and peer review as:

Gitter, J.H.¹; Geidobler, R.²; Halbinger, W.³, Presser, I.²; Winter, G.¹
100 % Control of controlled ice nucleation vials by camera-supported optical inspection in freeze-drying.

¹ Ludwig-Maximilians-Universität München, Department of Pharmacy, Pharmaceutical Technology and Biopharmaceutics, Butenandstr. 5, 81377 Munich, Germany

² Boehringer Ingelheim Pharma GmbH & Co. KG, Birkendorfer Str. 65, 88307 Biberach an der Riß, Germany

³ Seidenader Maschinenbau GmbH, Lilienthalstr. 8, 85570 Markt Schwaben, Germany

Author contributions:

Conceptual guidance, I.P. and G.W.; Data curation, J.H.G.; Formal analysis, J.H.G., W.H.; Investigation, J.H.G.; Methodology, J.H.G., W.H.; Project administration, J.H.G., R.G., I.P., and G.W.; Resources, R.G., I.P., and G.W.; Supervision, R.G., I.P., and G.W.; Validation, J.H.G.; Visualization, J.H.G.; Writing—Original draft, J.H.G.; Writing—Review & editing, R.G., W.H., I.P., and G.W.

VI.1 Abstract

Freeze-drying is the drying technology of choice for sensitive biological drugs. On the one side, it is admired for its suitability for the stabilization of sensitive molecules. On the other side, it is a time-consuming production step posing challenges in process development and technology transfer. The application of controlled ice nucleation is one elegant approach to shorten freeze-drying times significantly and at the same time increasing batch homogeneity. However, a reliable 100 % control of the controlled nucleation step in each vial is essential considering the impact of the nucleation temperature on product quality attributes. In this study, we introduce a camera-supported optical inspection method which utilizes the different superficial cake structures seen in controlled and random nucleated lyophilizates. Derived from the grayscale analysis the new distinguishing criterion “average edge brightness” is introduced. Four different formulations containing Sucrose, Trehalose, and/or BSA were freeze-dried with random or controlled nucleation and analyzed with the new technology. A proof of concept is provided by the analysis of a similar-to-market lyophilized monoclonal antibody formulation freeze-dried with three different freezing protocols covering different nucleation profiles. For all investigated formulations and process conditions, the clear discrimination of controlled and randomly nucleated vials was possible. By this, the technology allowed for reliable, non-invasive, and automatable 100 % monitoring of controlled nucleation success after freeze-drying.

Keywords

Lyophilization; Freeze-drying; Cake structure; Controlled nucleation; Inspection; Morphology; Visualization; Protein

Abbreviations

ANOVA	Analysis of variance
BET	Brunauer–Emmet–Teller krypton gas adsorption
BSA	Bovine serum albumin
CI	Confidence interval of the mean
CN	Controlled ice nucleation
FD	Freeze-drying
FMS	Frequency-modulated spectroscopy
ICH	International conference on harmonization
IQR	Interquartile range
<i>M</i>	Mean
mAb	Monoclonal antibody
p_{Chamber}	Chamber pressure
PES	Polyethersulfone

RN	Random shelf-ramped nucleation
RM	Residual moisture content
<i>SD</i>	Standard deviation
SSA	Specific surface area
T_N	Ice nucleation temperature
T_{Shelf}	Shelf temperature setpoint
WFI	Water for injection

VI.2 Introduction

In the field of biologicals, freeze-drying is still the method of choice to improve long-term stability compared to liquid formulations.^{69,158} By 2018, freeze-dried products represented a 33 % share of all parenteral protein formulations approved by the European Medicines Agency.¹¹¹ This is an impressive percentage keeping in mind the disadvantages of an additional production step resulting in often long processes and complex scale-up challenges.^{41,67,69,113,145} One approach intensively discussed in the freeze-drying community to alleviate such downsides is the application of controlled ice nucleation (CN) during freezing.^{40,41,50,53–56} In brief, it refers to the control of the nucleation temperature (T_N) of all vials and thus control of the degree of supercooling by setting a stimulus to the supercooled solutions. Depending on the technology, the most common stimuli types can be (1) the introduction of ice seeds by ice fog^{41,44–49}, (2) the application of rapid pressure changes^{48,50,51} or (3) the application of vacuum to induce local surface freezing^{52–54}. In general, controlled ice nucleation was reported to improve both process times^{40,43,50,52,53,55} and batch or product quality attributes^{40,43,54–59} of the lyophilizates. To our knowledge, first companies already started to implement commercial controlled ice nucleation processes into their production facilities. By this, the question of nucleation success and how to monitor it raises. Geidobler et al.²¹ reviewed different published CN methods and found no technology which could reliably prove to succeed in 100 % of the vials. Therefore, a full batch control of the nucleation success seems essential to overcome this uncertainty for quality assurance and regulatory reasons, e.g. if the application of controlled ice nucleation is performed to improve reconstitution times or other product quality attributes. Also, reliable discrimination of nucleated vs. non-nucleated samples can be used for process validation. The only published method for nucleation success control was recently described by Vollrath et al.¹⁵⁹ They discriminated CN failure vials by the calculated parameter water activity (a_w) derived from frequency-modulated spectroscopy (FMS). They confirmed the FMS results by visual assessment of macroscopic cake appearance and found the FMS method to be suitable for the determination of nucleation success. FMS is determining the partial pressure

of water in the headspace of the primary container as a surrogate for residual moisture content which in turn is highly dependent on the specific surface area of the cake. The latter is directly affected by the ice nucleation temperature/ice morphology.^{18,41,44} Additionally, the determined partial pressure values are strongly time-dependent, resulting in a minimum equilibration time of days needed before a meaningful measurement can take place.¹⁶⁰ That is why we alternatively focused on macroscopic differences in the superficial cake structure. We developed a new technique that is assessing these structural differences with a camera-supported optical inspection. It mainly determines differences in grayscale values which are dependent on the porosity, granularity, and looseness (density) of the cake. The main advantage of this technology would be the potential to be fully implemented in automated visual inspection to ensure a 100 % control of the batch after FD. It would allow discriminating vials that failed during the controlled ice nucleation step and consequently nucleated at a later point in freezing. These vials would resemble randomly nucleated vials. The current study examines the feasibility of camera-supported optical inspection for the discrimination between random shelf-ramped (RN) and controlled ice nucleated (CN) samples. A sample that has not undergone controlled nucleation during a respective freeze-drying protocol is assumed to be similar to a randomly nucleated sample which is in accordance with a report by Vollrath et al.¹⁵⁹. In the first part of this study, we investigated the glass-forming excipients Sucrose and Trehalose as placebos and with bovine serum albumin added. These formulations were freeze-dried with three different drying protocols, i.e. with controlled ice nucleation applied at -5 °C or random shelf-ramped nucleation with or without a secondary drying step. The latter was varied to investigate the robustness of the method over a broad range of residual moisture contents. In the second part, we studied the effect of three different freezing protocols covering random nucleation and controlled ice nucleation at -5 °C and -10 °C on a similar-to-market highly concentrated mAb formulation containing 120 g/L mAb and 8 % Trehalose. The parameter “average edge brightness” was introduced and examined for its feasibility as a distinction criterion under different conditions. We hypothesize that on the one hand the visually assessable superficial differences between random shelf-ramped and controlled nucleated samples can be assessed by a camera-supported inspection system. On the other hand, we anticipate the “average edge brightness” to be a reliable distinguishing criterion for all investigated conditions.

VI.3 Materials and methods

VI.3.1 Materials

Bovine serum albumin (BSA) which contained the heat shock fraction and was protease, fatty acid, and essentially globulin free (pH 7, ≥ 98 %) was purchased from Sigma-Aldrich (Steinheim, Germany). A formulation with a monoclonal antibody IgG type 1 (mAb) containing 120 g/L mAb, 8 % (w/v) Trehalose, histidine buffer, and polysorbate 80 was on stock at LMU and stored at < -65 °C before usage.

For the placebo and BSA formulations, the following excipients were used: D(+)-Sucrose, Extra Pure, SLR was obtained from Fisher Chemical (Leicestershire, UK). D(+)-Trehalose dihydrate, 99 %, Acros Organics™ was purchased from Acros Organics BVBA (Geel, Belgium). EMPROVE® exp sodium dihydrogen phosphate dihydrate was obtained from Merck KGaA (Darmstadt, Germany). Di-sodium hydrogen phosphate dihydrate (≥ 98.5 %) was purchased from Honeywell Fluka™ (Morris Plains, NJ, USA). Acetic acid 99/100 % chem. (BP) was obtained from Brenntag GmbH (Essen, Germany).

For the preparation of buffers and stock solutions, water for injection (WFI; Milli-Q® Advantage A10, Merck KGaA, Darmstadt, Germany) was used. For reconstitution of the lyophilizates WFI (Purelab Plus, USF Elga, Celle, Germany) was used, too.

VI.3.2 Preparation of formulations

50 g/L of BSA were dissolved in the respective placebo formulation in a 25 mM sodium phosphate buffer at pH 7.4 (Table VI-1).

Table VI-1 Formulations used in the study.

Formulation	mAb [g/L]	BSA [g/L]	Sucrose [% (w/v)]	Trehalose dihydrate [% (w/v)]	Methionine [% (w/v)]	Polysorbate 20 [% (w/v)]
Sucrose	/	/	5	/	/	/
Sucrose + BSA	/	50	5	/	/	/
Trehalose	/	/	/	5	/	/
Trehalose + BSA	/	50	/	5	/	/
mAb formulation	120	/	/	8	0.15	0.04

All placebo and BSA formulations were formulated in a 25 mM sodium phosphate buffer at pH 7.4. The mAb formulation was formulated in 20 mM histidine buffer at pH 5.5.

The mAb formulation was stored as a deep-frozen bulk drug substance. An aliquot was thawed in a water bath at room temperature and homogenized by gentle swaying. All formulations were filtered using a 0.22 μm PES Sartolab® RF vacuum filter unit (Sartorius AG, Goettingen, Germany). Subsequently, their concentration was measured with a NanoDrop™ 2000 UV photometer (Thermo Scientific, Wilmington, Delaware) at 280 nm using an extinction coefficient of $\epsilon_{0.1\%} = 0.667 \text{ g}/100 \text{ mL}^{-1} \text{ cm}^{-1}$ and an extinction coefficient of $\epsilon = 225,000 \text{ M}^{-1} \text{ cm}^{-1}$ with a molecular weight of $\text{MW} = 145.5 \text{ kDa}$ for BSA and mAb, respectively. 3 mL of each formulation was filled in 10R tubing vials (MGlaser AG, Muennerstadt, Germany) and semi-stoppered with lyophilization stoppers (FluroTec® rubber stopper, West Pharmaceuticals, Eschweiler, Germany).

VI.3.3 Freeze-drying processes

All placebo and BSA formulations (Table VI-1) were freeze-dried with three different protocols: two with random shelf-ramped nucleation with (RN w SD) or without secondary drying (RN w/o SD) and one with controlled ice nucleation at $-5 \text{ }^\circ\text{C}$ shelf temperature setpoint (CN) using depressurization technique on a Christ $\epsilon 2\text{-}12\text{D}$ pilot-scale freeze-dryer (Martin Christ Gefriertrocknungsanlagen GmbH, Osterode am Harz, Germany) as summarized in Table VI-2. Non-optimized conservative cycles were used.

Table VI-2 Overview of the applied freezing and drying protocols for the placebo and BSA formulations.

FD process	Setpoint	Freezing			Primary Drying	Secondary Drying	
RN w SD	TShelf [°C]	20	5	-50	-20	30	
	Ramp [K/min]	-	1	1	1	0.25	
	Hold time [min]	10	60	120	3060	540	
	pChamber [μbar]	-	-	-	90	90	
RN w/o SD	TShelf [°C]	20	5	-50	-20	-	
	Ramp [K/min]	-	1	1	1	-	
	Hold time [min]	10	60	120	3060	-	
	pChamber [μbar]	-	-	-	90	-	
CN	TShelf [°C]	20	-5	-5	-50	-15	35
	Ramp [K/min]	-	1	-	1	1	0.22
	Hold time [min]	10	30	60	120	1644	540
	Stabilization time [min]	-	30*	-	-	-	-
	pChamber [μbar]	-	2.7 x 106*	-	-	90	90

* Settings for the depressurization ice nucleation technique were as follows: chamber was pressurized to 2.7 bar ± 0.15 bar absolute pressure with pressurized air and nitrogen with a stabilization time of 30 minutes and a subsequent rapid pressure release to introduce controlled nucleation. The stabilization time and pressure setpoint were applied after the hold time stated in the same section.

The mAb formulation (Table VI-1) was freeze-dried using three different processes which mainly differed in the applied freezing protocol. These protocols comprised random shelf-ramped nucleation (RN) and controlled ice nucleation at both -5 °C (CN @ -5°C) and -10 °C (CN @ -10°C) using an ice fog technique on a Christ ε2-6D laboratory-scale freeze-dryer (Martin Christ Gefriertrocknungsanlagen GmbH, Osterode am Harz, Germany) as summarized in Table VI-3. Non-optimized cycles were used.

Table VI-3 Overview of the applied freezing and drying protocols for the mAb formulation.

Freeze-drying process	Setpoint	Freezing				Primary Drying	Secondary Drying
RN	TShelf [°C]	20	5	-50	30	30	
	Ramp [K/min]	-	1	1	1	-	
	Hold time [min]	10	60	180	540 ^b	420	
	pChamber [μbar]	-	-	-	90	90	
CN @ -5°C	TShelf [°C]	20	-5	-5	-50	30	40
	Ramp [K/min]	-	1	-	1	1	1
	Hold time [min]	10	60	60	180	717 ^c	480
	pChamber [μbar]	-	- / ^a	-	-	90	90
CN @ -10°C	TShelf [°C]	20	-10	-10	-50	30	40
	Ramp [K/min]	-	1	-	1	1	1
	Hold time [min]	10	60	60	180	457 ^d	480
	pChamber [μbar]	-	- / ^a	-	-	90	90

^a Settings for the ice fog ice nucleation technique were as follows: chamber pressure was reduced to 15 mbar ± 10 mbar with a subsequent introduction of ice crystals in the chamber by aeration through the ice condenser utilizing the external volume of the LyoCoN (Martin Christ Gefriertrocknungsanlagen GmbH, Osterode am Harz, Germany). Before the evacuation of the chamber, the designated hold time was held at atmospheric pressure.

^b Primary drying endpoint was determined automatically by comparative pressure measurement using a relative $\Delta p = 15\%$.

^c Primary drying endpoint was determined automatically by comparative pressure measurement using a relative $\Delta p = 15\%$ and $\Delta T = 1\text{ °C}$ between the lowest thermocouple and the shelf temperature.

^d Primary drying endpoint was determined automatically by comparative pressure measurement using a relative $\Delta p = 15\%$ and $\Delta T = 8\text{ °C}$ between the lowest thermocouple and the shelf temperature.

VI.3.4 Karl Fischer titration

Karl Fischer titration equipped with a headspace module was used to determine residual water content after freeze-drying. Due to huge expected differences in residual moisture content, sample aliquots between 6 mg and 59 mg were prepared in a glove box filled with pressurized air with a relative humidity of less than 10 %, filled into 2R vials and stoppered. The samples were then placed in an oven with 100 °C to enable the fast extraction of water. The headspace moisture is transported into a coulometric Karl Fischer titrator (Aqua 40.00, Elektrochemie Halle, Halle (Saale), Germany). Results are calculated in relative water content (w/w). For verification of equipment performance, three aliquots of Apura® water

standard oven 1 % by Merck KGaA (Darmstadt, Germany) were measured within a sequence. Results are given as mean \pm standard deviation (n=3).

VI.3.5 Brunauer-Emmet-Teller krypton gas adsorption

The specific surface area of dried samples was determined using Brunauer–Emmet–Teller (BET) krypton gas adsorption in a liquid nitrogen bath at 77.3 K (Autosorb 1; Quantachrome, Odelzhausen, Germany). Approximately 100 to 400 mg of a sample was gently crushed with a spatula and weighed into glass tubes. Prior to measurement, an outgassing step was performed for at least 6 h at room temperature. An 11-point gas adsorption curve was measured, covering a p/p_0 ratio of approximately 0.05– 0.30. Data evaluation was performed according to the multi-point BET method fit of the Autosorb 1 software. Results are given as mean \pm standard deviation (n=3).

VI.3.6 Reconstitution of lyophilizates

The lyophilized cakes were reconstituted by the addition of WFI. The WFI volume for each formulation was calculated to match the volume of the water removed during freeze-drying. Reconstitution time was determined by recording the time between adding the respective formulation-specific volume of water for injection and obtaining a clear solution without visible matter. This observation was performed by manual visual inspection. Reconstitution was performed applying gentle swirling for 5 s directly after the addition of water and then letting the vial stand without further swirling.

VI.3.7 Camera-supported optical inspection

The vials were placed centrally on top of a laboratory manual camera build with a centric white ring light above it as illustrated in Figure VI-1 (Seidenader Maschinenbau GmbH, Markt Schwaben, Germany). The camera in use was a monochromic 1.2 megapixel TXG12-type (Baumer Holding AG, Frauenfeld, Switzerland).

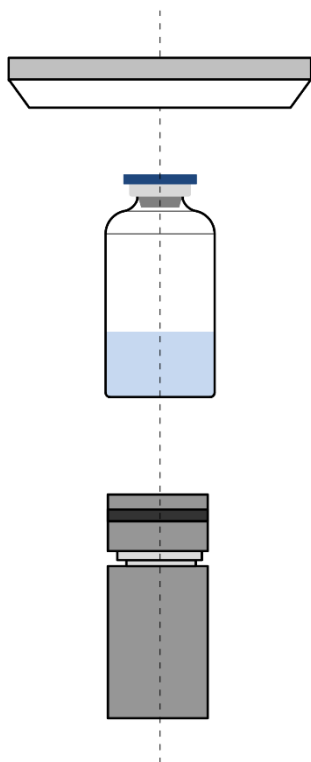


Figure VI-1 Schematic illustration of the laboratory camera setup with the vial containing the lyophilizate placed centrally above a camera equipped with a ring light centric above the vial.

The ring light illuminated the lyophilized cake from above so that the camera was taking an image of the scattered light. Dependent on the looseness (density), porosity, and granularity of the cake a grayscale image of the bottom cake structure was taken (Figure VI-2 and Figure VI-3A).

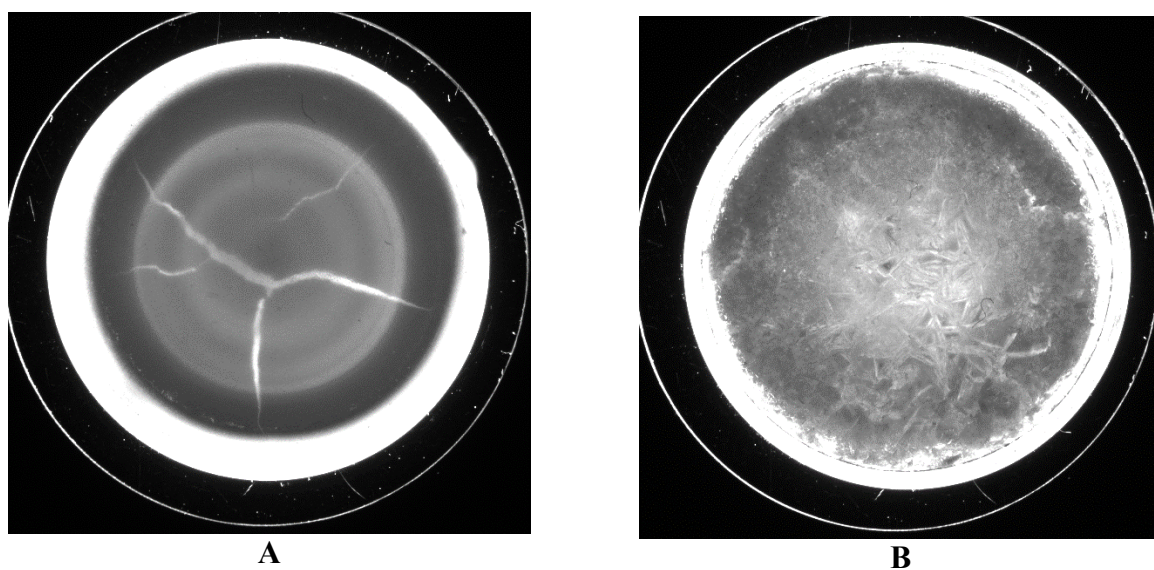


Figure VI-2 Raw example pictures of **A** the mAb formulation dried with protocol RN from **Table VI-3** and **B** the same formulation processed with protocol CN @ -5°C from **Table VI-3**.

The underlying algorithm is described briefly in the following: the differentiation was realized by the comparison of grayscale-associated parameters. Cracks within a cake would have caused artificially high grayscale values. In order to exclude these cracks from further investigation, an average grayscale value of the image was calculated. Larger areas of the picture exceeding a certain average grayscale range threshold were excluded. The resulting image is shown in Figure VI-3B and represented the mask image.

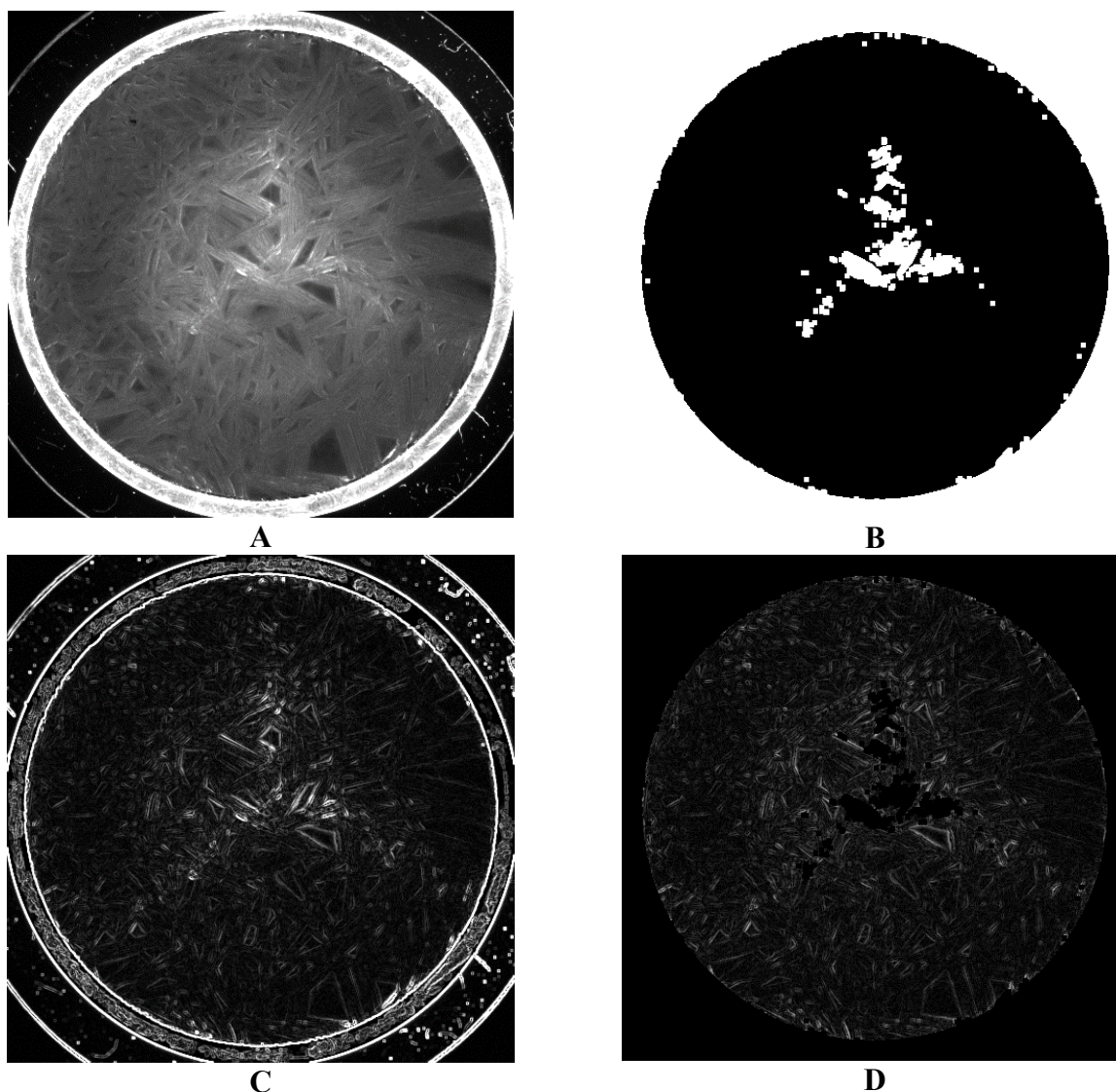


Figure VI-3 Image processing by the algorithm at the example of Sucrose+BSA formulation dried with protocol CN from **Table VI-2**. **A** raw image, **B** mask image representing areas exceeding the average grayscale range threshold **C** first derivative of the raw picture revealing edges **D** difference image of the first derivative (C) and the mask image (B) for the determination of the “average edge brightness”.

The first derivative of the raw image was calculated to amplify light-dark-transitions revealing edges (Figure VI-3C). These are small-sized pixel areas with strong grayscale differences inside the investigated pixels. Eventually, the difference image of the first

derivative of the raw picture (Figure VI-3C) and the mask image (Figure VI-3B) was generated. By that, the absolute grayscale value became negligible. The resulting difference image was used for calculation of the “average edge brightness” which was the main distinguishing criterion based on grayscale and edges (Figure VI-3D). The technical set-up and algorithm can be implemented on all machine platforms of the provider and is therefore integrable in an automated inspection station.

VI.3.8 Statistical analysis

For statistical analysis and regression analysis, Minitab 19 Statistical Software (Minitab, LLC., State College, PA, USA) and OriginPro 2017 (OriginLab Corporation, Northampton, MA, USA) were used. A one-way ANOVA with Tukey’s method was used for statistical testing at a significance level of $\alpha = 5\%$ or $\alpha = 0.1\%$. The normal distribution of the data sets was tested using the Anderson-Darling test. Due to the small sample size for specific surface area and reconstitution time ($n=3$), all tests for normal distribution (Anderson-Darling, Ryan-Joiner, Kolmogorov-Smirnov) of the samples resulted in a normally distributed population. This was in agreement with the authors’ expectations based on the nature of investigated data (specific surface area, reconstitution times). Hence, a normal distribution of these parameters was assumed.

VI.4 Results

VI.4.1 Residual moisture content and specific surface area

The results for residual moisture (RM) and specific surface area (SSA) analysis are presented in Figure VI-4. Due to the different freeze-drying protocols used (Table VI-2), a range of lyophilizates with different RM was produced. For the Sucrose placebo formulations (Figure VI-4A) residual moisture values between $2.2 \% \pm 0.1 \%$ and $1.6 \% \pm 0.2 \%$ for CN and RN w SD, respectively, were obtained. As expected, the application of controlled nucleation reduced the specific surface area. The drying protocol with random nucleation and without a secondary drying step (Table VI-2, RN w/o SD) resulted in partially liquid collapsed samples for Sucrose placebos which have not been used for further analysis.

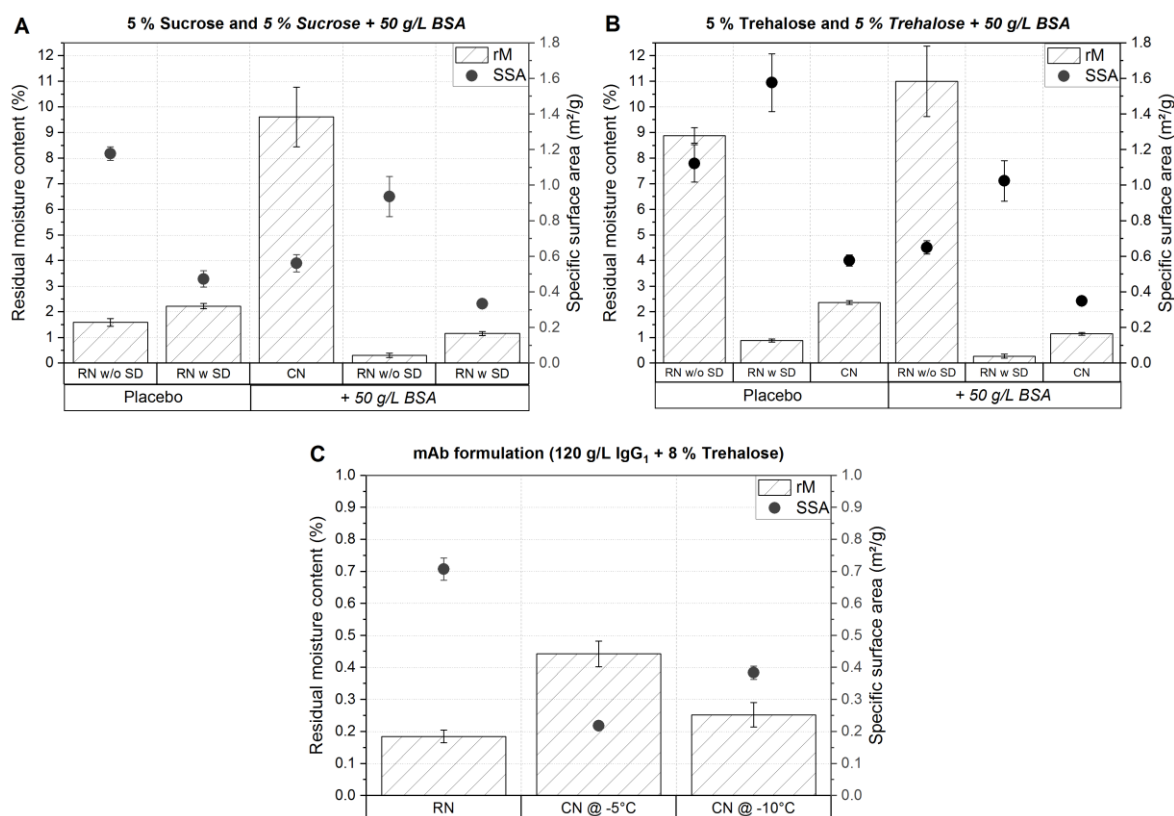


Figure VI-4 Residual moisture content (bars) and specific surface area (symbols) results for the different formulations. **A** Sucrose and Sucrose+BSA, **B** Trehalose and Trehalose+BSA, and **C** IgG₁ mAb formulation. Values shown represent the mean value ($n = 3$) \pm standard deviation.

In contrast, Sucrose + BSA samples resulted in cake-like structures for all applied freeze-drying protocols revealing moisture contents in a range of $1.2 \% \pm 0.1 \%$, $0.3 \% \pm 0.1 \%$, and $9.6 \% \pm 1.2 \%$ for CN, RN w SD and RN w/o SD, respectively. The corresponding specific surface areas indicate a microscopic collapse for the random shelf-ramped nucleated

samples which did not undergo secondary drying by a 40 % reduced SSA of $0.56 \text{ m}^2/\text{g} \pm 0.05 \text{ m}^2/\text{g}$. In contrast to that, CN samples revealed an even smaller specific surface area of $0.33 \text{ m}^2/\text{g} \pm 0.00 \text{ m}^2/\text{g}$ which was determined by the freezing step and by elevated residual moisture.

Similar observations were made for Trehalose placebo and Trehalose + BSA samples (Figure VI-4B). The former covered a range of residual moisture contents from $2.4 \% \pm 0.1 \%$, $0.9 \% \pm 0.1 \%$ and $8.9 \% \pm 0.3 \%$ for CN, RN w SD and RN w/o SD, respectively. A smaller extent of microscopic collapse by a 29 % reduction in SSA was observed for the RN w/o SD samples compared to the corresponding samples with secondary drying (RN w SD). Controlled nucleated samples again showed a strongly decreased specific surface area of $0.58 \text{ m}^2/\text{g} \pm 0.03 \text{ m}^2/\text{g}$ in comparison to $1.58 \text{ m}^2/\text{g} \pm 0.16 \text{ m}^2/\text{g}$ obtained for RN w SD solids. Trehalose + BSA lyophilizates revealed lower residual moisture contents and specific surface areas compared to placebo except for the moisture content of RN w/o SD. The BSA containing Trehalose samples showed moisture levels of $1.1 \% \pm 0.1 \%$, $0.3 \% \pm 0.1 \%$ and $11.0 \% \pm 1.4 \%$ for CN, RN w SD and RN w/o SD, respectively. Overall, as mentioned, specific surface areas were found to be smaller with $0.35 \text{ m}^2/\text{g} \pm 0.01 \text{ m}^2/\text{g}$ for CN, $1.02 \text{ m}^2/\text{g} \pm 0.11 \text{ m}^2/\text{g}$, and $0.65 \text{ m}^2/\text{g} \pm 0.04 \text{ m}^2/\text{g}$ for RN w SD and RN w/o SD, respectively, than for the pure placebo. The investigated IgG₁ mAb formulation underwent three different freezing procedures whereas drying conditions were kept similar (Table VI-3). Samples were found to be dry with only slightly higher moisture levels of 0.4 % (CN @ -5°C) and 0.3 % (CN @ -10°C) compared to 0.2 % residual moisture within random shelf-ramped nucleated samples (RN). However, specific surface areas differed statistically significant as indicated by non-overlapping 95 % confidence intervals of the mean (Figure VI-5).

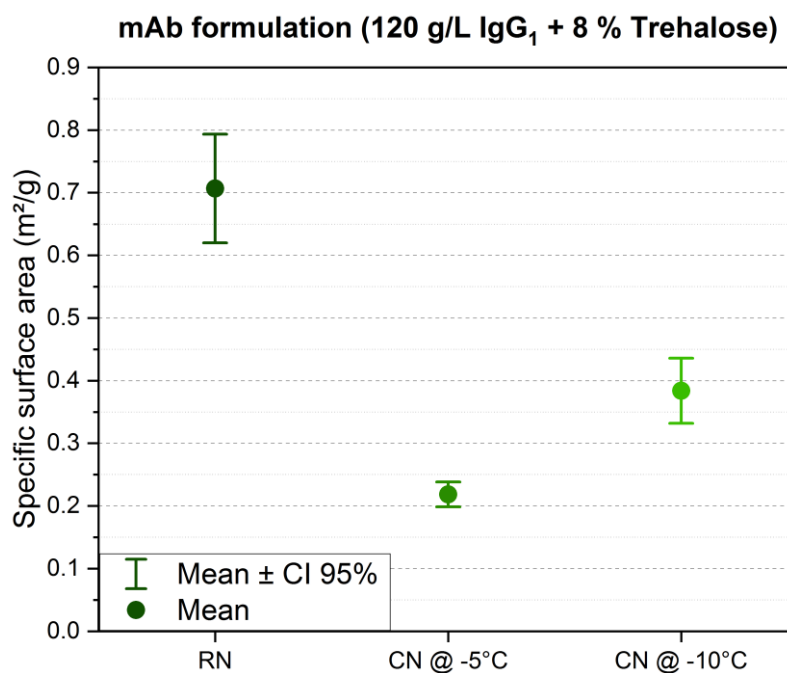


Figure VI-5 Specific surface area of the mAb formulation dependent on the nucleation temperature. Symbols represent the mean value with its 95 % confidence interval.

VI.4.2 Average edge brightness

The “average edge brightness” values derived from the raw image analysis for the different formulations and freeze-drying protocols are presented in Figure VI-6. Sucrose placebos revealed a significant difference in the determined “average edge brightness” of 10.48 ± 0.15 (95 % CI = 10.42, 10.53) compared to 41.15 ± 3.20 (95 % CI = 39.95, 42.34) for RN and CN, respectively (Figure VI-6A).

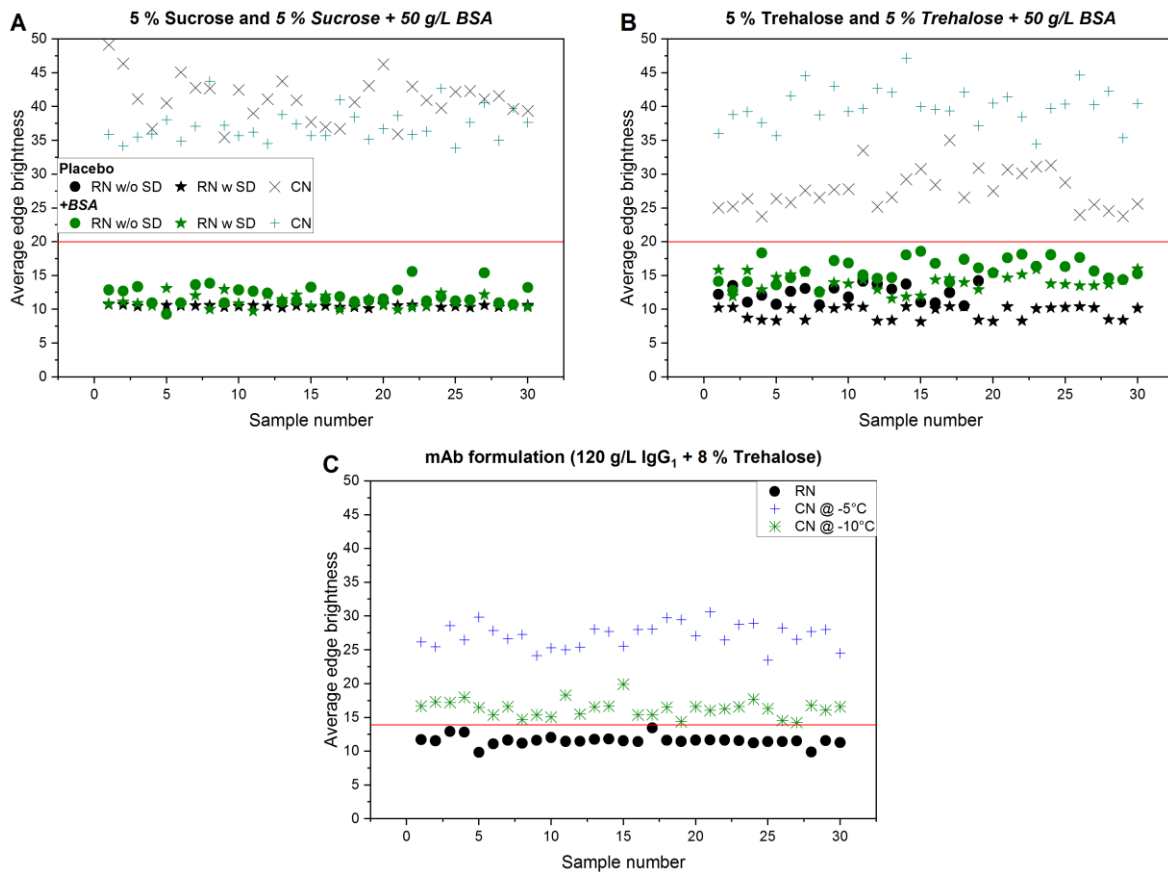


Figure VI-6 “Average edge brightness” depending on the different formulations and freeze-drying protocols. **A** Sucrose and Sucrose+BSA, **B** Trehalose and Trehalose+BSA, and **C** IgG1 mAb formulation. The red horizontal line represents the individually set distinction limit of 20 and 13.9 for A/B and C, respectively. Individual values of 30 different vials were recorded per data set.

The same clear discrimination between random shelf-ramped nucleated samples and controlled ice nucleated samples was found for Sucrose-based BSA samples. These exhibited values of 11.09 ± 0.91 (95 % CI = 10.75, 11.43) for RN w SD-samples and 37.19 ± 2.43 (95 % CI = 36.28, 38.09) for samples which underwent the CN-protocol. Even high residual moisture content within the Sucrose + BSA-matrix (RN w/o SD) only slightly increased the “average edge brightness” to 12.13 ± 1.40 (95 % CI = 11.61, 12.65) compared to identical samples which underwent a desorption step. Moreover, the slight yellow cake color introduced by the addition of BSA did not decrease the resolution of the discrimination parameter.

Similar results were found for both Trehalose lyophilizates with and without BSA (Figure VI-6B). On the one hand, absolute differences in Trehalose placebo decreased between RN without SD ($M = 12.35$, $SD = 1.25$, 95 % CI = 11.75, 12.95) and with a secondary drying step ($M = 9.51$, $SD = 0.95$, 95 % CI = 9.16, 9.87) compared to CN samples ($M = 27.70$, SD

= 2.91, 95 % CI = 26.62, 28.79). On the other hand, no such reduction was found for Trehalose formulations with BSA neither for RN without SD ($M = 15.82$, $SD = 1.71$, 95 % CI = 15.18, 16.46) or for RN with secondary drying ($M = 14.02$, $SD = 1.28$, 95 % CI = 13.54, 14.50) nor for CN samples ($M = 40.08$, $SD = 2.85$, 95 % CI = 39.01, 41.14). As a proof of concept, the newly introduced discrimination parameter of “average edge brightness” was investigated for a similar-to-market highly concentrated IgG₁ formulation nucleated with three different freezing protocols (Figure VI-6C). Values obtained for random shelf-ramped nucleated samples (RN) of 11.57 ± 0.69 (95 % CI = 11.32, 11.83) were in between the “average edge brightness” obtained for Trehalose placebos (9.51 ± 0.95) and Trehalose + BSA (14.02 ± 1.28). Interestingly, the “average edge brightness” of 27.16 ± 1.79 (95 % CI = 26.49, 27.83) for CN @ -5°C was found to be essentially the same as for the Trehalose placebo formulation with CN (27.70 ± 2.91) but not for the Trehalose + BSA with CN (40.08 ± 2.85). However, clear discrimination between RN and CN @ -5°C samples was possible. For controlled ice nucleation at -10 °C lower values of 16.30 ± 1.23 (95 % CI = 15.84, 16.75) were found; slowly approximating to the value of RN. Yet, the mean values of the two populations, RN and CN @ -10°C, were still different on a significance level of $p < .001$ as shown in Figure VI-7A and analyzed by a one-way ANOVA. Moreover, a clear distinction between the two populations can be seen in the box-plot (Figure VI-7B) showing the measure of location and statistical dispersion for the different freezing protocols. Only single outliers of the RN sample set approximated close to the distinction limit. Overall, the method was still capable to discriminate between RN and CN @ -10°C for all samples.

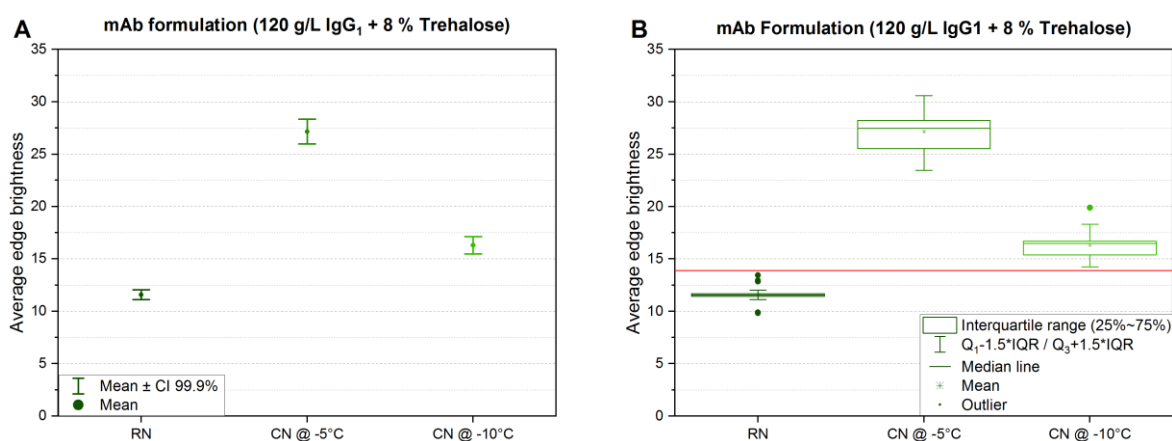


Figure VI-7 “Average edge brightness” of the mAb formulation dependent on the nucleation temperature. **A** 99.9 % confidence intervals of the mean. **B** Box-plot of differently frozen populations showing the measure of location and statistical dispersion. The red horizontal line represents the individually set distinction limit of 13.9.

VI.4.3 Reconstitution time

Controlled nucleation was reported to reduce reconstitution times in protein formulations^{48,56,57,161}, especially in highly concentrated protein formulations^{57,161}. Figure VI-8 shows the 95 % confidence intervals of the mean reconstitution times for the different freezing protocols used for the highly concentrated similar-to-market formulation. Surprisingly, no positive effect on reconstitution behavior was found. We, therefore, suggest that this is highly dependent on the chosen formulation (mAb, excipients) and applied process conditions.

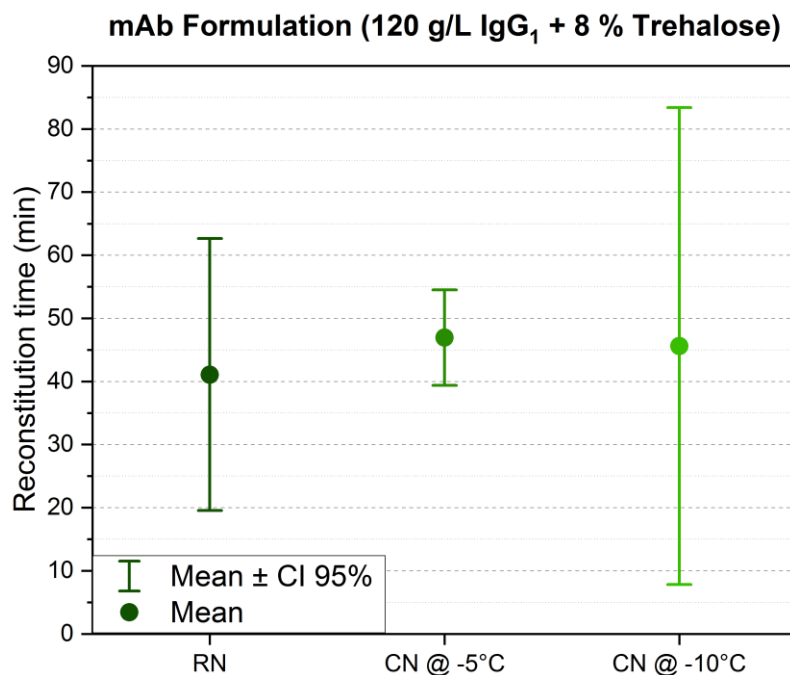


Figure VI-8 Reconstitution time of the mAb formulation dependent on the nucleation temperature. Symbols represent the mean value with its 95 % confidence interval.

VI.5 Discussion

VI.5.1 The feasibility of optical camera inspection for determination of nucleation success

Controlled ice nucleation has been intensively discussed in the literature for its potential advantages over random shelf-ramped nucleation in terms of process improvements^{40,43,50,52,53,55} and critical product quality attributes^{40,43,54-59}. However, especially due to potentially more aggressive cycles that can be applied with controlled ice nucleation, assurance of 100 % nucleation success becomes essential. For example, Goshima et al.¹⁶² showed that the design space of a product is directly affected by the ice morphology with larger pores significantly enlarging the design space. The design space as part of quality by design is expected by regulatory agencies based on ICH Q8(R2) and was investigated for its implementation in freeze-drying process development.¹⁶³⁻¹⁶⁶ The application of controlled ice nucleation can be seen as one control strategy to fulfill regulatory expectations. However, its implementation requires a reliable assessment of the nucleation success batch by batch for validation, scale-up, and quality assurance purposes. Hence, the need for an easy-implementable and non-invasive method for 100 % controlled ice nucleation success assessment is high.

The only published method for nucleation success control was recently described by Vollrath et al.¹⁵⁹. They discriminated CN failure vials by the application of frequency-modulated spectroscopy (FMS). FMS is determining the partial pressure of water in the headspace of the primary container as a surrogate for residual moisture content. The latter is highly dependent on the specific surface area which is directly affected by the ice nucleation temperature/ice morphology.^{18,41,44} Partial pressure values are strongly time-dependent and, therefore, several days of holding or intermediate storage time would be needed after a batch has been unloaded from the freeze-dryer.¹⁶⁰ Our alternative approach, the camera-supported optical inspection, is based on the assessment of macroscopic differences in the cake surface structure. It was noticed by several authors that controlled nucleated lyophilization cakes reveal a more porous, loose, i.e. less dense, and more or less granular structure with a higher rate of cracks compared to random shelf-ramped lyophilizates.^{159,167} Figure VI-6 demonstrates that the “average edge brightness” derived from the optical inspection was a good and reliable distinguishing criterion for discrimination between RN and CN. It was shown that a clear and reproducible differentiation in different pharmaceutically relevant amorphous excipient systems was feasible. In Sucrose formulations with or without bovine

serum albumin the best resolution, i.e. the greatest distance of single values to the distinction limit, between randomly and controlled nucleated vials was found (Figure VI-6A). For Trehalose-based formulations resolution decreased slightly, but yet differently treated populations were very well distinguishable (Figure VI-6B). Based on these results, the authors conclude that the method was neither affected by the change in composition (type of excipient, total solid content, introduction of polymer-like BSA) nor by extremely different residual moisture content (Figure VI-4A+B). In fact, the “average edge brightness” was almost unaffected by residual moisture differences, even though BET measurements indicated differences in microscopic structure. For example, for BSA-containing Trehalose lyophilizates with and without secondary drying, residual moisture contents of 0.3 % and 11.0 %, respectively, were found. Corresponding “average edge brightness” values were 14.02 ± 1.28 (w SD) and 15.82 ± 1.71 (w/o SD), although specific surface areas were found to be apparently different with $1.02 \text{ m}^2/\text{g} \pm 0.11 \text{ m}^2/\text{g}$ and $0.65 \text{ m}^2/\text{g} \pm 0.04 \text{ m}^2/\text{g}$ for RN w SD and RN w/o SD, respectively. Although both microscopic collapse due to high RM content and application of CN led to a significant decrease in SSA, “average edge brightness” was still capable of distinguishing between randomly and controlled nucleated samples. Moreover, it seems obvious that regularly found moisture differences between center- and edge-vials within one freeze-drying run would not affect the resolution of the newly proposed method.

The proof of concept of our approach was provided by the investigation of a similar-to-market formulation with a highly concentrated IgG₁ in a Trehalose-based formulation. In contrast to the placebo + BSA formulations, two different controlled ice nucleation protocols were applied and compared to a random shelf-ramped freeze-drying cycle (Table VI-3). Figure VI-5 shows that the different species are statistically significantly different concerning the specific surface area. These SSA values translated into a pronounced macroscopic difference between RN and CN @ -5°C samples as shown exemplarily in Figure VI-2. Consequently, the clear discrimination of these two populations based on “average edge brightness” was possible (Figure VI-6C, Figure VI-7). A distinction between samples produced by random nucleation and controlled nucleation at -10 °C was still feasible (Figure VI-6C). However, a few individual outliers of the RN population appeared to result in quite similar “average edge brightness” values as obtained for CN @ -10°C (Figure VI-7B). This is because the morphology and specific surface area of the cake are primarily determined by the nucleation temperature.^{18,50} Experimentally obtained nucleation temperatures for random shelf-ramped nucleation were reported by Konstantinidis et al.⁵⁰

to be in the range of -7.2 °C to -16.6 °C for a 5 % Sucrose formulation in a laboratory setup. The freezing behavior of Sucrose and Trehalose is presumably the same, wherefore RN samples were probably stochastically nucleating within the same temperature range. This resulted in a potential overlap with samples that were controlled nucleated at -10 °C. However, all different mAb formulation samples were still reliably distinguished.

VI.5.2 Average edge brightness as a surrogate with reservations for specific surface area

The specific surface area determined by BET measurement is a sensitive measure for freezing-^{41,44} or drying-induced¹⁶⁸ changes. However, its destructive and time-consuming character are typical drawbacks. In contrast, a non-invasive, rapid surrogate for routine measurements could be attractive. The newly introduced “average edge brightness” showed the potential to distinguish between samples nucleated at different nucleation temperatures corresponding to different SSA values. A simple linear regression model revealed already a good negative correlation as shown in Figure VI-9. Such a model could be used for routine verification during production instead of SSA analysis.

However, the prognostic R^2 is rather low and needs to be improved to predict specific surface area values accurately for a known formulation. This could be particularly of interest when platform formulations are used. In the course of freeze-drying process development, the collection of a sufficiently big data set for a formulation-specific mathematical model is imaginable which could allow for “designing” the drying characteristics of a new product based on porosity indirectly assessed by rapid camera inspection. Consequently, the “average edge brightness” could be of value as a surrogate with reservations for SSA in future development processes.

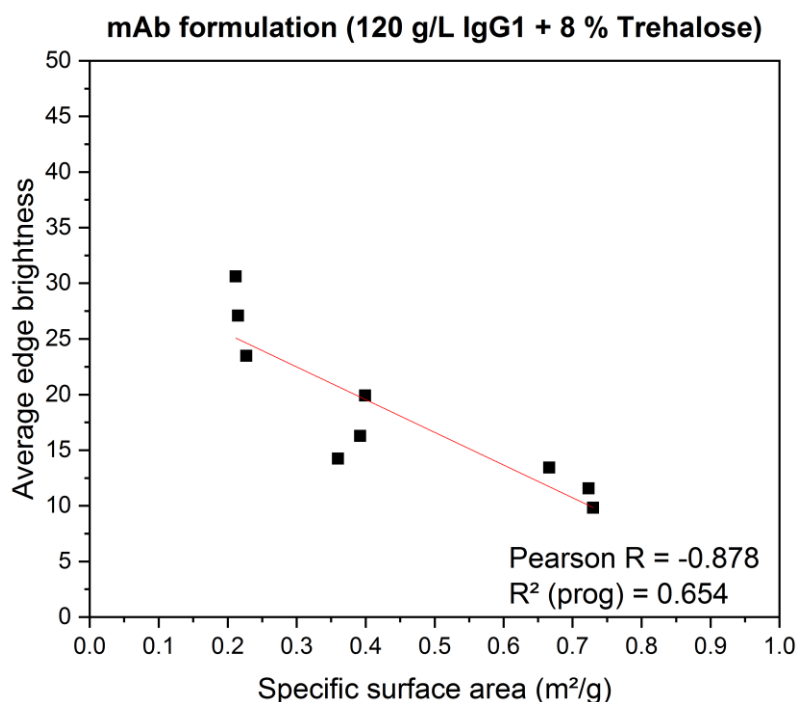


Figure VI-9 Linear regression model with “average edge brightness” over the specific surface area containing data of the mAb formulation processed at three different freezing protocols (Table VI-3).

VI.5.3 Limitations

Based on the results obtained for the mAb formulation (Figure VI-6C, Figure VI-7B) the discrimination of CN samples nucleated at low nucleation temperatures (i.e. ≤ -10 °C) could be limiting. However, the resolution may be improved with lyophilizates produced in a Class 100 cleanroom environment. This assumption is based on theoretical considerations and practical observations described in the literature for random shelf-ramped freezing. The cleaner the environment, the lesser potential airborne nucleation sites are present, leading to a higher degree of supercooling and thus, huger differences in nucleation temperatures compared to those obtained in controlled ice nucleation.^{18,41,44,58,169} Rambhatla et al. estimated that solutions in the manufacturing scale would typically experience approximately 20 °C supercooling⁴¹ compared to ~ 13 °C – 14 °C supercooling observed by Searles et al.¹⁸ and Fang et al.⁵⁸ in a laboratory environment. Additionally, the applied algorithm for raw image processing was kept rather simple. By changes in thresholds or further addition of filters to the image processing procedure, an optimization of the resolution is feasible as well.

VI.6 Conclusion

We describe a new method to discriminate in freeze-drying with controlled ice nucleation between vials that nucleate at controlled nucleation conditions and others that fail and nucleate at a later stage in freezing, using camera-supported optical inspection. The parameter “average edge brightness” which can be easily derived from a raw image taken from the bottom of the vial with a simple raw image processing is introduced. It is successfully applied to Sucrose- and Trehalose-based placebo and BSA formulations resulting in a clear distinction between random shelf-ramped (i.e. vials that failed CN) and controlled nucleated samples. A proof of concept is provided by applying the technology to a similar-to-market high concentrated IgG₁ mAb formulation with Trehalose which underwent three different freezing protocols, i.e. random nucleation and controlled ice nucleation at -5 °C and -10 °C. The sample populations were found to be statistically significantly different with a significance level of $p < .001$ with respect to the “average edge brightness”. By this, the technology allows for reliable, non-invasive, and potentially automatable 100 % monitoring of controlled nucleation success after freeze-drying.

Acknowledgments

The support from the Global Technology Management from Boehringer Ingelheim Pharma GmbH & Co. KG is kindly acknowledged. Also, the authors thank Manuel Breitfeld and Tiziana Bummer for help with the preparation of the placebo and BSA batches. Katharina Kopp is acknowledged for her help with the reconstitution studies.

Conflicts of Interest

Werner Halbinger is an employee of Seidenader Maschinenbau GmbH. The company is the manufacturer and distributor of the visual inspection equipment used in the study. However, Seidenader was neither involved in the conceptualization of the study nor the interpretation of results or drawing of conclusions. The authors, therefore, declare no conflict of interest.

Chapter VII Final summary and conclusion of the thesis

The primary aim of the first part of this thesis was to study the feasibility and applicability of microwave-assisted freeze-drying to monoclonal antibody formulations in vials. **Chapter I** gave a general introduction to the basic principles of conventional freeze-drying and a brief overview of emerging technologies like MFD with their reported advantages and associated challenges. With this background, I investigated in **Chapter II** the applicability of MFD to established excipients used in conventional freeze-drying with a low concentration antibody formulation. The excipients studied comprised sucrose, trehalose, a 4:1 mannitol:sucrose-mixture, a sucrose formulation with only 1 % (w/v) sucrose content, a 1:1 sucrose:HP- β -CD-mixture as well as an ionic stabilizer system with arginine phosphate. I found that microwave-assisted freeze-drying (1) was able to shorten the drying process by more than 75 % compared to a conservative CFD cycle and that (2) it could be successfully applied for the drying of these formulations. However, higher variances in solid state analysis of the samples processed with MFD were found indicating an inferior drying and batch homogeneity. Moreover, information on product quality over storage was still lacking. For this reason, I studied in **Chapter III** the storage stability of four different formulations with 5 g/L or 50 g/L mAb concentration for six months. Also, I introduced a new generator set up to investigate its effect on batch homogeneity. Besides the significant time savings in MFD; I was able to elucidate comparable stability profiles for the different antibody formulations composed of classical lyophilization excipients like sucrose, trehalose and, selected due to findings from Chapter II, arginine phosphate. Even with the extended analytical toolbox applied and accelerated stress conditions of 40 °C for 24 weeks, no differences in product quality and stability were found between CFD and MFD. Yet again, I found indications for an increased batch heterogeneity within MFD batches produced with the indirect magnetron generator setup introduced in Chapter II. Especially with respect to residual moisture content which is considered one critical quality attribute of lyophilizates the first setup appeared less favorable. In contrast, the data of the product batch produced with the modern semiconductor solid-state microwave generator (Chapter III) indicated a batch homogeneity comparable to the conventionally freeze-dried samples. However, future investigations should systematically study the potential and limitations of modern generator setups as well as new machinery concepts complying with the manufacturing requirements of (sterile) pharmaceutical dosage forms. Besides, the

evaluation of critical product quality attributes focusing on chemical changes within a protein drug and investigating batch homogeneity analysis could be of particular interest.

In the second part of this thesis, the focus was on unresolved issues of controlled ice nucleation like process design, comparability of mechanistically different techniques, and non-invasive monitoring of the nucleation success.

The first two commercially available CN techniques, ice fog and depressurization, were compared for the similarity of process performance and critical product quality attributes in a case study in **Chapter IV**. I found that regarding nucleation behavior and resulting process length both techniques are well comparable. Moreover, I was able to show that the resulting products were practically identical in all three pharmaceutically relevant model formulations (sucrose-, trehalose, mannitol-sucrose-based) with respect to solid state properties and in protein-related analyses. Therefore, I concluded that the control of ice nucleation as such is more relevant than the applied mechanism concerning depressurization and ice fog. However, formulation aspects (e.g. mAb and excipient concentration) and different process conditions (e.g. different T_N or CN protocols) were out of the scope of this study but could be of interest for future investigations.

To deepen the process understanding of different factors on the success of controlled ice nucleation, I performed freezing studies in **Chapter V** taking formulation aspects like solid content or filling volume as well as process aspects like shelf temperature or post-CN hold time into consideration. A regression model was generated to elucidate the mutual interplay of these factors. I demonstrated that in particular, the shelf temperature setpoint for pre-CN equilibration and subsequent initiation of the nucleation event is key for a desirable nucleation result. Based on the literature and my findings, I made general recommendations for the controlled ice nucleation process design (section V.3.4). Still, extensive systematic investigations on a good nucleation practice are strongly needed in the future. In order to be able to control the nucleation success of a full freeze-dried batch, I developed a new camera-supported optical inspection method to particularly detect the vials that failed to nucleate during CN. In **Chapter VI**, I introduced the distinction parameter “average edge brightness” which was successfully applied to sucrose- and trehalose-based placebos and BSA formulations processed with different freezing protocols and with different residual moisture contents. With a high concentration IgG₁ mAb formulation freeze-dried with different protocols, I demonstrated the proof of concept of this new non-invasive and non-destructive method with an extremely significant difference of $p < .001$ for the two sample

populations with respect to the introduced parameter “average edge brightness”. By this, I described a new simple method to reliably perform a 100 % control of controlled ice nucleation success after freeze-drying.

Ultimately, this work contains various significant findings in the field of pharmaceutical freeze-drying of biologicals. I was able to show the potential of microwave-assisted freeze-drying for the optimization of freeze-drying in terms of process time while maintaining overall product quality. However, also the pitfalls and limitations of the technology as well as of the currently available prototype are discussed. In the field of controlled ice nucleation, several benefits related to the application of controlled ice nucleation have been reported before, so that my findings should rather support process scientists in the data-driven implementation of CN. I demonstrated the interchangeability of CN techniques depressurization and ice fog. Additionally, I systematically investigated the effects of different formulation and CN process parameters on the success of controlled nucleation leading to general recommendations for process design. Furthermore, I developed a new simple method using camera-supported optical inspection for the 100 % control of nucleation success to overcome disadvantages of current headspace-based methods which often need long equilibration times to deliver reliable and reproducible results.

References

1. Flosdorf, E. W., Stokes, F. J. & Mudd, S. The desivac process for drying from the frozen state. *J. Am. Med. Assoc.* 115, 1095–1097 (1940).
2. Greaves, R. I. N. *The preservation of proteins by drying*. (His Majesty's stationery office, 1946).
3. Rey, L. Glimpses into the Realm of Freeze-Drying: Classical Issues and New Ventures. in *Freeze-Drying/Lyophilization of Pharmaceutical and Biological Products* (eds. Rey, L. & May, J. C.). Vol. 206. (Informa Healthcare, 2010).
4. Wang, W. Lyophilization and development of solid protein pharmaceuticals. *Int. J. Pharm.* 203, 1–60 (2000).
5. Manning, M. C., Patel, K. & Borchardt, R. T. Stability of Protein Pharmaceuticals. *Pharm. Res.* 6, 903– 918 (1989).
6. Arakawa, T., Prestrelski, S. J., Kenney, W. C. & Carpenter, J. F. Factors affecting short-term and long term stabilities of proteins. *Adv. Drug Deliv. Rev.* 10, 1–28 (1993).
7. Franks, F. Freeze-drying of bioproducts: Putting principles into practice. *Eur. J. Pharm. Biopharm.* 45, 221–229 (1998).
8. Manning, M. C., Chou, D. K., Murphy, B. M., Payne, R. W. & Katayama, D. S. Stability of protein pharmaceuticals: An update. *Pharm. Res.* 27, 544–575 (2010).
9. Manning, M. C., Liu, J., Li, T. & Holcomb, R. E. Rational Design of Liquid Formulations of Proteins. in *Advances in Protein Chemistry and Structural Biology* Vol. 112. 1–59 (Elsevier Inc., 2018).
10. Chi, E. Y., Krishnan, S., Randolph, T. W. & Carpenter, J. F. Physical Stability of Proteins in Aqueous Solution: Mechanism and Driving Forces in Nonnative Protein Aggregation. *Pharm. Res.* 20, 1325–1336 (2003).
11. Tang, X. & Pikal, M. J. Measurement of the kinetics of protein unfolding in viscous systems and implications for protein stability in freeze-drying. *Pharm. Res.* 22, 1176–1185 (2005).
12. Wang, W. & Ohtake, S. Science and art of protein formulation development. *Int. J. Pharm.* 568, 118505 (2019).
13. Ohtake, S., Izutsu, K. & Lechuga-Ballesteros, D. *Drying Technologies for Biotechnology and Pharmaceutical Applications*. (Wiley-VCH Verlag GmbH, 2020).
14. Rey, L. Glimpses into the Realm of Freeze-Drying: Fundamental Issues. in *Freeze-Drying/Lyophilization of Pharmaceutical and Biological Products* (eds. Rey, L. & May, J. C.) (CRC Press, 2004).
15. Ó'Fágáin, C. Lyophilization of Proteins. in *Protein Purification Protocols* Vol. 368. 309–322 (Humana Press, 2007).
16. Jennings, T. A. *Lyophilization: Introduction and Basic Principles*. (Taylor & Francis, 1999).
17. Kasper, J. C. & Friess, W. The freezing step in lyophilization: Physico-chemical fundamentals, freezing methods and consequences on process performance and quality attributes of biopharmaceuticals. *Eur. J. Pharm. Biopharm.* 78, 248–263 (2011).
18. Searles, J. A., Carpenter, J. F. & Randolph, T. W. The ice nucleation temperature determines the primary drying rate of lyophilization for samples frozen on a temperature-controlled shelf. *J. Pharm. Sci.* 90, 860–871 (2001).
19. Hillig, W. B. & Turnbull, D. Theory of Crystal Growth in Undercooled Pure Liquids. *J. Chem. Phys.* 24, 914–914 (1956).
20. Burke, M. J., Gusta, L. V., Quamme, H. A., Weiser, C. J. & Li, P. H. Freezing and Injury in Plants. *Annu. Rev. Plant Physiol.* 27, 507–528 (1976).
21. Geidobler, R. & Winter, G. Controlled ice nucleation in the field of freeze-drying: Fundamentals and technology review. *Eur. J. Pharm. Biopharm.* 85, 214–222 (2013).
22. Searles, J.A. Freezing and Annealing Phenomena in Lyophilization. in *Freeze Drying/Lyophilization of*

References

- Pharmaceutical and Biological Products* (eds. Rey, L. & May, J. C.) 52–81 (CRC Press, **2004**).
23. Mattern, M., Winter, G., Kohnert, U. & Lee, G. Formulation of proteins in vacuum-dried glasses. II. Process and storage stability in sugar-free amino acid systems. *Pharm. Dev. Technol.* 4, 199–208 (**1999**).
 24. Mackenzie, A. P. Basic principles of freeze-drying for pharmaceuticals. *Bull. Parenter. Drug Assoc.* 20, 101–130 (**1966**).
 25. Schersch, K. B. Effect of Collapse on Pharmaceutical Protein Lyophilizates. *Dissertation*. (Ludwig-Maximilians-Universität München, **2009**).
 26. Pansare, S. K. & Patel, S. M. Practical Considerations for Determination of Glass Transition Temperature of a Maximally Freeze Concentrated Solution. *AAPS PharmSciTech* 17, 805–819 (**2016**).
 27. Depaz, R. A., Pansare, S. & Patel, S. M. Freeze-Drying Above the Glass Transition Temperature in Amorphous Protein Formulations While Maintaining Product Quality and Improving Process Efficiency. *J. Pharm. Sci.* 105, 40–49 (**2015**).
 28. Pikal, M. J. & Shah, S. The collapse temperature in freeze drying: Dependence on measurement methodology and rate of water removal from the glassy phase. *Int. J. Pharm.* 62, 165–186 (**1990**).
 29. Meister, E. & Gieseler, H. Freeze-dry microscopy of protein/sugar mixtures: Drying behavior, interpretation of collapse temperatures and a comparison to corresponding glass transition data. *J. Pharm. Sci.* 98, 3072–3087 (**2009**).
 30. Bhatnagar, B. S., Bogner, R. H. & Pikal, M. J. Protein stability during freezing: separation of stresses and mechanisms of protein stabilization. *Pharm. Dev. Technol.* 12, 505–523 (**2007**).
 31. Hatley, R. H. M. & Franks, F. The cold-induced denaturation of lactate dehydrogenase at sub-zero temperatures in the absence of perturbants. *FEBS Lett.* 257, 171–173 (**1989**).
 32. Lazar, K. L., Patapoff, T. W. & Sharma, V. K. Cold denaturation of monoclonal antibodies. *MAbs* 2, 42–52 (**2010**).
 33. Roessler, U., Leitgeb, S. & Nidetzky, B. Protein freeze concentration and micro-segregation analysed in a temperature-controlled freeze container. *Biotechnol. Reports* 6, 108–111 (**2015**).
 34. Bhatnagar, B. S., Pikal, M. J. & Bogner, R. H. Study of the Individual Contributions of Ice Formation and Freeze-Concentration on Isothermal Stability of Lactate Dehydrogenase during Freezing. *J. Pharm. Sci.* 97, 798–814 (**2008**).
 35. Gómez, G., Pikal, M. J. & Rodríguez-Hornedo, N. Effect of initial buffer composition on pH changes during far-from-equilibrium freezing of sodium phosphate buffer solutions. *Pharm. Res.* 18, 90–97 (**2001**).
 36. Bhatnagar, B. *et al.* Protein/ice Interaction: High-Resolution Synchrotron X-Ray Diffraction Differentiates Pharmaceutical Proteins From Lysozyme. *J. Phys. Chem. B* 123, 5690–5699 (**2019**).
 37. Schwegman, J. J., Carpenter, J. F. & Nail, S. L. Evidence of partial unfolding of proteins at the ice/freezing-concentrate interface by infrared microscopy. *J. Pharm. Sci.* 98, 3239–3246 (**2009**).
 38. Assegehegn, G., Brito-de la Fuente, E., Franco, J. M. & Gallegos, C. The Importance of Understanding the Freezing Step and Its Impact on Freeze-Drying Process Performance. *J. Pharm. Sci.* 108, 1378–1395 (**2019**).
 39. Tang, X. & Pikal, M. J. Design of Freeze-Drying Processes for Pharmaceuticals: Practical Advice. *Pharm. Res.* 21, 191–200 (**2004**).
 40. Esfandiary, R., Gattu, S. K., Stewart, J. M. & Patel, S. M. Effect of Freezing on Lyophilization Process Performance and Drug Product Cake Appearance. *J. Pharm. Sci.* 105, 1427–1433 (**2016**).
 41. Rambhatla, S., Ramot, R., Bhugra, C. & Pikal, M. J. Heat and mass transfer scale-up issues during freeze drying: II. Control and characterization of the degree of supercooling. *AAPS PharmSciTech.* 5, 54–62 (**2004**).
 42. Hsu, C. C. *et al.* Surface denaturation at solid-void interface--a possible pathway by which opalescent particulates form during the storage of lyophilized tissue-type plasminogen activator at high temperatures. *Pharm. Res.* 12, 69–77 (**1995**).
 43. Oddone, I., Barresi, A. A. & Pisano, R. Influence of controlled ice nucleation on the freeze-drying of

-
- pharmaceutical products: the secondary drying step. *Int. J. Pharm.* 524, 134–140 (2017).
44. Patel, S. M., Bhugra, C. & Pikal, M. J. Reduced pressure ice fog technique for controlled ice nucleation during freeze-drying. *AAPS PharmSciTech.* 10, 1406–1411 (2009).
 45. Chakravarty, P., Lee, R., DeMarco, F. & Renzi, E. Ice Fog as a Means to Induce Uniform Ice Nucleation During Lyophilization. *BioPharm Int.* 25, (2012).
 46. Ling, W. Controlled Nucleation During Freezing Step of Freeze Drying Cycle Using Pressure Differential Ice Crystals Distribution From Condensed Frost. US Patent no. US8875413 B2. (2014).
 47. Ling, W. Controlled Nucleation During Freezing Step of Freeze Drying Cycle Using Pressure Differential Ice Fog Distribution. US Patent no. US8839528 B2. (2014).
 48. Gitter, J. H., Geidobler, R., Presser, I. & Winter, G. A Comparison of Controlled Ice Nucleation Techniques for Freeze-Drying of a Therapeutic Antibody. *J. Pharm. Sci.* 107, 2748–2754 (2018).
 49. Geidobler, R., Mannschedel, S. & Winter, G. A New Approach to Achieve Controlled Ice Nucleation of Supercooled Solutions During the Freezing Step in Freeze-Drying. *J. Pharm. Sci.* 101, 4409–4413 (2012).
 50. Konstantinidis, A. K., Kuu, W., Otten, L., Nail, S. L. & Sever, R. R. Controlled nucleation in freeze-drying: Effects on pore size in the dried product layer, mass transfer resistance, and primary drying rate. *J. Pharm. Sci.* 100, 3453–3470 (2011).
 51. Gasteyer III, T. H., Rex Sever, R., Hunek, B., Grinter, N. & Verdone, M. L. Method of Inducing Nucleation of a Material. US Patent no. US9453675 B2. (2016).
 52. Kramer, M., Sennhenn, B. & Lee, G. Freeze-drying using vacuum-induced surface freezing. *J. Pharm. Sci.* 91, 433–443 (2002).
 53. Oddone, I., Pisano, R., Bullich, R. & Stewart, P. Vacuum-induced nucleation as a method for freeze-drying cycle optimization. *Ind. Eng. Chem. Res.* 53, 18236–18244 (2014).
 54. Oddone, I., Van Bockstal, P. J., De Beer, T. & Pisano, R. Impact of vacuum-induced surface freezing on inter- and intra-vial heterogeneity. *Eur. J. Pharm. Biopharm.* 103, 167–178 (2016).
 55. Awotwe-Otoo, D. *et al.* Impact of controlled ice nucleation on process performance and quality attributes of a lyophilized monoclonal antibody. *Int. J. Pharm.* 450, 70–78 (2013).
 56. Awotwe-Otoo, D. *et al.* Product and process understanding to relate the effect of freezing method on glycation and aggregation of lyophilized monoclonal antibody formulations. *Int. J. Pharm.* 490, 341–350 (2015).
 57. Geidobler, R., Konrad, I. & Winter, G. Can controlled ice nucleation improve freeze-drying of highly-concentrated protein formulations? *J. Pharm. Sci.* 102, 3915–3919 (2013).
 58. Fang, R., Tanaka, K., Mudhivarathi, V., Bogner, R. H. & Pikal, M. J. Effect of Controlled Ice Nucleation on Stability of Lactate Dehydrogenase During Freeze-Drying. *J. Pharm. Sci.* 107, 824–830 (2018).
 59. Oddone, I. *et al.* Vacuum-Induced Surface Freezing for the Freeze-Drying of the Human Growth Hormone: How Does Nucleation Control Affect Protein Stability? *J. Pharm. Sci.* 109, 254–263 (2019).
 60. Pikal, M. J., Roy, M. L. & Shah, S. Mass and heat transfer in vial freeze-drying of pharmaceuticals: role of the vial. *J. Pharm. Sci.* 73, 1224–1237 (1984).
 61. Pikal, M. J. Freeze-drying of proteins. Part II: formulation selection. *BioPharm* 3, 26–30 (1990).
 62. Pikal, M. J. Freeze-drying of proteins. Part I: process design. *BioPharm* 3, 18–27 (1990).
 63. Pikal, M. J. & Lang, J. E. Rubber closures as a source of haze in freeze dried parenterals: test methodology for closure evaluation. *J. Parenter. Drug Assoc.* 32, 162–173 (1978).
 64. Pikal, M. J., Shah, S., Senior, D. & Lang, J. E. Physical chemistry of freeze-drying: measurement of sublimation rates for frozen aqueous solutions by a microbalance technique. *J. Pharm. Sci.* 72, 635–650 (1983).
 65. Pikal, M. J. Use of Laboratory Data in Freeze Drying Process Design: Heat and Mass Transfer Coefficients and the Computer Simulation of Freeze Drying. *PDA J. Pharm. Sci. Technol.* 39, 115–139 (1985).
 66. Nail, S. L. The Effect of Chamber Pressure on Heat Transfer in the Freeze Drying of Parenteral Solutions. *PDA*

References

- J. Pharm. Sci. Technol.* 34, 358–368 (1980).
67. Rambhatla, S. & Pikal, M. J. Heat and mass transfer scale-up issues during freeze-drying, I: Atypical radiation and the edge vial effect. *AAPS PharmSciTech.* 4, 22–31 (2003).
68. Franks, F. *Freeze-drying of Pharmaceuticals and Biopharmaceuticals*. (The Royal Society of Chemistry, 2007).
69. Carpenter, J. F., Pikal, M. J., Chang, B. S. & Randolph, T. W. Rational Design of Stable Lyophilized Protein Formulations: Some Practical Advice. *Pharm. Res.* 14, 969–975 (1997).
70. Yoshioka, S., Aso, Y. & Kojima, S. Dependence of the Molecular Mobility and Protein Stability of Freeze-Dried gamma-Globulin Formulations on the Molecular Weight of Dextran. *Pharm. Res.* 14, 736–741 (1997).
71. Hellman, K., Miller, D. S. & Cammack, K. A. The effect of freeze-drying on the quaternary structure of l-asparaginase from *Erwinia carotovora*. *Biochim. Biophys. Acta - Protein Struct. Mol. Enzymol.* 749, 133–142 (1983).
72. Hsu, C. C. *et al.* Determining the optimum residual moisture in lyophilized protein pharmaceuticals. in *Developments in biological standardization*. 255–271 (Karger, 1992).
73. Breen, E. D., Curley, J. G., Overcashier, D. E., Hsu, C. C. & Shire, S. J. Effect of Moisture on the Stability of a Lyophilized Humanized Monoclonal Antibody Formulation. *Pharm. Res.* 18, 1345–1353 (2001).
74. Duralliu, A. *et al.* The Influence of Moisture Content and Temperature on the Long-Term Storage Stability of Freeze-Dried High Concentration Immunoglobulin G (IgG). *Pharmaceutics* 12, 303 (2020).
75. Pikal, M. J., Shah, S., Roy, M. L. & Putman, R. The secondary drying stage of freeze drying: Drying kinetics as a function of temperature and chamber pressure. *Int. J. Pharm.* 60, 203–217 (1990).
76. Emami, F., Vatanara, A., Park, E. & Na, D. Drying Technologies for the Stability and Bioavailability of Biopharmaceuticals. *Pharmaceutics* 10, 131 (2018).
77. Sebastião, I. B. *et al.* Bulk Dynamic Spray Freeze-Drying Part 1: Modeling of Droplet Cooling and Phase Change. *J. Pharm. Sci.* 108, 2063–2074 (2019).
78. Sebastião, I. B. *et al.* Bulk Dynamic Spray Freeze-Drying Part 2: Model-Based Parametric Study for Spray-Freezing Process Characterization. *J. Pharm. Sci.* 108, 2075–2085 (2019).
79. Wanning, S., Süverkrüp, R. & Lamprecht, A. Pharmaceutical spray freeze drying. *Int. J. Pharm.* 488, 136–153 (2015).
80. Xu, Y. *et al.* Protein Quantity on the Air-Solid Interface Determines Degradation Rates of Human Growth Hormone in Lyophilized Samples. *J. Pharm. Sci.* 103, 1356–1366 (2014).
81. Gitter, J. H., Geidobler, R., Presser, I. & Winter, G. Significant Drying Time Reduction Using Microwave-Assisted Freeze-Drying for a Monoclonal Antibody. *J. Pharm. Sci.* 107, 2538–2543 (2018).
82. Metaxas, A. C. Microwave heating. *IEE Power Eng. J.* 5, 237–247 (1991).
83. Vadivambal, R. & Jayas, D. S. Non-uniform temperature distribution during microwave heating of food materials—A review. *Food Bioprocess Technol.* 3, 161–171 (2010).
84. Chandrasekaran, S., Ramanathan, S. & Basak, T. Microwave food processing—A review. *Food Res. Int.* 52, 243–261 (2013).
85. Gitter, J. H., Geidobler, R., Presser, I. & Winter, G. Microwave-Assisted Freeze-Drying of Monoclonal Antibodies: Product Quality Aspects and Storage Stability. *Pharmaceutics* 11, 674 (2019).
86. Kelen, A., Pallaivarsanyi, E., Röss, S., Nagy, T. & Pintyehodi, K. Practical method for choosing diluent that ensures the best temperature uniformity in the case of pharmaceutical microwave vacuum drying of a heat sensitive product. *Eur. J. Pharm. Biopharm.* 62, 101–109 (2006).
87. Khinast, J. & Bresciani, M. Continuous Manufacturing: Definitions and Engineering Principles. in *Continuous Manufacturing of Pharmaceuticals* (eds. Kleinebudde, P., Khinast, J. & Rantanen, J.) (John Wiley & Sons, Ltd, 2017).
88. Pisano, R., Arsiccio, A., Capozzi, L. C. & Trout, B. L. Achieving continuous manufacturing in lyophilization:

-
- Technologies and approaches. *Eur. J. Pharm. Biopharm.* 142, 265–279 (2019).
89. Corver, J. A. W. M. Method and system for freeze-drying injectable compositions, in particular pharmaceutical compositions. US Patent no. US 2014/0215845 A1. (2012).
90. De Meyer, L. *et al.* Evaluation of spin freezing versus conventional freezing as part of a continuous pharmaceutical freeze-drying concept for unit doses. *Int. J. Pharm.* 496, 75–85 (2015).
91. Lammens, J. *et al.* The relevance of shear, sedimentation and diffusion during spin freezing, as potential first step of a continuous freeze-drying process for unit doses. *Int. J. Pharm.* 539, 1–10 (2018).
92. Van Bockstal, P. J. *et al.* Developing a framework to model the primary drying step of a continuous freeze-drying process based on infrared radiation. *Eur. J. Pharm. Biopharm.* 127, 159–170 (2018).
93. Van Bockstal, P. J. *et al.* Mechanistic modelling of infrared mediated energy transfer during the primary drying step of a continuous freeze-drying process. *Eur. J. Pharm. Biopharm.* 114, 11–21 (2017).
94. Van Bockstal, P. J. *et al.* Global Sensitivity Analysis as Good Modelling Practices tool for the identification of the most influential process parameters of the primary drying step during freeze-drying. *Eur. J. Pharm. Biopharm.* 123, 108–116 (2018).
95. Van Bockstal, P. J., De Meyer, L., Corver, J., Vervaet, C. & De Beer, T. Noncontact Infrared-Mediated Heat Transfer During Continuous Freeze-Drying of Unit Doses. *J. Pharm. Sci.* 106, 71–82 (2017).
96. Capozzi, L. C., Trout, B. L. & Pisano, R. From Batch to Continuous: Freeze-Drying of Suspended Vials for Pharmaceuticals in Unit-Doses. *Ind. Eng. Chem. Res.* 58, 1635–1649 (2019).
97. Patel, S. M., Doen, T. & Pikal, M. J. Determination of end point of primary drying in freeze-drying process control. *AAPS PharmSciTech.* 11, 73–84 (2010).
98. Walters, R. H. *et al.* Next-Generation Drying Technologies for Pharmaceutical Applications. *J. Pharm. Sci.* 103, 2673–2695 (2014).
99. Duan, X., Zhang, M., Mujumdar, A. S. & Wang, S. Microwave freeze drying of sea cucumber (*Stichopus japonicus*). *J. Food Eng.* 96, 491–497 (2010).
100. Jiang, H., Zhang, M., Liu, Y., Mujumdar, A. S. & Liu, H. The energy consumption and color analysis of freeze/microwave freeze banana chips. *Food Bioprod. Process. Trans. Inst. Chem. Eng. Part C* 91, 464–472 (2013).
101. Duan, X., Zhang, M. & Mujumdar, A. S. Studies on the Microwave Freeze Drying Technique and Sterilization Characteristics of Cabbage. *Dry. Technol.* 25, 1725–1731 (2007).
102. Rynnänen, S. The Electromagnetic Properties of Food Materials: A Review of the Basic Principles. *J. Food Eng.* 26, 409–429 (1995).
103. Barba, A. A. & D'Amore, M. Relevance of Dielectric Properties in Microwave Assisted Processes. in *Microwave Materials Characterization* (ed. Costanzo, P. S.) 91–118 (InTech, 2012).
104. Meredith, R. *Engineers' Handbook of Industrial Microwave Heating*. (The Institution of Engineering and Technology, 2007).
105. Evans, R. Applications of Microwave Vacuum Drying and Lyospheres to Freeze-Drying of Vaccines and Biologics. in *CPPR: Freeze-Drying of Pharmaceuticals and Biologicals*. Conference Proceedings. (CPPR, 2014).
106. Bhambhani, A., Evans, R. K., Sinacola, J. & Jones, M. Method of Obtaining Thermostable Dried Vaccine Formulations. WIPO Patent no. WO 2015/057541 A1. (2015).
107. Püschner GmbH+Co KG. Püschner Vacuum Drying / Freeze-Drying. Available at: <http://www.pueschner.com/en/products/vacuum-drying-freeze-drying>. (Accessed July 10, 2018).
108. Püschner GmbH+Co KG. Good Manufacturing Practise (GMP) for Industrial Microwave Plants. Available at: <http://www.pueschner.com/en/microwave-technology/gmp-microwaves>. (Accessed July 10, 2018).
109. Yu, L., Milton, N., Groleau, E. G., Mishra, D. S. & Vansickle, R. E. Existence of a mannitol hydrate during freeze-drying and practical implications. *J. Pharm. Sci.* 88, 196–195 (1999).

References

110. Mehta, M., Bhardwaj, S. P. & Suryanarayanan, R. Controlling the physical form of mannitol in freeze-dried systems. *Eur. J. Pharm. Biopharm.* 85, 207–213 (2013).
111. Gervasi, V. *et al.* Parenteral protein formulations: An overview of approved products within the European Union. *Eur. J. Pharm. Biopharm.* 131, 8–24 (2018).
112. Franks, F. Long-term stabilization of biologicals. *Biotechnology. (N. Y.)* 12, 253–256 (1994).
113. Patel, S. M. & Pikal, M. J. Emerging freeze-drying process development and scale-up issues. *AAPS PharmSciTech.* 12, 372–378 (2011).
114. Bjelošević, M. *et al.* Aggressive conditions during primary drying as a contemporary approach to optimise freeze-drying cycles of biopharmaceuticals. *Eur. J. Pharm. Sci.* 122, 292–302 (2018).
115. Zhang, M., Jiang, H. & Lim, R. X. Recent developments in microwave-assisted drying of vegetables, fruits, and aquatic products-drying kinetics and quality considerations. *Dry. Technol.* 28, 1307–1316 (2010).
116. Jiang, H., Zhang, M. & Mujumdar, A. S. Physico-chemical changes during different stages of MFD/FD banana chips. *J. Food Eng.* 101, 140–145 (2010).
117. Datta, a. K. & Davidson, P. M. Microwave and Radio Frequency Processing. *J. Food Sci.* 65, 32–41 (2000).
118. Ambros, S., Mayer, R., Schumann, B. & Kulozik, U. Microwave-freeze drying of lactic acid bacteria: Influence of process parameters on drying behavior and viability. *Innov. Food Sci. Emerg. Technol.* 48, 90–98 (2018).
119. Durance, T. D. & Fu, J. Apparatus and Method for Dehydrating Biological Materials. US Patent no. 2016/0137997 A1. (2016).
120. Bhambhani, A., Evans, R. K., Sinacola, J. & Lizzano, R. Method of Microwave Vacuum Drying Spherical-shaped Pellets of Biological Materials. US Patent no. US 2016/0252300 A1. (2016).
121. Sundaramurthi, P. & Suryanarayanan, R. Trehalose crystallization during freeze-drying: Implications on lyoprotection. *J. Phys. Chem. Lett.* 1, 510–514 (2010).
122. Sundaramurthi, P. & Suryanarayanan, R. Influence of crystallizing and non-crystallizing cosolutes on trehalose crystallization during freeze-drying. *Pharm. Res.* 27, 2384–2393 (2010).
123. Liu, J. Physical characterization of pharmaceutical formulations in frozen and freeze-dried solid states: techniques and applications in freeze-drying development. *Pharm. Dev. Technol.* 11, 3–28 (2006).
124. Burfoot, D., Griffin, W. J. & James, S. J. Microwave pasteurisation of prepared meals. *J. Food Eng.* 8, 145–156 (1988).
125. Vilayannur, R. S., Puri, V. M. & Anantheswaran, R. C. Size and shape effect on nonuniformity of temperature and moisture distributions in microwave heated food materials: Part II experimental validation. *J. Food Process Eng.* 21, 235–248 (1998).
126. Zhang, Z., Su, T. & Zhang, S. Shape Effect on the Temperature Field during Microwave Heating Process. *J. Food Qual.* 2018, 1–24 (2018).
127. James, C., Swain, M. V., James, S. J. & Swain, M. J. Development of methodology for assessing the heating performance of domestic microwave ovens. *Int. J. Food Sci. Technol.* 37, 879–892 (2002).
128. Rattanadecho, P. Theoretical and experimental investigation of microwave thawing of frozen layer using a microwave oven (effects of layered configurations and layer thickness). *Int. J. Heat Mass Transf.* 47, 937–945 (2004).
129. Lobo, S. & Datta, A. K. Characterization of Spatial Non-Uniformity in Microwave Reheating of High Loss Foods. *J. Microw. Power Electromagn. Energy* 33, 158–166 (1998).
130. Pikal, M. J. & Shah, S. Moisture transfer from stopper to product and resulting stability implications. *Dev. Biol. Stand.* 74, 165–179 (1992).
131. Meng, C. *et al.* A new approach to microwave food research: Analyzing the electromagnetic response of basic amino acids. *Innov. Food Sci. Emerg. Technol.* 41, 100–108 (2017).
132. Aoki, K., Nagano, K. & Iitaka, Y. The crystal structure of L -arginine phosphate monohydrate . *Acta Crystallogr.*

-
- Sect. B Struct. Crystallogr. Cryst. Chem.* 27, 11–23 (1971).
133. Izutsu, K. I., Fujimaki, Y., Kuwabara, A. & Aoyagi, N. Effect of counterions on the physical properties of L-arginine in frozen solutions and freeze-dried solids. *Int. J. Pharm.* 301, 161–169 (2005).
134. Stärtzel, P. *et al.* Freeze Drying of L-Arginine/Sucrose-Based Protein Formulations, Part I: Influence of Formulation and Arginine Counter Ion on the Critical Formulation Temperature, Product Performance and Protein Stability. *J. Pharm. Sci.* 104, 2345–2358 (2015).
135. Bianchi, C., Schmid, R., Frick, D. & Kurtz, S. Microwave Assisted Vacuum Drying Processing: Magnetron vs Solid State. Case Study: Apple Drying. in *COMSOL Conference*. Conference Proceedings. (2018).
136. Du, Y. *et al.* Chromatographic analysis of the acidic and basic species of recombinant monoclonal antibodies. *MAbs* 4, 578–585 (2012).
137. Fekete, S., Beck, A., Veuthey, J. L. & Guillarme, D. Ion-exchange chromatography for the characterization of biopharmaceuticals. *J. Pharm. Biomed. Anal.* 113, 43–55 (2015).
138. Harris, R. J. *et al.* Identification of multiple sources of charge heterogeneity in a recombinant antibody. *J. Chromatogr. B Biomed. Sci. Appl.* 752, 233–245 (2001).
139. Stärtzel, P. Arginine as an Excipient for Protein Freeze-Drying: A Mini Review. *J. Pharm. Sci.* 107, 960–967 (2018).
140. Abdul-Fattah, A. M. *et al.* Drying-Induced Variations in Physico-Chemical Properties of Amorphous Pharmaceuticals and Their Impact on Stability (I): Stability of a Monoclonal Antibody. *J. Pharm. Sci.* 96, 1983–2008 (2007).
141. Craig, D. Q. M., Royall, P. G., Kett, V. L. & Hopton, M. L. The relevance of the amorphous state to pharmaceutical dosage forms: Glassy drugs and freeze dried systems. *Int. J. Pharm.* 179, 179–207 (1999).
142. Yoshioka, S. & Aso, Y. Correlations between Molecular Mobility and Chemical Stability During Storage of Amorphous Pharmaceuticals. *J. Pharm. Sci.* 96, 960–981 (2007).
143. Abdul-Fattah, A. M., Kalonia, D. S. & Pikal, M. J. The Challenge of Drying Method Selection for Protein Pharmaceuticals: Product Quality Implications. *J. Pharm. Sci.* 96, 1886–1916 (2007).
144. Schersch, K. *et al.* Systematic Investigation of the Effect of Lyophilizate Collapse on Pharmaceutically Relevant Proteins, Part 2: Stability During Storage at Elevated Temperatures. *J. Pharm. Sci.* 101, 2288–2306 (2012).
145. Chang, B. S. & Patro, S. Y. Freeze-drying Process Development for Protein Pharmaceuticals. in *Lyophilization of Biopharmaceuticals* (eds. Constantino, H. R. & Pikal, M. J.) vol. 2, 113–138 (Springer, 2004).
146. Konstantinidis, A. K., Kuu, W. Y., Otten, L., Nail, S. L. & Sever, R. R. Controlled nucleation in freeze-drying: effects on pore size in the dried product layer, mass transfer resistance, and primary drying rate. *J. Pharm. Sci.* 100, 3453–3470 (2011).
147. Allmendinger, A. *et al.* Controlled nucleation during freeze drying using vacuum-induced surface freezing. *Res. Discl. data base no. 633018*. Available at: <http://www.researchdisclosure.com>. (accessed July 20, 2018) (2017).
148. Martin Christ Gefriertrocknungsanlagen GmbH. LyoCam – Greater Transparency in Freeze-Drying. Available at: <https://www.martinchrist.de/en/freeze-drying/camera-system-lyocam/>. (accessed July 20, 2018).
149. Nunes, C., Suryanarayanan, R., Botez, C. E. & Stephens, P. W. Characterization and crystal structure of D-mannitol hemihydrate. *J. Pharm. Sci.* 93, 2800–2809 (2004).
150. Cao, W., Xie, Y., Krishnan, S., Lin, H. & Ricci, M. Influence of Process Conditions on the Crystallization and Transition of Metastable Mannitol Forms in Protein Formulations During Lyophilization. *Pharm. Res.* 30, 131–139 (2013).
151. Vollrath, I., Friess, W., Freitag, A., Hawe, A. & Winter, G. Does controlled nucleation impact the properties and stability of lyophilized monoclonal antibody formulations? *Eur. J. Pharm. Biopharm.* 129, 134–144 (2018).
152. Patapoff, T. W. & Overcashier, D. E. The Importance of Freezing on Lyophilization Cycle Development. *BioPharm* 15, 16-21 & 72 (2002).

References

153. Searles, J. A., Carpenter, J. F. & Randolph, T. W. Annealing to optimize the primary drying rate, reduce freezing-induced drying rate heterogeneity, and determine T_g pharmaceutical lyophilization. *J. Pharm. Sci.* 90, 872–887 (2001).
154. Tang, X. & Pikal, M. J. The effect of stabilizers and denaturants on the cold denaturation temperatures of proteins and implications for freeze-drying. *Pharm. Res.* 22, 1167–1175 (2005).
155. Wenzel, T., Gieseler, M. & Gieseler, H. Investigation of Two Different Pressure-Based Controlled Ice Nucleation Techniques in Freeze-Drying: The Integral Role of Shelf Temperature After Nucleation in Process Performance and Product Quality. *J. Pharm. Sci.* 109, 2746–2756 (2020).
156. Schott AG. SCHOTT Vials. Available at: https://www.schott.com/d/pharmaceutical_packaging/33243f84-657e-49f9-97b4-06180b08ac7e/1.6/schott-brochure-schott-vials-english-20092017.pdf (accessed December 07, 2018) (2017).
157. Wenzel, T., Gieseler, M. & Gieseler, H. Design of Vacuum-Induced Freezing Protocols for High Fill Volume Formulations in Freeze-Drying: A Strategic Approach. *J. Pharm. Sci.* 109, 3035–3044 (2020).
158. Pikal, M. J. Mechanisms of Protein Stabilization During Freeze-Drying and Storage: The Relative Importance of Thermodynamic Stabilization and Glassy State Relaxation Dynamics. in *Freeze-Drying/Lyophilization of Pharmaceutical and Biological Products* (eds. Rey, L. & May, J. C.) (CRC Press, 2004).
159. Vollrath, I., Friess, W., Freitag, A., Hawe, A. & Winter, G. Comparison of ice fog methods and monitoring of controlled nucleation success after freeze-drying. *Int. J. Pharm.* 558, 18–28 (2019).
160. Lin, T. P., Hsu, C. C., Kabakoff, B. D. & Patapoff, T. W. Application of Frequency-Modulated Spectroscopy in Vacuum Seal Integrity Testing of Lyophilized Biological Products. *PDA J. Pharm. Sci. Technol.* 58, 106–115 (2004).
161. Singh, S. N. *et al.* Unexplored benefits of controlled ice nucleation: Lyophilization of a highly concentrated monoclonal antibody solution. *Int. J. Pharm.* 552, 171–179 (2018).
162. Goshima, H., Do, G. & Nakagawa, K. Impact of Ice Morphology on Design Space of Pharmaceutical Freeze-Drying. *J. Pharm. Sci.* 105, 1920–1933 (2016).
163. Nail, S. L. & Searles, J. A. Elements of quality by design in development and scale-up of freeze-dried parenterals. *BioPharm Int.* 21, 40–45 (2008).
164. Sundaram, J., Shay, Y. H. M., Hsu, C. C. & Sane, S. U. Design space development for lyophilization using Doe and process modeling. *BioPharm Int.* 23, 40–45 (2010).
165. Koganti, V. R. *et al.* Investigation of design space for freeze-drying: Use of modeling for primary drying segment of a freeze-drying cycle. *AAPS PharmSciTech.* 12, 854–861 (2011).
166. Patel, S. M. & Pikal, M. J. Lyophilization Process Design Space. *J. Pharm. Sci.* 102, 3883–3887 (2013).
167. Awotwe-Otoo, D., Agarabi, C. & Khan, M. A. An integrated process analytical technology (PAT) approach to monitoring the effect of supercooling on lyophilization product and process parameters of model monoclonal antibody formulations. *J. Pharm. Sci.* 103, 2042–52 (2014).
168. Schersch, K. *et al.* Systematic investigation of the effect of lyophilizate collapse on pharmaceutically relevant proteins I: Stability after freeze-drying. *J. Pharm. Sci.* 99, 2256–2278 (2010).
169. Roy, M. L. & Pikal, M. J. Process Control in Freeze Drying: Determination of the End Point of Sublimation Drying by an Electronic Moisture Sensor. *PDA J. Pharm. Sci. Technol.* 43, 60–66 (1989).

Appendix

A.1 List of publications

Publications associated with this work:

Gitter, J. H., Geidobler, R., Presser, I. & Winter, G. Microwave-Assisted Freeze-Drying of Monoclonal Antibodies: Product Quality Aspects and Storage Stability. *Pharmaceutics* 11, 674 (2019).

Gitter, J. H., Geidobler, R., Presser, I. & Winter, G. A Comparison of Controlled Ice Nucleation Techniques for Freeze-Drying of a Therapeutic Antibody. *J. Pharm. Sci.* 107, 2748–2754 (2018).

Gitter, J. H., Geidobler, R., Presser, I. & Winter, G. Significant Drying Time Reduction Using Microwave-Assisted Freeze-Drying for a Monoclonal Antibody. *J. Pharm. Sci.* 107, 2538–2543 (2018).

Gitter, J.H., Geidobler, R., Halbinger, W., Presser, I. & Winter, G. 100% Control of Controlled Ice Nucleation Vials by Camera-supported Optical Inspection in Freeze-Drying (*Manuscript ready for submission*)

Further publications:

Krieg, D., Svilenov, H., **Gitter, J. H.** & Winter, G. Overcoming challenges in co-formulation of proteins with contradicting stability profiles - EPO plus G-CSF. *Eur. J. Pharm. Sci.* 105073 (2019).

A.2 List of presentations

Oral presentations:

***Gitter J.H.**, Geidobler R., Presser I., Winter G. Microwave-assisted Freeze-Drying of a mAb: Time Savings and Product Quality Aspects. *aaps PharmSci 360*, Rapid Fire Talk, Washington, DC, USA (2018).

***Gitter J.H.**, Häupler B., Geidobler R., Presser I., Winter G. Tert-Butyl Alcohol as an Excipient in Freeze-Drying of a Monoclonal Antibody. *PDA Europe Pharmaceutical Freeze-Drying Technology*, Seville, Spain (2018).

***Gitter J.H.**, Häupler B., Geidobler R., Presser I., Winter G. Accelerating the Freeze Drying Process of a Monoclonal Antibody by Addition of tert-Butyl Alcohol. *11th PBP World Meeting*, Granada, Spain (2018).

#Gitter J.H., Häupler B., Geidobler R., Presser I., Winter G. How to Accelerate the Freeze Drying Process of a Monoclonal Antibody? A Case Study on the Usage of tert-Butyl Alcohol. *PDA Europe: Freeze Drying in Practice*, Martin Christ Gefriertrocknungsanlagen GmbH, Osterode (Harz), Germany (2018).

Poster presentations:

***Gitter J.H.**, Geidobler R., Presser I., Winter G. Significant Drying Time Reduction Using Microwave-assisted Freeze-Drying for a Monoclonal Antibody. *aaps PharmSci 360*, Washington, DC, USA (2018).

***Gitter J.H.**, Geidobler R., Presser I., Winter G. A Comparison of Ice Fog and Depressurization for Freeze-Drying of a Therapeutic Antibody. *Freeze Drying of Pharmaceuticals and Biologicals - Short Course and Conference*, Garmisch-Partenkirchen, Germany (2018).

**Selected by peer review process.*

Selected by invitation.

A.3 Curriculum vitae

Personal data:

Name: Julian Hendryk Gitter
Date of birth: 2 September 1989
Place of birth: Dessau, Germany
Nationality: German
Languages: German, English

Work experience:

01/2020 – present Laboratory Head
Bayer AG, Wuppertal, Germany
Formulation development for Parenteral drug delivery

04/2015 – 05/2019 Ph.D. student
Ludwig-Maximilians-Universität München, Munich, Germany
Department of Pharmacy, Pharmaceutical Technology and Biopharmaceutics
Supervisor: Prof. Dr. Gerhard Winter

01/2015 – 04/2015 Pharmacist
Holsten-Apotheke, Schacht-Audorf, Germany

07/2014 – 12/2014 Pharmacist trainee
Flora Apotheke, Elmshorn, Germany

01/2014 – 06/2014 Research assistant (pharmacist trainee)
Trinity College Dublin, Ireland
The School of Pharmacy and Pharmaceutical Sciences, Pharmaceutics and
Pharmaceutical Technology
Host: Prof. Dr. Anne Marie Healy

Education:

04/2015 – 05/2019 PhD Studies, Ludwig-Maximilians-Universität München, Munich, Germany
Department of Pharmacy,
Chair of Pharmaceutical Technology and Biopharmaceutics
Supervisor: Professor Dr. Gerhard Winter

01/2015 Licensure as pharmacist (Approbation)

10/2009 – 11/2013 Pharmacy studies, University of Kiel, Germany

08/2002 – 07/2008 Certificate of matriculation (Abitur), Gymnasium Philanthropinum, Dessau,
Germany